4-14-2009

Clay Mineralogy and Illite Crystallinity in the Late Devonian to Early Mississippian Woodford Shale in the Arbuckle Mountains, Oklahoma, USA

Richard Allen Whittington II

CLAY MINERALOGY AND ILLITE CRYSTALLINITY IN THE LATE DEVONIAN TO EARLY MISSISSIPPIAN WOODFORD SHALE IN THE ARBUCKLE MOUNTAINS, OKLAHOMA, USA

by

RICHARD ALLEN WHITTINGTON II

Under the Direction of Dr. W. Crawford Elliott

ABSTRACT

Commonly the thermal maturity of the Late Devonian to Early Mississippian Woodford shale found on the flanks of the Arbuckle Mountains of Oklahoma is determined by vitrinite reflectance, values ranging from 0.3-1.5%. Using phyllosilicate minerals, specifically diagenetic mixed layer illite/smectite and diagenetic illite, an understanding of the extent and processes leading to the thermal maturation may be developed. Analysis by XRD of the clay mineralogy of the Woodford shale found kaolinite and mixed layer illite/smectite with <5% smectite and R≥3 stacking order. Modeling of the Woodford shale also suggests the percentage of smectite present in mixed layer illite/smectite to be <5% and commonly <2.5%. Deconvolution of the illite (001) peak supports the low smectite content and high illite crystallinity. The long range ordered illite, R≥3, and high illite crystallinity values are indicative of diagenesis to anchizone conditions suggesting a higher thermal maturity relative to previously measured values of vitrinite reflectance.

INDEX WORDS: Mixed layer illite/smectite, Thermal maturity, Illite polytype, Peak deconvolution, Kübler Crystallinity Index

CLAY MINERALOGY AND ILLITE CRYSTALLINITY IN THE LATE DEVONIAN TO EARLY MISSISSIPPIAN WOODFORD SHALE IN THE ARBUCKLE MOUNTAINS, OKLAHOMA, USA

by

RICHARD ALLEN WHITTINGTON II

A Thesis Submitted in Partial Fulfillment of the Requirements for the Degree of

Master of Science

in the College of Arts and Sciences

Georgia State University

2009

CLAY MINERALOGY AND ILLITE CRYSTALLINITY IN THE LATE DEVONIAN TO EARLY MISSISSIPPIAN WOODFORD SHALE IN THE ARBUCKLE MOUNTAINS, OKLAHOMA, USA

by

RICHARD ALLEN WHITTINGTON II

Committee Chair: Dr. W. Crawford Elliott

Committee: Dr. Seth E. Rose
Dr. Daniel M. Deocampo
Dr. R. Douglas Elmore

Electronic Version Approved:

Office of Graduate Studies
College of Arts and Sciences
Georgia State University
May 2009

I would like to dedicate this thesis to my wife- Laura, my family and Dr. D. Bran Potter Jr. Laura has supported me tirelessly throughout the past two and a half years. She made sure that I was staying current on my work, quizzed me before tests and occasionally when I requested has proofed my "boring" papers. I could not have completed this program without your steadfast support. Laura, you are the best! My family supported me 100% when I decided to pursue my passion and I thank them for that. Their constant enthusiasm and advice have been greatly appreciated.

I would not have discovered that my passion is geology if not for an 8:00 a.m. Introduction to Geology class taught by Dr. Potter (the only 8:00 a.m. class I have ever taken). This was a class everyone said you should take while at Sewanee. I enjoyed the class and followed it up with Structural Geology, Western Geology and a field course. All helped solidify my love of geology. I stayed in contact with Dr. Potter and several years after graduating from Sewanee and deciding what direction to go, Dr. Potter was instrumental in guiding me to pursue a Masters in geology.

ACKNOWLEDGEMENTS

The journey that this thesis culminates has been supported by many. Dr. Elliott was my first contact at Georgia State University and as fortune would have it, he also became my thesis advisor. I greatly appreciate the opportunity that he provided me to work on a project that interests and challenges me. Dr. Elliott has been very patient and helpful with my many questions, providing direction in the lab and with revisions of this thesis, even as his other duties pulled him in many other directions.

I thank Dr. Elmore (University of Oklahoma) for providing the samples and allowing me to work on this project. Feedback from my committee of Dr. Rose (Georgia State University), Dr. Deocampo (Georgia State University) and Dr. Elmore helped improve this work greatly. All were very willing to answer my many questions and that was truly appreciated.

Thank you to all other faculty, staff, graduate and undergraduate students. Being a student is easy when you are challenged academically by the professors and when fellow students act professionally. The community of budding geologists found in the Green Room and the adjacent Graduate Offices helped to balance the rigors of academics while also providing focus for the tasks at hand.

TABLE OF CONTENTS

LIST OF TABLES

LIST OF FIGURES

CHAPTER 1- INTRODUCTION

1.1 Overview

The Late Devonian to Early Mississippian Woodford shale is an important hydrocarbon source rock in Oklahoma. The exploration of the Woodford shale within Oklahoma began over 75 years ago with the first Woodford shale well being completed in 1939 (Wang and Philp, 1997; Vulgamore, 2008). Due to the recent success of the Barnett shale in Texas over the past decade, the interest in the lithologic correlative Woodford shale has grown considerably from only 22 completed Woodford shale wells in 2004 to over 500 completed wells in 2007 (Vulgamore, 2008). Rocks present in Oklahoma range in lithology from metasedimentary Precambrian basement rocks to Permian evaporites (Johnson and Cardott, 1992). Carbonates are the predominate lithology in the lower Paleozoic rocks; siliciclastic rocks, including the Woodford shale, account for the majority of upper Paleozoic rocks (Carter et al., 1998).

Thermal history data provides an understanding of both the extent of and the processes leading to the maturation of organic matter and the subsequent generation of crude oil and natural gas from the Woodford shale. Cardott and Lambert (1985) list multiple methods used to determine the maturation of source rocks at the range of temperatures corresponding to the generation of crude oil and natural gas (100-200^{o}C): 1) conodont-color alteration; 2) palynomorph or kerogen color; 3) spore translucency; 4) organic geochemistry; 5) vitrinite reflectance (VR_o); and 6) clay mineralogy (mixed layer illite/smectite and illite). This study focuses on using the clay mineralogy (mixed layer illite/smectite and illite) in order to better understand the thermal history of the Woodford shale from several locations in Oklahoma.

Clay minerals, specifically diagenetic illite and diagenetic mixed layer illite/smectite, are useful in determining the degree of thermal maturation and frequently track vitrinite reflectance

(Hoffman and Hower, 1979; Pevear, 1999). Much like VR_o which increases as thermal maturity increases, the percentage of illite layers in mixed layer illite/smectite and the illite crystallinity of diagenetic illite are also temperature proxies used to estimate the temperatures associated with the maturation of organic matter in petroleum source rocks (e.g. Waples, 1980; Kübler, 1968; Guthrie et al., 1986; Pevear, 1999). Unlike VR_o which records only maximum temperature, illite may be used to determine the time of maximum temperature provided the kinetics of this transformation are favorable (time, temperature and K availability) (Pevear, 1999). The range of time corresponding to maximum temperature can be established by measuring the ^{40}K-^{40}Ar or ^{40}Ar -^{39}Ar ages of diagenetic mixed layer illite/smectite while the maximum temperature may be determined by illite crystallinity and/or the stacking order of illite/smectite (Hoffman and Hower, 1979; Pevear, 1999).[1]

Diagenetic illite (or mixed layer illite/smectite) is found in altered volcanic rocks like bentonites (and potassium bentonites) and sedimentary rocks such as shales and sandstones. Smectite is the predominant phyllosilicate phase that forms soon after hydrolysis of precursor ash or glass (Altaner, 1989). When bentonites are buried or otherwise heated to temperatures >50 °C and/or experience long reaction times, then diagenetic illite begins to form from smectite (Hower et al, 1976; Pevear et al., 1980). During diagenesis, it is understood from X-ray diffraction data, that smectites convert to illite via mixed layer illite/smectite having various stacking orders [random (R=0), short range ordered (R≥1) and long range ordered (R≥3)] (e.g. Hower et al., 1976; Pevear, 1999). Bentonites or potassium bentonites allow for more accurate age analysis by ^{40}K-^{40}Ar or ^{40}Ar -^{39}Ar dating procedures, because only diagenetic, $1M_d$, illite is

[1] Stacking order of illite and smectite layers in mixed layer illite/smectite is described using R-notation where R means Reichweite (or reachback) (Moore and Reynolds, 1997). For example, R≥1 means there are one or more illite layers following a smectite layer (Moore and Reynolds, 1997).

present (Pevear, 1999). Separating diagenetic illite from detrital illite has not been accomplished at the precision needed for ^{40}K-^{40}Ar or ^{40}Ar -^{39}Ar methods. Therefore, if a rock is analyzed that contains only diagenetic illite, then the range of ages determined by radioactive dating techniques will have greater certainty than the range of ages from rocks with mixtures of detrital and diagenetic illite such as shales (Pevear, 1999; Elliott et al., 2006).

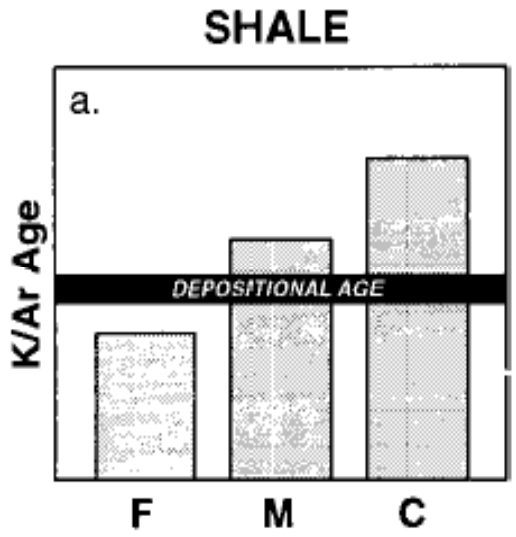

Figure 1.1- Three size fractions commonly found in shales. C- Coarse, M- medium and F- fine. Showing the change in age with each size fraction, (from Pevear, 1999).

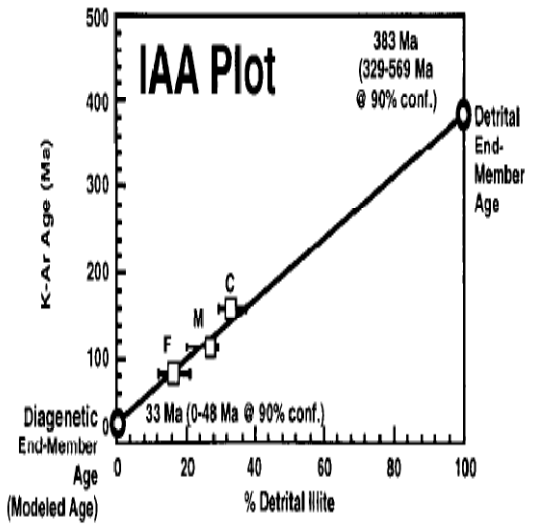

Figure 1.2- Plot of three size fractions with K-Ar dates vs. percent detrital illite (% $2M_1$ polytype). End members are determined through the use of X-ray diffraction, (from Pevear, 1999).

Shales often contain both detrital and diagenetic illite (Pevear, 1999). Pevear (1999) presents the use of ^{40}K-^{40}Ar dating of different size fractions to determine the age of diagenesis. Depending on the amount of detrital illite present (% $2M_1$ polytype), the coarse fraction (2.0- 0.2 μm), may represent the oldest age. Finer fractions- medium (0.2-0.02 μm) and fine (<0.02 μm), represent younger ages due to a greater abundance of diagenetic illite (Figure 1.1). The ages from each size fraction form what Pevear (1999) refers to as a "mixochron" (Figure 1.2). The age of diagenetic illite can be extrapolated to the 0% detrital illite end member, and that age of

the "mixochron" may represent an approximate age of hydrocarbon generation. Of note, Pevear, in developing this idea, measured the ^{40}K-^{40}Ar age of diagenetic mixed layer illite/smectite separated from a bentonite interbedded in a shale and found the measured diagenetic ^{40}K-^{40}Ar age of the bentonite and shale agreed demonstrating the utility and success of this concept. Pevear (1999) also presents evidence where this procedure was applied to date the timing of hydrocarbon generation relative to the formation of traps and to the growth of diagenetic illite in sandstone reservoirs where permeability was reduced. All three applications provide important information for understanding the thermal history (e.g. Elliott et al., 1991; Pevear, 1999).

1.2 Objectives

The objective of this study is to derive a better understanding of the thermal maturity of the Woodford shale in select locations in Oklahoma. Understanding the thermal maturity of the Woodford shale is also important in the pursuit of exploitable hydrocarbon deposits. The Woodford shale is a source rock of hydrocarbons and the hydrocarbons produced from the Woodford shale are dependent upon the degree thermal maturation. This data can also be useful in the study of paleomagnetics due to the release of Fe^{3+} during the conversion of smectite to illite (e.g. Elliott et al., 2006). The Fe^{3+} can then precipitate and record the paleomagnetic orientation of the rock. This signature can then be related to known paleo-wanderer paths.

Using the clay mineralogy, we hope to provide new information to the thermal history which here to fore has been derived from VR_o and other organic geochemistry measurements. VR_o studies of the Woodford shale and adjacent strata have found that thermal maturity corresponds to orogenic belts and stratigraphic age (Houseknecht and Mathews, 1985; Comer, 2005). Likewise, we expect mixed layer illite/smectite to display similarly high thermal maturity within orogenic belts and with increasing depositional age. The five samples analyzed in this

study were collected from the flanks of the Arbuckle Mountains, a structure bounded by thrust faults and created by the Ouachita Orogeny (Comer, 2005; Nance and Linnemann, 2008). We would expect mixed layer illite/smectite to exhibit long range ordered illite, R≥3, suggesting high thermal maturity. If the samples are not of high thermal maturity as suggested by Comer (2008) who reported the Woodford shale on the flanks of the Arbuckle Mountains is in the oil generation window (VR_o =0.3-1.5%), we would expect to see mixed layer illite/smectite with a low-percentage of illite layers of either random (R=0) or short range (R≥1) ordering.

An understanding of the thermal maturity of the Woodford shale will be accomplished by detailed analysis of the diagenetic and detrital clay mineralogy. Previous mineralogical studies have been done before and have found illite and kaolinite present in the clay fractions of the Woodford shale (Lewan, 1983; Cardott, 2007). Few studies have treated mixed layer illite/smectite as a semi-quantitative geothermometer for thermal maturity. The thermal maturity indicated by illite crystallinity measurements may be influenced by detrital illite present in the Woodford shale. Quantifying the influence and presence of detrital illite will help us to better understand the thermal history of the Woodford shale and will be done during this study.

The ability to date illite by ^{40}K-^{40}Ar or ^{40}Ar -^{39}Ar procedures is an excellent tool in the study of illite. For this study, ^{40}K-^{40}Ar dating was not attempted on these samples. This is due to the large inherent error that comes with dating shales containing both detrital and diagenetic illite. If the content of detrital illite can be determined then estimating the ^{40}K-^{40}Ar age of the diagenetic illite is possible (e.g. Pevear, 1999; Środoń et al., 1999). If bentonites or potassium bentonites are found in these strata then the application of ^{40}K-^{40}Ar or ^{40}Ar -^{39}Ar dating of the mixed layer illite/smectite is more feasible to determine the timing of thermal maturation of the Woodford shale.

1.3 Conversion of Smectite to Illite

The clay minerals smectite and illite can be found in many sedimentary units as a result of both detrital and diagenetic processes. Understanding these processes is helpful in understanding the history of a given rock. Smectite and illite may be considered end-members of a series and form under many different conditions ranging from the weathering of volcanic ashes to precipitating in pore spaces (Moore and Reynolds, 1997). The end-members illite and smectite and the resulting mixed layer illite/smectite (I/S) constitute approximately 30% of all sedimentary rocks making their study warranted (Środoń, 1990; Lynch et al., 1997).

One important path linking the two minerals is the conversion of smectite to illite during burial diagenesis which has been studied extensively. Many of these early studies have shown the conversion of smectite to illite occurs during burial diagenesis at the same temperature and pressure regimes as the formation of crude oil and natural gas. The ability to interpret the paleo-temperature from the stacking order and to determine the age of diagenetic mixed layer illite/smectite show that the conversion of smectite to illite is a useful geologic tool for the study of thermal histories of sedimentary basins.

Studies of the conversion of smectite to illite began in the late 1950s and the 1960s. The mineralogy of mixed layer illite/smectite as distinct from illite was first described by Velde and Hower (1963) and Hower and Mowatt (1966). During the 1970s, the work on the Gulf Coast and other sedimentary basins being explored for oil and gas focused on the conversion of smectite to illite and its use as a geothermometer. With a basic understanding of the conversion of smectite to illite, the work done in the 1980s radically questioned the conversion based on S-TEM evidence (e.g. Nadeau et al., 1984) and the conversion was also linked to larger scale tectonic processes such as convergent tectonism (e.g. Elliott and Aronson, 1987). During the

1990s and 2000s, work progressed in the directions of determining the amounts of diagenetic illite in shales, modeling the conversion, crystal growth models and further applications to geologic study of sedimentary basins. With over four decades of research on the conversion of smectite to illite the amount of information available is vast. In the following pages I aim to synthesize some of this information to present how smectite converts to illite and its many variables.

1.3.1 Overview of Smectite, Illite and Mixed Layer Illite/Smectite

Smectite is a 2:1 dioctahedral[2], expandable clay mineral with a layer charge of 0.2-0.6 found in the dioctahedral sheet (Figure 1.3) (Moore and Reynolds, 1997). Due to its ability to expand and low layer charge, smectites have a high cation-exchange capacity when compared to other clay minerals (Moore and Reynolds, 1997). Generally the most abundant cation within the interlayer of smectite controls the interlayer spacing, ranging from 10-17 Å (Ransom and Helgeson, 1994; Moore and Reynolds, 1997).

Illite is a 2:1 dioctahedral and rarely trioctahedral, non-expandable, mineral with a layer charge of approximately 0.9 and originates mostly in the tetrahedral sheet (Figure 1.3) (Moore and Reynolds, 1997). K^+ is strongly held in the interlayer preventing expansion and allows illite to be dated using ^{40}K-^{40}Ar or ^{40}Ar -^{39}Ar dating techniques (Pevear, 1999). Nadeau and Bain (1986) write the half-cell formula for illite as:

$$(K^+E^+)_{x+y}(Al^{3+}_{2-y}Mg^{2+}_{y})(Si_{4-x}Al_x)O_{10}(OH)_2$$

K^+ represents a non-exchangeable monovalent cation (generally K^+) and E^+ represents any exchangeable monovalent cation. The exchangeable and non-exchangeable cations balance the

---

[2] Smectite and illite are found mostly as dioctahedral 2:1 phyllosilicate minerals in bentonites, sandstones and shales. Some occurrences of trioctahedral smectite and illite have been identified (Moore and Reynolds, 1997).

negative layer charge resulting from the substitution of Al^{3+} for Si^{4+} within the tetrahedral sheet and Mg^{2+} for Al^{3+} in the octahedral sheet (Nadeau and Bain, 1986). Fe is not represented but if present, the cation may be found in the octahedral sheet as Fe^{3+} in smectites and Fe^{2+} in more illitic clays (Nadeau and Bain, 1986).

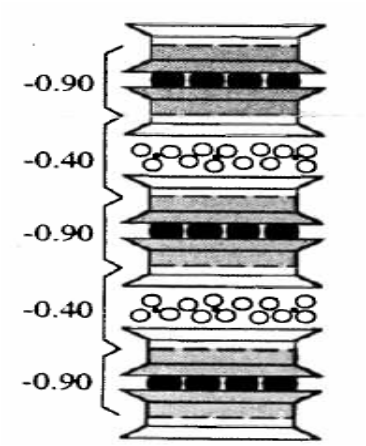

Figure 1.3- Ordered interstratification of smectites and illite with layer charges (from Altaner and Ylagan, 1997).

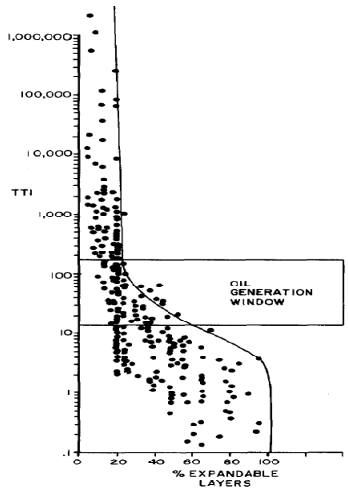

Figure 1.4- Time-temperature index vs. % expandable layer clays (smectite) (from Waples, 1980).

Smectite converts to illite and forms a mixed layer complex illite/smectite during diagenesis; this process is called illitization (Hoffman and Hower, 1979; Altaner, 1989). Illitization occurs at a similar time-temperature index as the generation of hydrocarbons (Figure 1.4) (Waples, 1980). As burial diagenesis progresses, smectite rich illite/smectite becomes illite rich illite/smectite as a function of time (Pytte and Reynolds, 1989), temperature (Hower et al., 1976), and the concentration of K^+ in pore fluids (Huang et al., 1993). Hoffman and Hower (1979) found the percentage of illite layers present in mixed layer illite/smectite to be a reliable geothermometer sensitive to the metamorphic grade of the rock. No structural formula is possible for mixed layer clays, i.e. illite/smectite, because it is not by definition compositionally homogeneous (Hower and Mowatt, 1966).

Three common rocks where smectite, illite and illite/smectite can be found are sandstones, bentonites (and potassium bentonites) and shales. The nature of the sandstone affects the nature of the illite present. If a sandstone has a matrix of clays then the presence of both detrital and diagenetic illite should be assumed (Pevear, 1999). If, however, the sandstone is clean and lacks a clay matrix, indicating a high energy depositional environment, then the presence of detrital illite will be low (Pevear, 1999). The illite present will have precipitated within the pore spaces, evidenced by its hairy texture due to unconfined growth, with no smectite precursor and should be considered diagenetic (Figure 1.5) (Pevear, 1999). How and why illite precipitates in sandstones is not fully understood (Güven, 2001). One hypothesis begins with the weathering of potassium feldspar impurities found within the sandstone resulting in the precipitation of kaolinite, the precipitated kaolinite then becomes the core of the fibrous illite overgrowth (Güven, 2001).

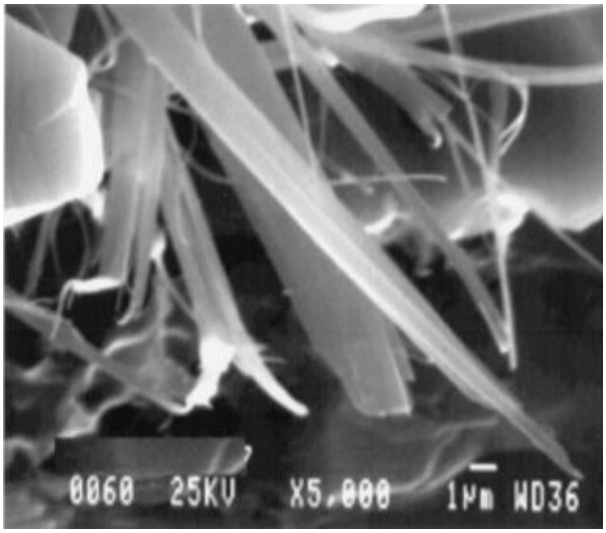

Figure 1.5- Image of "hairy illite" commonly found filling the pores of sandstones (from Pevear, 1999).

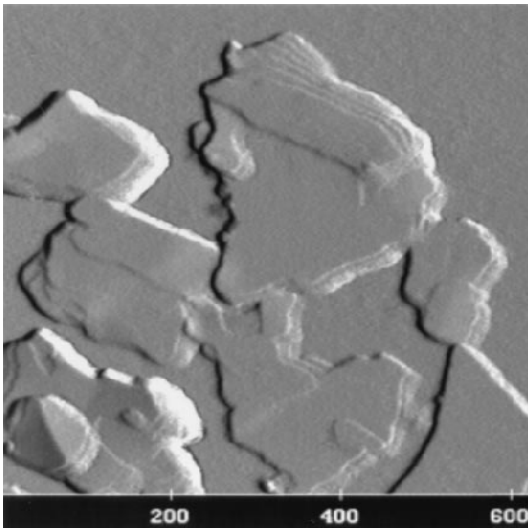

Figure 1.6- Image of illite crystals from the Tioga K-bentonite (from Pevear, 1999). Scale is in nm

Bentonites are the result of volcanic ash falls which have been altered to smectite (Altaner, 1989). If the bentonite undergoes diagenesis then smectite will convert to diagenetic mixed layer illite/smectite with negligible detrital illite present (Figure 1.6) (Pevear, 1999).

Shales contain both detrital and diagenetic illite. Coarser clay fractions (1-2 μm) contain more detrital illite than smaller clay fractions (<0.25 μm) due to the inefficiencies of physical weathering very fine grained particles (Moore and Reynolds, 1997; Pevear, 1999). The influence of physical weathering becomes very small for particles <4 μm, the inertia of the particles is small compared to the viscous forces in the water reducing the grinding or chipping action responsible for creating ever finer grains (Moore and Reynolds, 1997).

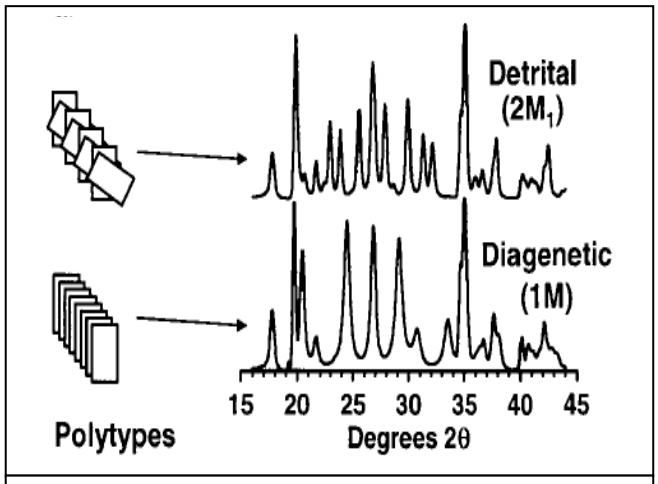

Figure 1.7- X-ray diffraction patterns for 1*M* and 2M_1 polytypes (from Pevear, 1999).

Differentiating the detrital and diagenetic illite present in a shale or sandstone is done by polytype determination (Figure 1.7) (Grathoff and Moore, 1996). Three polytypes have been identified for illite, with a possible progressive sequence of 1M_d→1*M*→2M_1 where the 2M_1 polytype is found at the beginning of low grade metamorphism (epizone) (280 to 360°C) (Velde, 1980; Weaver and Brockstra, 1984). If no other parameters of a rock indicate the rock had experienced low grade metamorphism temperatures (280 to 360°C) then the presence of the 2M_1

polytype should be considered the result of detrital input. Velde and Hower (1963) found the most abundant polytype present in the <1 μm fraction of Paleozoic rocks to be the $1M_d$ polytype followed by the $2M_1$ polytype. The $1M_d$ polytype was found in all samples while the $2M_1$ polytypes was absent from some samples. The absence of $2M_1$ from some samples suggested $1M_d$ to be a product of diagenesis and $2M_1$ to be a product of detrital input, likely the weathering of igneous/metamorphic rocks (Velde and Hower, 1963). $2M_1$ polymorphs have been shown to weather to other 2:1clays with greater d-spacings than 10Å by the removal of K^+ (vermiculite, hydroxyl interstratified vermiculite), when K^+ is reintroduced to the system, the clay will return to a $2M_1$ structure (Weaver, 1958).

Supporting this hypothesis of $1M_d$ representing diagenetic illite are examples of bentonites, sandstones and shales from Pevear (1999). Pevear (1999) presents results from multiple studies for bentonites, sandstones and shales- within bentonites $1M$ polytypes are found but never any detrital $2M_1$, while clean sandstones contain $1M$ polytypes and never $2M_1$, and shales contain $1M_d$ and $2M_1$ illite indicating both a diagenetic and a detrital source.

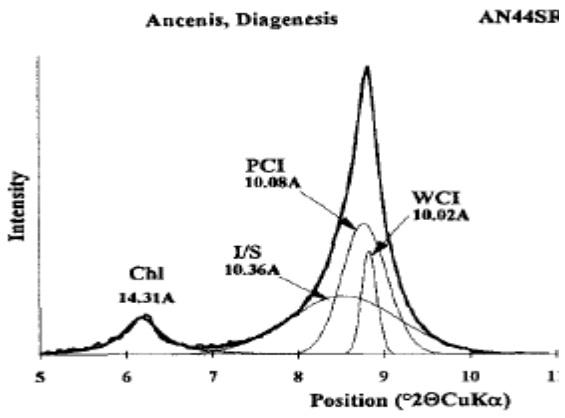

Figure 1.8- Deconvolution of a diagenetic illite (001) peak. The three sub-populations and d-spacings noted (from Gharrabi et al., 1998).

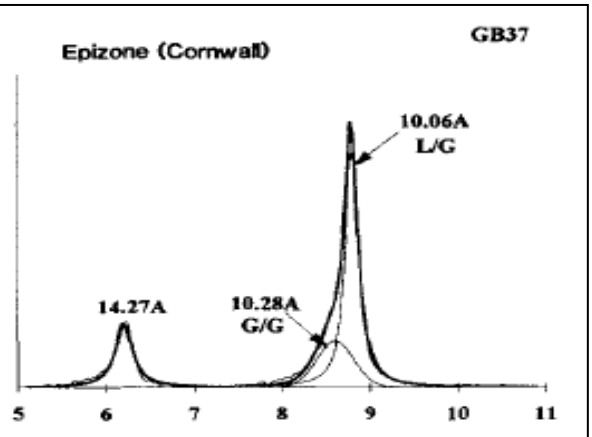

Figure 1.9- Deconvolution of the illite (001) peak from a sample indicative of the epizone. PCI and WCI d-spacings noted (from Gharrabi et al., 1998).

Illite can be classified by the crystallinity which is determined by the width of the (001) peak at half-height (i.e. the Kübler Index) (Eberl and Velde, 1989 and references therein). In addition three discrete subpopulations of illite are identified from the deconvolution of the illite (001) peak- mixed layer illite/smectite (I/S), poorly crystallized illite (PCI) and well crystallized illite (WCI) (Figure 1.8) (Lanson et al., 1998). As time and temperature increase the physical characteristics of mixed layer illite/smectite change, illite crystals grow at the expense of mixed layer illite/smectite (Lanson et al., 1998). Mixed layer illite/smectite converts to poorly crystallized illite and then to well crystallized illite as thermal maturity increases (Lanson et al., 1998). The number of peaks necessary to deconvolve the illite (001) peak of more thermally mature illite decreases from three peaks in samples of diagenesis to two peaks for samples displaying crystallinity indicative of epizone due to the increase in peak symmetry (Figure 1.9) (Gharrabi et al., 1998).

1.3.2 Role of Organic Acids

As temperature and depth increase, fluid flow causes a chemical disequilibrium and in order to attain chemical equilibrium dissolution and precipitation reactions occur (Berger et al., 1997). Most mineralogical reactions may be considered isochemical because the sources and sinks for the reaction are in close proximity to the reaction sites (Berger et al., 1997). During diagenesis, illite is a sink for K^+ and Al^{3+}, the presence or absence of their sources- K-feldspar, kaolinite and smectite represent the limiting factors on illitization (Figure 1.10a and 1.10b) (Lynch et al., 1997). At the same time thermal maturation of organic material releases organic acids aiding the dissolution of feldspars and releasing K^+ and Al^{3+} for use during illitization (MacGowan and Surdam, 1990).

a-

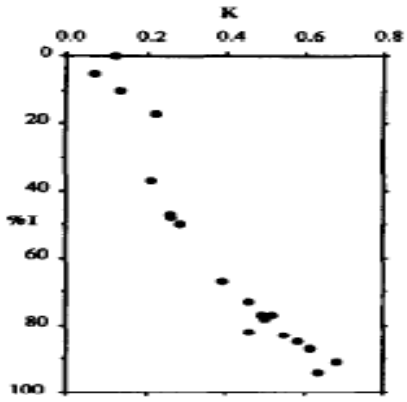

Figure 1.10a- The concentration of potassium versus the percentage of illite layers in mixed layer illite/smectite. The concentration of potassium is increasing with illitization (from Lynch et al., 1997).

b-

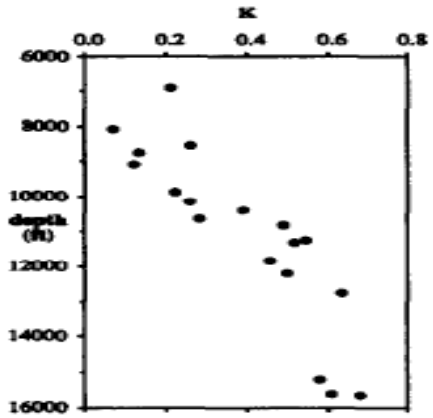

Figure 1.10b- The concentration of potassium versus burial depth. The concentration of potassium is increasing with illitization of illite/smectite (from Lynch et al., 1997).

As organic matter matures, CO_2, organic acids and CH_4 are the main water-soluble species generated (Berger et al., 1997). The acids released by organic material are dominated by acetate, a monofunctional acid, and bicarbonate (Palandri and Reed, 2001; Harrison and Thyne, 1992). This is followed with minor amounts of monofunctional acid anions (formic and propionic), difunctional acid anions (malonic, oxalic and succinic), monocarboxylic, dicarboxylic and C^{3+} acid ions (Palandri and Reed, 2001; Harrison and Thyne, 1992). During sedimentary rock diagenesis, difunctional acids are thermally less stable than monofunctional acids (Lundegard and Kharaka, 1990). The stability of monofunctional acids, i.e. acetate, may be enhanced due to the formation of more stable complexes with the divalent metal cations such as Mg^{2+}, Ca^{2+} and Fe^{2+} than difunctional acids (Harrison and Thyne, 1992).

Bicarbonate is formed when CO_2, largely generated between 100-135°C and formed from the thermal breakdown of organic material and/or organic acids, reacts with water (Capuano, 1990; Berger et al., 1997):

$$CO_{2(aq)} + H_2O_{(l)} \rightarrow HCO_3^-{}_{(aq)} + H^+{}_{(aq)}$$

This reaction may lower the pH but is limited due to the solubility of the gasses (Capuano, 1990). Reduction of Fe^{3+} and simultaneous oxidation of carbon may also lower the pH (Lynch et al., 1997):

$$4Fe^{+3}{}_{(aq)} + CH_2O_{(aq)} + H_2O_{(l)} \rightarrow 4Fe^{+2}{}_{(aq)} + CO_{2(aq)} + 4H^+{}_{(aq)}$$

Acetate accounts for 94% of organic acids present in solution (Palandri and Reed, 2001). The stability of acetate is dependent on temperature, fluid chemistry and the minerals exposed to pore waters (Berger et al., 1997). Under unstable conditions acetate may decompose into CH_4 and H_2CO_3 (Berger et al., 1997). Acetate and other organic acids may serve several different purposes: act as a buffer to the pH and Eh of the solutions, promote the growth of end-member illite, reduce the energy barrier for nucleation and/or act as a complexing agent increasing the solubility of cations (Kharaka et al., 1986; Berger et al., 1997).

The solubility of Al^{3+} and Si^{4+} are enhanced in the presence of short-chain organic acid anions particularly the difunctional acids (MacGowan and Surdam, 1990; Harrison and Thyne, 1992). Carbonic acids and dissociated bases ability to complex with metals is very low, therefore their ability to transport cations such as Al^{3+} and Si^{4+} is not favorable (MacGowan and Surdam, 1990). Difunctional organic acids, such as oxalic acid, are the preferred complexing agent with Al^{3+} through a pH interval from 4 to 6.5 (Harrison and Thyne, 1992). The presence of oxalate and its affinity to complex with Al^{3+} may destabilize plagioclase and carbonate minerals in slightly acidic environments common in subsurface waters (Harrison and Thyne, 1992).

Dissolution of potassium feldspar within a slightly acidic environment can be explained by this reaction where kaolinite is precipitated (Lynch et al., 1997):

$$2KAlSi_3O_{8(s)} + 2H^+{}_{(aq)} + 9H_2O_{(l)} \rightarrow Al_2Si_2O_5(OH)_{4(s)} + 2K^+{}_{(aq)} + 4H_4SiO_{4(aq)}$$

The dissolution of potassium feldspar may be due to acidic conditions created when CO_2 is generated while the rate of the reaction may be enhanced by the presence of organic acids (Harrison and Thyne, 1992). The above reaction is not dependent upon organic acids, only the rate of the reaction is affected by the presence of organic acids; the end point, whether organic acids are present or not, is the same (Harrison and Thyne, 1992). The lack of organic matter and subsequent acids in addition to the lack of a source of K^+ within bentonites may explain the slower illitization within some bentonites when compared to adjacent sedimentary rocks (Altaner, 1989; Dong et al., 2000).

This hypothesis was tested by Oelkers and Schott (1998) and they found that in mildly acidic to neutral environments aqueous aluminum-organic acid anion complexes increase the solubility of feldspars. Oelkers and Schott (1998) describe a three step process for the dissolution of alkali feldspars:

1) A relatively rapid exchange of hydrogen and alkali ions near the surface.
2) Three hydrogen atoms in solution reacting with one aluminum atom in the mineral structure, breaking the Al-O bonds, in conjunction with the rate controlling Si^{4+} rich precursor complexes.
3) Hydrolysis of Si-O bonds releasing the precursor complexes into solution.

Equilibrium is attained when the organic matter matures and the generation of CO_2 diminishes, potassium feldspar will continue hydrolysis increasing the solution pH back to neutral (Capuano, 1990).

1.3.3 Conversion of Smectite to Illite

The conversion of smectite to illite progresses as temperature and pressure increase and K^+ and Al^{3+} are added to the system (Altaner, 1989). The burial conditions necessary for the

conversion of smectite to illite are thought to occur over a narrow depth interval in the Gulf Coast whose temperature range is dependent upon the geothermal gradient (Ohr et al., 1991). While the formation of mixed layer illite/smectite occurs in a narrow range, mixed layer illite/smectite is more common than either end member, illite or smectite, in the sedimentary rock record (Moore and Reynolds, 1997).

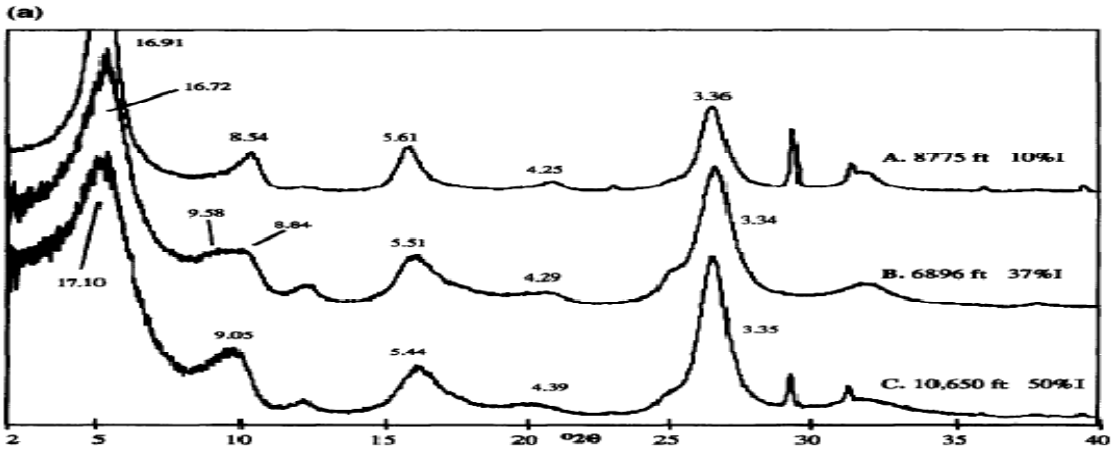

Figure 1.11a- X-ray diffraction patterns of illite/smectite with ordering of R=0 (from Lynch et al., 1997). Peaks positions are in Angstroms.

Classification of the resultant mixed layer illite/smectite begins with randomly ordered illite/smectite, where the percentage of illite layers in illite/smectite is <50% (SISSSIS…) and the stacking order is referred to as R=0 (Figure 1.11a) (Reynolds and Hower, 1970; Hower, 1981). "Short range" ordering occurs where illite/smectite composition is approximately 50% smectite to 50% illite (ISISISIS…) and is noted as R≥1(Figure 1.11b) (Hoffman and Hower, 1979; Meunier and Velde, 2004). "Long range" ordering ranges in composition from 50-95% illite (ISIIISI…) and is noted as R≥3 (Hoffman and Hower, 1979; Meunier and Velde, 2004). Historically, R≥1and R≥3 illite/smectite assemblages were referred to as allevardite type and Kalkberg type ordering, respectively (Hower and Mowatt, 1966; Hoffman and Hower, 1979).

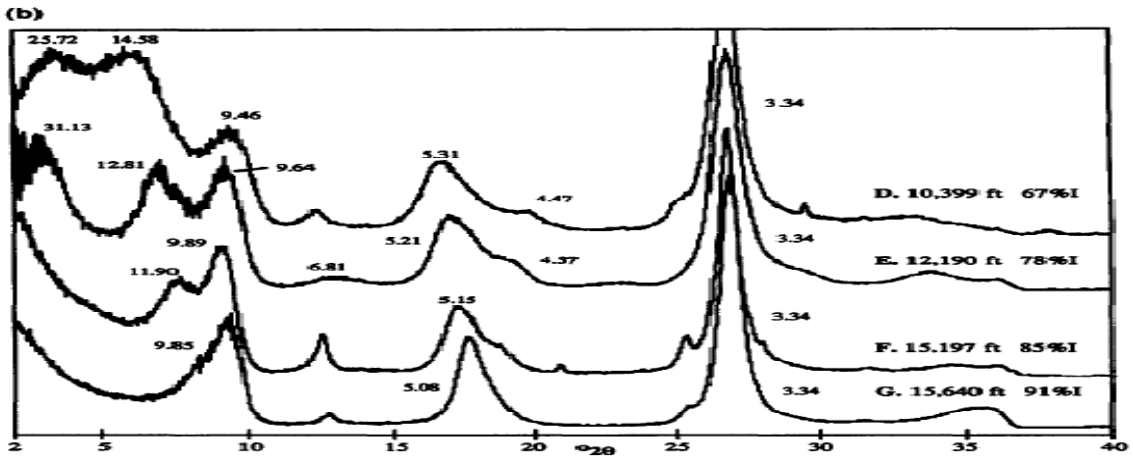

Figure 1.11b- X-ray diffraction patterns of illite/smectite with ordering of R>0 (from Lynch et al., 1997). Peaks positions are in Angstroms.

The study of how smectite converts to illite has yielded three potential mechanisms- 1) Solid-state transformation (SST), 2) Dissolution and crystallization (DC) and 3) Oswald ripening (OR). Researchers have yet to reach a consensus on a model because no model adequately describes all environments and reactions. Depending upon the geologic setting or which stage of the reaction one is studying, one model may be more applicable than the next (Altaner and Ylagan, 1997).

Solid-state transformation is characterized by the gradual replacement of smectite by illite in close topotactic contact (Altaner and Ylagan, 1997), and was first proposed by Hower et al. (1976) as a layer-to-layer conversion. Solid-state transformation is done by increasing the layer charge by the substitution of Al^{3+} for Si^{4+} in the tetrahedral layer (Nadeau and Bain, 1986). When K^{+} is incorporated in the interlayer, a ten angstrom illite layer is formed (Nadeau and Bain, 1986). Bell (1986) used transmission electron microscope (TEM) to observe the lateral solid-state transformation of smectite to illite.

Nadeau et al. (1984) proposed a dissolution and crystallization model where smectite under increased temperature and pressure became unstable and dissolved. Diagenetic illite is then precipitated; one layer upon the next, creating assemblages of illite of *n* layers (Nadeau et al. 1984). Whitney and Velde (1993) proposed a multi-step dissolution and crystallization model where smectite is dissolved and illite nucleates on a smectite particle followed by coalescence and growth of illite crystals. Nucleation on a preexisting particle (heterogeneous nucleation) is favored compared to new crystal growth (homogeneous nucleation) due to energy barriers of homogeneous nucleation (Altaner and Ylagan, 1997). Continuous chemical changes observed in the tetrahedral and octahedral layers combined with the oxygen isotopic composition of the minerals strongly supports the dissolution and crystallization model (Ahn and Peacor, 1986; Lynch et al., 1997). Ahn and Peacor (1986) proposed a dissolution and crystallization model where smectite particles dissolved and illite particles crystallized from an aqueous solution containing components of the parent smectite.

Eberl and Środoń (1988) and Inoue et al. (1988) found illitization to occur due to Oswald ripening. In order to minimize the interfacial free energy, the smallest crystals dissolved and reprecipitated onto larger crystals resulting in crystals with a core of progressively younger overgrowths (Eberl and Środoń, 1988; Inoue et al., 1988; Altaner and Ylagan, 1997). The smallest crystals have a higher free energy due to their higher solubility (Altaner and Ylagan, 1997). Altaner and Ylagan (1997) found that this model for illitization, due to its large chemical and mineralogical changes, is not a realistic explanation.

These models follow the first model proposed by Hower et al. (1976) showing the reaction for illitization where X represents various interlayer cations- Na^+, K^+, etc.:

$$\text{X-Smectite} + K^+ + Al^{3+} = \text{Illite} + Si^{4+} + H_2O$$

Quartz is produced from the substitution of Al^{3+} for Si^{4+} and water is expelled from the interlayer. During illitization the ratio of Si/Al decreases from ≥2.0 in smectite to ≤1.5 in illite, while the Si/Al ratio in muscovite is =1.0 (Figure 1.12a and 1.12b) (Charpentier et al., 2003). The amount of silica released during the illitization of illite/smectite, when Al^{3+} is substituted for Si^{4+}, is dependent on whether the smectite present is dioctahedral or trioctahedral (Peltonen et al., 2008). For every one mole of illite formed where Al was conserved 24.66 moles of Si^{4+} was released compared to a non Al-conserved illitization reaction where three moles of Si^{4+} were released for every one mole of illite formed (Elliott and Matisoff, 1996 and references there in).

a-

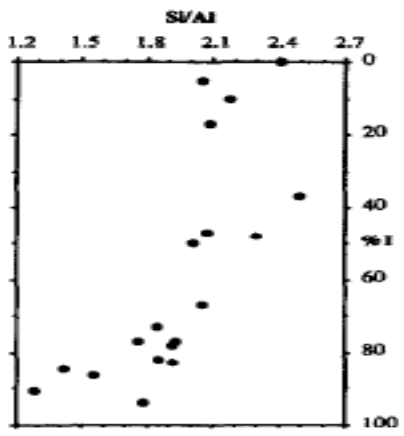

Figure 1.12a- The Si/Al versus the percentage of illite layers in mixed layer illite/smectite. The Si/Al ratio is decreasing during illitization of illite/smectite (from Lynch et al., 1997).

b-

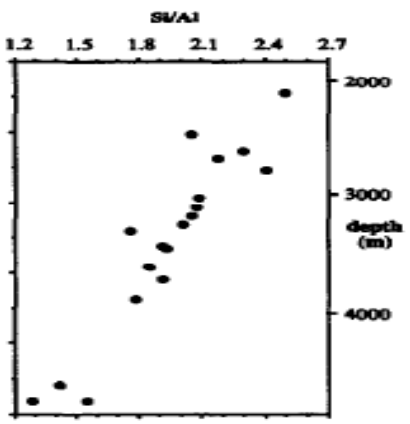

Figure 1.12b- The Si/Al vs. burial depth. The Si/Al ratio is decreasing with increasing burial depth (from Lynch et al., 1997).

The ^{40}K resides in the interlayer between illite crystals and as the ^{40}K ages it decays to ^{40}Ar, the resultant ratio of ^{40}K-^{40}Ar or ^{40}Ar -^{39}Ar can be used to determine an approximate age of heating (Pevear, 1999). In addition to the Si^{4+} and H_2O proposed to be released during illitization by Hower et al. (1976), Fe has also been found to be released during illitization which may later precipitate as magnetite (Boles and Franks, 1979; Elliott el al, 2006). The interaction

of these reactants and products with variables such as temperature and time help to describe the many processes occurring during illitization. The factors of time and temperature are believed to be independent where rocks exposed to high temperatures for short periods of time will display the same maturity as rocks exposed to low temperatures for long periods of time (Waples, 1980).

Smectite and illite are stable and coexist at low temperatures, <50°C, and high temperatures, >200°C; between these temperatures smectite converts to illite (Sass et al., 1987; Lynch et al., 1997). During hydrocarbon maturation organic matter begins to form hydrocarbons at ≈60°C and the degree of maturation is measured by vitrinite reflectance (VR_o) (North, 1985; Pevear, 1999). Randomly ordered illite begins to form at temperatures >50°C, corresponding with VR_o values <0.5% (Perry and Hower, 1970; Abid and Hesse, 2007). The transition from R=0 to R≥1 corresponded with VR_o values ranging from 0.5-0.66% (Abid and Hesse, 2007). Experiments by Sass et al. (1987) found illite and smectite experience a phase change between 90° and 110°C when the Gibbs free energy of illite and smectite decrease by approximately the same amount. The phase change may relate to a change in ordering from R=0 to R≥1 which was observed by Hower et al. (1976) at ≈100°C.

Illitization may occur over two stages, the increase in illite ordering from R=0 to R≥1 represents the first stage and the second stage occurs when R≥1 illite ordering increases to R≥3 (Saleemi and Ahmed, 2000). The first stage of the conversion of smectite to illite occurs when illite accounts for ≈20% of the mixed layer illite/smectite (Saleemi and Ahmed, 2000). This conversion occurs rapidly and is associated with an increase of ordering from R=0 to R≥1 (Figure 1.13) (Saleemi and Ahmed, 2000). Interestingly, the activation energy necessary for the dissolution of potassium feldspar is 68.8 KJ mol^{-1}, very similar to the activation energy for the conversion of R=0 ordering to R≥1 ordering of 69.7 KJ mol^{-1}, releasing K^+ into solution at the

height of illitization (Berger et al., 1997). Aplin et al. (2003) found the Gulf of Mexico mudstones they studied to almost completely convert from R=0 to R≥1 within a range of 10°C. Ramseyer and Boles (1986) found the transition from R=0 to R≥1 in the Tertiary sandstones and shales they studied, occurred between 120-140°C in Miocene rocks and 100-120°C in Oligocene rocks.

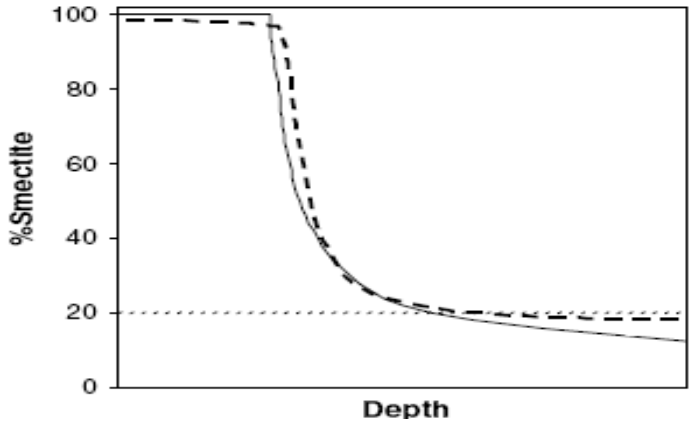

Figure 1.13- "Z" shaped curve where the conversion of smectite to illite ordering of R=0 to R≥1 occurs rapidly over a short burial interval. The second stage conversion of R≥1 to R≥3 ordering at ≈80% illite proceeds more slowly (from Cuadros, 2006).

The second stage represents when the R≥1 ordering develops to R≥3 ordering (Saleemi and Ahmed, 2000). Developing R≥3 ordering proceeds more slowly than the R=0 to R≥1 conversion and occurs at ≈175±5°C (Abid and Hesse, 2007). Sass et al. (1987) found smectite to represent <5% of layers present in mixed layer illite/smectite at temperatures ≈200°C. This may represent natural end-member illite due to divalent cations, i.e. Mg^{2+}, restricting the flow of pore fluids carrying dissolved cations thereby reducing the ability of Al^{3+} to substitute for Si^{4+} and preserving some smectitic sheets (Berger et al., 1997). Above 200°C smectite and illite may coexist if quartz solubility is stable, illitization may occur if silica is under-saturated in solution (Sass et al., 1987).

1.3.4 Summary

Hoffman and Hower (1979) found the conversion of smectite to illite to be an excellent semi-quantitative geothermometer up to temperatures approaching 300°C. How this reaction proceeds has been studied extensively and some of the findings have been presented here. Two important factors in the conversion of smectite to illite, time and temperature, are also the same important factors in the generation of hydrocarbons (Waples, 1980). The conversion of smectite to illite begins at ≈50°C and proceeds to ≈200°C (Hoffman and Hower, 1979; North, 1985; Sass et al., 1987). When organic material is heated, CO_2 and organic acids are produced creating an acidic environment which promotes the dissolution of potassium feldspar releasing K^+, an important interlayer cation (Oelkers and Schott, 1998). Smectite may convert to illite by three possible processes- solid state transformation of smectite to illite, when smectite becomes unstable, dissolves and illite crystallizes in its place or by three dimensional growth (Altaner and Ylagan, 1997).

The illite within the rock unit can be described in terms of polytype as well as crystallinity. Three illite polytypes have been identified- $1M_d$ and $1M$ are both the result of diagenesis with $2M_1$ polytypes the result of low grade metamorphism and present in sedimentary rocks due to weathering (Velde and Hower, 1963; Velde, 1980). Illite crystallinity may be described in progression from mixed layer illite/smectite to poorly crystallized illite to well crystallized illite as thermal maturity increases (Lanson et al., 1998).

Use of the conversion of smectite to illite as a geothermometer is complicated because the illite present in sandstones and shales may be detrital or diagenetic. Bentonites contain only diagenetic illite but may convert to illite at a slower rate than shales or sandstones. The conversion is further complicated because the amount of organic material and potassium feldspar

present act as limiting agents. Thanks to many studies on the conversion of smectite and illite and its variables the conversion of smectite to illite can be used as a geothermometer to recreate the thermal history and assess the thermal maturity of a rock unit (Pevear, 1999).

1.4 Stratigraphy and Tectonic History of Oklahoma

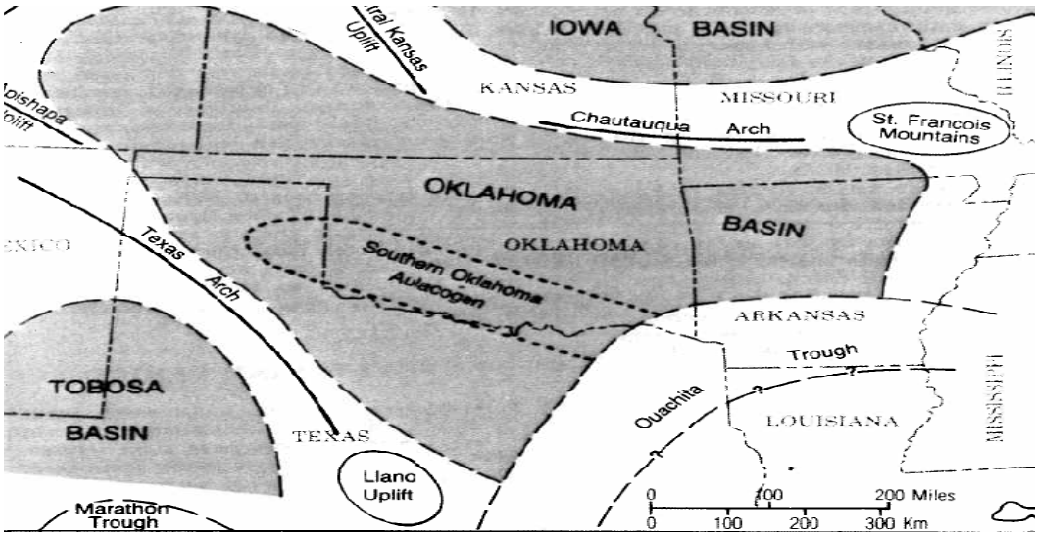

Figure 1.14- Map of the south-central United States with the approximate boundaries of the major tectonic/depositional features within Oklahoma. These features likely formed during Early and Middle Paleozoic time (from Northcutt et al. (2001) modified from Johnson et al., 1988).

Oklahoma's geology is very complex but well understood due in large part to the extensive drilling and seismic data collected in the pursuit of hydrocarbons (Johnson and Cardott, 1992). These data have led to the common interpretation of three distinct depositional structures within Oklahoma- the Oklahoma basin, Southern Oklahoma aulacogen and the Ouachita trough (Figure 1.14) (Johnson and Cardott, 1992; Northcutt et al., 2001). The Oklahoma basin represented a broad, shelf like area surrounding an area of increased deposition, known as the Southern Oklahoma aulacogen (Johnson and Cardott, 1992; Northcutt et al., 2001). The basin and aulacogen are bordered to the south/southeast by the Ouachita trough (Johnson and Cardott, 1992; Northcutt et al., 2001).

From Cambrian to Middle Mississippian periods, the Oklahoma basin and aulacogen were filled with southward-thickening strata dominated by shallow-water carbonates with interbedded shales and sandstones (Figure 1.15) (Johnson, 1989; Byrnes and Lawyer, 1999). These strata can be traced and correlated from the Oklahoma aulacogen out into the Oklahoma basin, demonstrating high lateral continuity from region to region (Johnson et al, 1988; Johnson and Cardott, 1992).

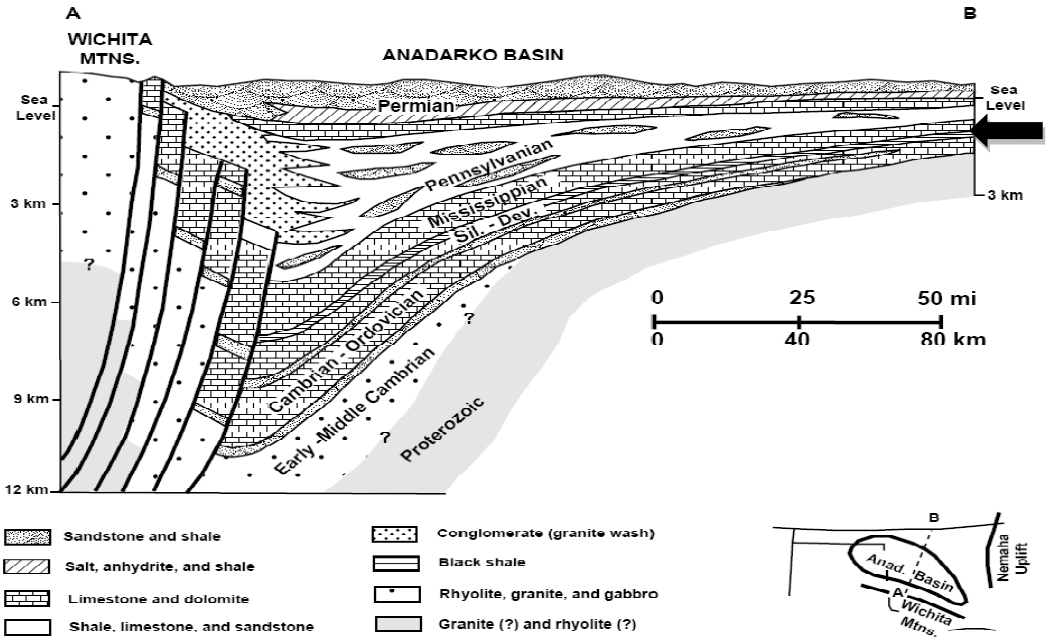

Figure 1.15- Simplified cross section of the Anadarko Basin within Oklahoma (from Johnson, 1989). The black arrow points to the Woodford Shale. A-B is perpendicular to the basin axis.

Due to the Ouachita-Marathon orogeny, the depositional regime within Oklahoma during Middle Mississippian, changed from shallow water carbonates to clastic sediment deposition (Burgess, 1976; Gallardo and Blackwell, 1999). This orogenic event transformed the Oklahoma basin and aulacogen into distinct foreland basins and areas of uplift, including the Anadarko, Ardmore and Marietta protobasins, the Arbuckle anticline and the Wichita Mountain uplift (Johnson and Cardott, 1992; Byrnes and Lawyer, 1999). The strata deposited within these

dissected basins are not laterally continuous but are specific to each basin while overlying strata deposited during Permian, Triassic and Holocene time are laterally continuous with variations in thickness and distribution (Johnson and Cardott, 1992).

1.4.1 Precambrian to Early Paleozoic

Basement rocks underlying Oklahoma range in age and type. The Precambrian basement rocks consist mainly of igneous rocks and some low-grade metasedimentary rocks that range in age from 1.3-1.6 Ga (Denison et al., 1984; Johnson, 1989). Early Cambrian and Middle Cambrian basement rocks consist of granites, rhyolites, gabbros, anorthosites and basalt, they were emplaced approximately 525-550 Ma (Johnson, 1989). These rocks were formed during the initial rifting associated with the formation of the Oklahoma aulacogen and include the Carlton Rhyolite Group and the emplacement of the Wichita Granite Group (Denison, 1982; Gilbert, 1983; Gallardo and Blackwell, 1999).

The Precambrian basement is unconformably overlain by the basal, transgressive Reagan Sandstone which grades up into bioclastic limestones and sandy dolomites of the Honey Creek Limestone (Johnson and Cardott, 1992). The Reagan Sandstone and the Honey Creek Limestone were deposited in open, shallow marine environments and together they comprise the Late Cambrian Timbered Hills Group (Johnson and Cardott, 1992). The overlying Late Cambrian/Early Ordovician Arbuckle Group was deposited almost continuously and consists of shallow-water marine limestones and secondary dolomites (Johnson, 1989). The dolomite likely formed from the diagenesis of carbonates deposited in alternating shallow-marine and supratidal environments (Johnson and Cardott, 1992). The Timbered Hills Group and the Arbuckle Group are >6,000 ft thick within the Oklahoma aulacogen and thin to ~2,000 ft thick in the Oklahoma basin (Johnson, 1989).

1.4.2 Early to Middle Paleozoic

Middle Ordovician to Early Mississippian strata is composed of mainly fossiliferous shallow-water carbonates interbedded with fine-grained to moderately coarse-grained siliciclastic sediments (Johnson et al., 1989). The clastic sediments were derived from the Mid-Continent region to the northeast and east of Oklahoma (Cardott and Lambert, 1985; Johnson et al., 1989).

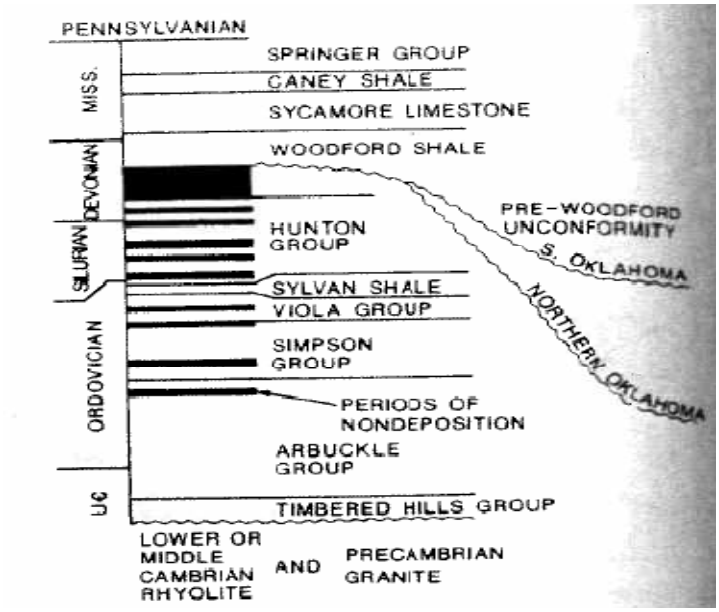

Figure 1.16- Generalized stratigraphic column from Pre-Cambrian basement through Mississippian time. Areas of black are non-deposition and the extent of the Woodford unconformity is shown (after Ham, 1969; Amsden, 1973; Ross and Bergstrom, 1982; from Kirkland et al., 1992).

The Early to Middle Paleozoic succession ranges in total thickness from 500 to 4,000 feet and from bottom to top consists of the Simpson Group overlain by the Viola Group, the Sylvan shale, the Hunton Group and then by the Woodford shale (Johnson, 1989). Many episodes of non-deposition occurred in Middle Paleozoic time (Figure 1.16) (Kirkland et al., 1992). Two periods of non-deposition are associated with two major epeirogenic uplifts: 1) pre-middle Early Devonian before deposition of the Frisco member of the Hunton Group and, 2) pre-Late Devonian before deposition of the Woodford shale (Johnson, 1989).

The Middle Ordovician Simpson Group consists of clean, washed quartzose sandstone interbedded with thick, shallow-water marine limestones with some greenish-gray shales interbedded (Johnson and Cardott, 1992). The shales are more abundant within the Oklahoma aulacogen than the basin and range in color from dark-green to bright-green to bluish-green (Johnson and Cardott, 1992). The Late Ordovician Viola Group is a highly fossiliferous marine-limestone with chert present at several stratigraphic levels (Johnson and Cardott, 1992). The Viola grades upward from limestone interbedded with organic and graptolitic shale to clean-washed skeletal limestone indicating a decrease in water depth and an increase in energy and aerobic levels (Johnson and Cardott, 1992). The overlying Late Ordovician Sylvan shale is a green to greenish-gray shale ranging in thickness from 300-400 ft in the aulacogen to 30-200 ft in the basin (Johnson and Cardott, 1992). The Hunton Group deposited from Late Ordovician to Early Devonian contains three members: 1) the Chimneyhill Subgroup which is mainly shallow-water, clean-washed skeletal limestones, 2) the Henryhouse and Haragan-Bois d'Arc Formations are argillaceous and silty carbonates, 3) the Frisco Formation consists of clean limestone and was deposited after one of the epeirogenic uplifts (Johnson, 1989; Johnson and Cardott, 1992). Immediately following the deposition of the Frisco Formation the second epeirogenic uplift halted deposition resulting in one of the most widespread unconformities in the Mid-Continent region (Johnson, 1989). Transgression followed the uplift and the Woodford shale was deposited upon the unconformity in euxinic seas (Johnson, 1989). The euxinic sea allowed organic matter to be preserved, creating a dark-gray to black fissile siliceous shale containing interbedded chert (Johnson, 1989; Johnson and Cardott, 1992; Roberts and Mitterer, 1992).

The euxinic seas present during the deposition of the Woodford shale (Late Devonian-Early Mississippian) were replaced by shallow, well oxygenated, marine waters during the

Early/Middle Mississippian possibly due to the closing of the Rheic Ocean (Figure, 4) (Johnson, 1989; Nance and Linnemann, 2008). The Mississippian strata, deposited in mostly recessive seas, consist mainly of fossiliferous limestones with some interbedded shales and siltstones with some chert present (Johnson, 1989; Jorgensen, 1989). Total thickness of Mississippian strata ranges from ~2,500 to 3,000 ft within the aulacogen decreasing to 1,000 to 2,000 ft within the basin and were (Johnson, 1989).

1.4.3 Late Paleozoic

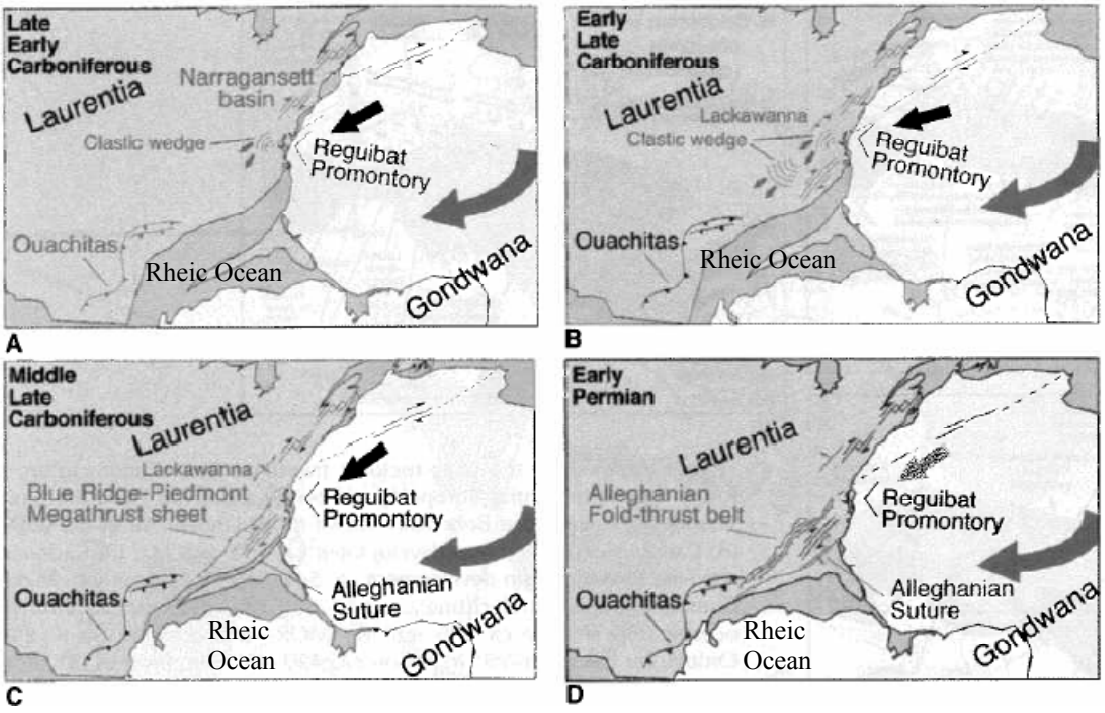

Figure 1.17- Oblique rotational collision between Laurentia and Gondwana. A) Initial contact during Late Mississippian. B) Clockwise rotation of Gondwana during Early Pennsylvanian. C) Continued rotation and southward movement of Gondwana during Late Pennsylvanian. D) Head-on collision of Gondwana and Laurentia during Early Permian (from Hatcher, 2002).

The Oklahoma region experienced significant change during Mississippian and Pennsylvanian time (Figure 1.17). The closure of the Rheic Ocean produced the Ouachita-Alleghanian-Variscan orogeny, the largest collisional orogeny of the Paleozoic, forming the

supercontinent Pangea (Nance and Linnemann, 2008). The Ouachita orogeny took place over several pulses during Early to Late Pennsylvanian time and was the result of Gondwana's Amazonian margin colliding with the southern margin of Laurentia (Gallardo and Blackwell, 1999; Nance and Linnemann, 2008). The Ouachita orogeny is distinctive in that evidence of metamorphism and magmatic activity are practically absent; with only subgreenschist facies found (Johnson, 1989; Nance and Linnemann, 2008).

The collision divided the Oklahoma basin and aulacogen, into a series of distinct uplifts and foreland basins including the Wichita, Criner, Arbuckle, Nemaha and Ozark uplifts and the down-warping of the Anadarko, Ardmore, Marietta, Arkoma and Hollis basins (Figure 1.18) (Johnson et al, 1988; Johnson, 1989).

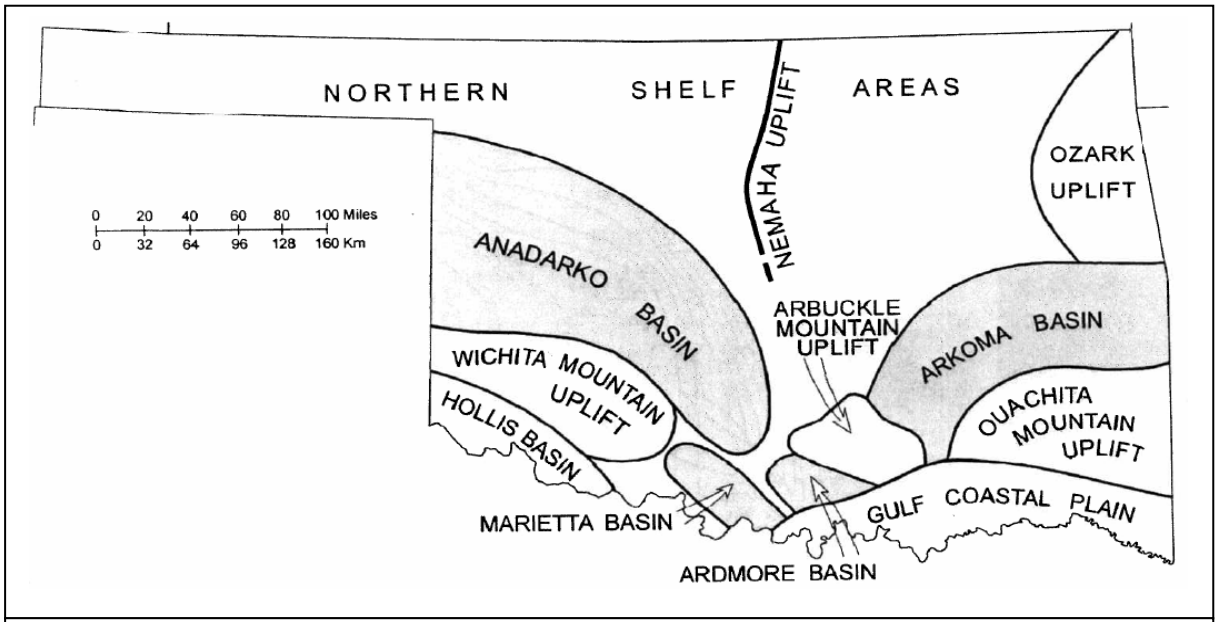

Figure 1.18- Overview of geologic provinces within Oklahoma (Cardott, 2007).

The subsidence and subsequent filling of these foreland basins, deeply buried the Early and Middle Paleozoic strata. For example, the Arbuckle Group within the Anadarko basin is believed to have been buried to a depth of ~2,500 ft to 9,000 ft, top to bottom at the end of

Ordovician time, subsiding to ~6,000 ft to 12,500 ft at the end of Mississippian, and ultimately subsiding to a depth of 26,000 ft to >30,000 ft at the end of Permian time (Johnson, 1989). Likewise, the Woodford shale was buried deeply in many of these basins, preserving its subsurface extent over much of Oklahoma (Roberts and Mitterer, 1992).

The Ouachitas are considered to be the result of foreland fold/thrust belts and represent the supracrustal toes of low-angle faults which rose progressively higher in stair-step fashion (Nance and Linnemann, 2008). Vertical displacement along the thrust faults within the Wichita Mountains, have been estimated to total 40,000 ft (Johnson, 1989). The Ouachitas appear to connect to the Marathon uplift under the Gulf Coastal plain connecting to the Appalachians under the Mississippi embayment to the east leading some to theorize that the Ouachitas may have formed synchronously to the Appalachians or formed as two separate orogenic events that occurred side by side (Flawn et al., 1961; Graham et al., 1975; Viele, 1982; Houseknecht and Mathews, 1985).

The closure of the Rheic Ocean changed the depositional environment from carbonate dominated to clastic dominated deposition filling the developing Anadarko, Ardmore and Arkoma foreland basins (Johnson and Cardott, 1992; Nance and Linnemann, 2008). Wedges of Pennsylvanian strata, 10,000-15,000 ft thick composed of marine and non-marine shale, sandstone, conglomerate and limestones were deposited within the aforementioned basins (Johnson and Cardott, 1992). These strata varied from basin to basin dependent upon their source and geologic history making a detailed description too lengthy for my purposes.

1.4.4 Permian to Holocene

The Ouachitas and Appalachian Mountains disrupted the sub-tropical winds during Early Permian time creating a severe rain shadow where Gondwana experienced a wet climate while

Laurasia experienced a dry and hot climate (Jorgensen, 1989). The dry and hot climate of Laurasia resulted in precipitation of evaporites over most of the central United States (Jorgensen, 1989). The flanks of the Ozark and Ouachita uplifts were the exception where severe erosion buried the uplifted blocks in their own debris and caused little relief to remain by the end of Early Permian time (Johnson, 1989; Jorgensen, 1989). This erosion exposed several outcrops of the Woodford shale within the Arbuckle-Ouachita region of Southern Oklahoma (Roberts and Mitterer, 1992).

Most Permian strata are limited to the western half of Oklahoma where the Wichita block of the Ouachitas provided clastic debris during Early Permian (Johnson, 1989). The resultant sandstones and shales were minor constituents of sediment which was dominated by evaporites and red beds, totaling up to 7,000 ft of strata deposited within the subsiding basins (Johnson and Cardott, 1992). The end of Permian time and the beginning of Triassic time marked an end to rapid sedimentation and a change from compressional to tensional forces over the region (Jorgensen, 1989; Lee and Deming, 1999).

Triassic and Jurassic strata were deposited in mixed fluvial, lacustrine and deltaic environments and consist mainly of red-bed shales and sandstones (Johnson and Cardott, 1992). These sediments have been eroded away and are limited to the panhandle of Oklahoma (Johnson and Cardott, 1992). Cretaceous shales, sandstones and limestones were deposited in southeast Oklahoma along the Gulf Coastal Plain as part of the Cretaceous seaway (Johnson and Cardott, 1992). The strata deposited within the seaway in southeast Oklahoma are 1,000-2,000 ft thick while the Cretaceous Gulf Coastal Plain deposits in western Oklahoma are 50-300 ft thick (Johnson and Cardott, 1992). During the uplift of the Rocky Mountains, much of Oklahoma was synchronously uplifted and subsequently eroded, removing most post-Permian strata (Wang and

Philp, 1997). Tertiary strata consist of fluvial and windblown sediments of the Ogallala Formation (Johnson and Cardott, 1992). The fluvial sediments of the Ogallala formation were deposited by low-gradient streams flowing form the Rocky Mountains to the west and range in thickness from 10-50 ft, but can be 100 ft thick next to major rivers (Johnson and Cardott, 1992).

1.5 Characteristics of the Woodford Shale

1.5.1 Deposition and Timing

The Woodford shale was deposited synchronously with the Chattanooga, New Albany, Ohio, Millboro, Bucket, Geneseo and Antrim shales (Figure 1.19) (Conant and Swanson, 1961; Ham and Wilson, 1967; Cardott and Lambert, 1985; Cardott, 2007). Deposition occurred during Late Devonian (Frasnian) to Early Mississippian (Tournaisian) time and marks a transition from the primarily carbonate sediments of Early to Middle Paleozoic to the clastic sediments of Late Paleozoic (Cardott and Lambert, 1985; Hester et al., 1992).

Conodonts found within the Woodford shale provide the basis for determining the depositional age (Kirkland et al., 1992). The oldest conodonts found are from the early Late Devonian period (Kirkland et al., 1992). The youngest conodonts, of Early Mississippian age, are found in the top 1-8 ft of the Woodford shale (Kirkland et al., 1992). Commonly the beginning of the earliest Mississippian stage (Tournaisian) is placed at the top of the Woodford because it is an easily recognizable rock/stratigraphic boundary representing both a paleotectonic change and a time-stratigraphic boundary (Northcutt et al., 2001).

The Woodford shale lithofacies indicates deposition occurred under a chemically reducing environment in quiet seas promoting the preservation of organic matter (Connant and Swanson, 1961; Kirkland et al., 1992). The ratio of organic sulfur to organic carbon is =0.02, and this value is consistent with source rocks deposited in marine environments (Lewan and

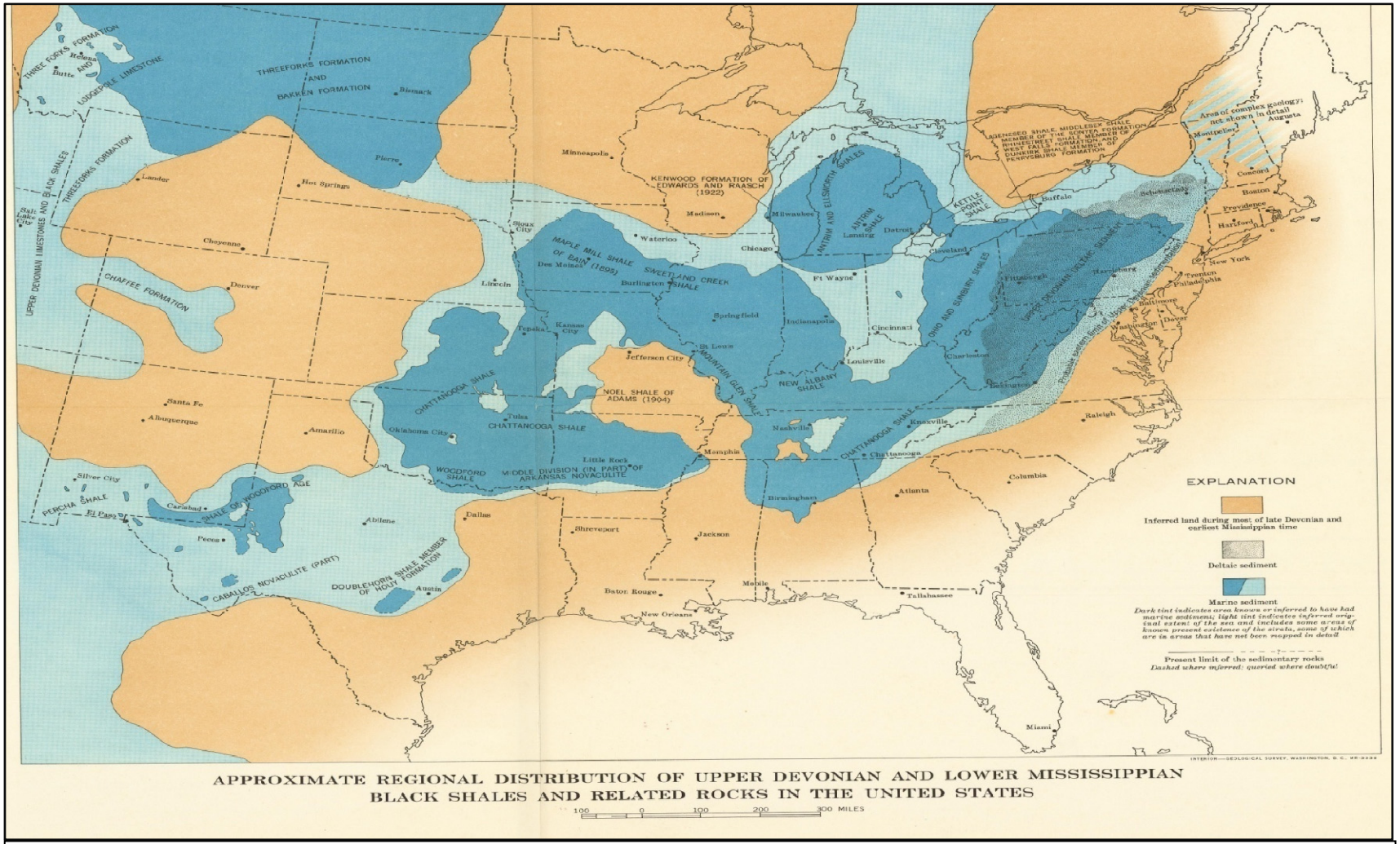

Figure 1.19- Distribution of Late Devonian and Early Mississippian shales across America (from Conant and Swanson, 1961).

Ruble, 2002). World wide sea levels had just reached a peak during early-Late Devonian time and began a long-term gradual sea-level decline lasting into Late Mississippian (Haq and Schutter, 2008).

The euxinic, shallow epicontinental sea was likely the result of thermal stratification and stretched from New York to North Dakota and south to Mexico (Kirkland et al., 1992; Wang and Philp, 1997). Kirkland et al. (1992) suggest two factors which may have allowed oxygen poor waters to persist: 1) thermal stratification within the sea may have prevented oxygen rich saline waters from moving downward, or 2) The relative shallowness of the sea, <200 ft, prevented oxygen rich saline waters from the open ocean from entering the sea and moving laterally beneath the thermocline. Comer (2008) supports the idea of stratification but attributes the stratification to local net evaporation resulting in hypersaline brine. The hypersaline brine restricted vertical circulation due to density stratification (Comer, 2008)

Deposition of the Woodford shale occurred on top of a regional unconformity on the Hunton Group extending locally into the Ordovician age Sylvan shale and Viola Group (Wang and Philp, 1997; Byrnes and Lawyer 1999). The previously mentioned epeirogenic uplift created the regional unconformity by halting deposition and the transgressive sea eroding the Hunton Group, Sylvan shale and Viola Group (Amsden, 1975; Kirkland et al., 1992; Johnson, 1992; Wang and Philp, 1997). The products of this erosion were incorporated into a basal sandstone member of the Woodford shale known as the Misener sandstone consisting of quartzose sand, phosphate and a limestone pebble conglomerate (Amsden, 1975; Kirkland et al., 1992; Wang and Philp, 1997; Over, 1990).

The average thickness of the Woodford shale is 200 ft but can range from near zero to ~125 ft in northern Oklahoma to >700 ft in the deep Anadarko basin (Amsden, 1975; Kirkland et

al., 1992; Wang and Philp, 1997). Local variations in thickness may be attributed to an irregular depositional surface due to the regional unconformity (Sullivan, 1985). Kirkland et al. (1992) studied an outcrop of the Woodford shale in the Arbuckle Mountains totaling 365 ft. They determined a rate of deposition of ~0.01 mm/year over ~15 million years (or 10 Bubnoffs[3]) would result in the deposition of 365 ft. of Woodford shale. Roberts and Mitterer (1992) estimated depositional rates based on couplets of shale and chert. Based upon a depositional time span of approximately 10-15 Ma the average couplet of 6.7 cm would have accumulated over 7.4-11.0 Ka or at a rate of 6-9 Bubnoffs (Roberts and Mitterer, 1992). Megacycles of two to ten couplets have a frequency of 15-21 Ka and 90-125 Ka respectively (Roberts and Mitterer, 1992). These very slow rates match estimates based on petrography (Kirkland et al., 1992).

1.5.2 Mineralogy

The Woodford shale is characterized by rhythmically interbedded shale and chert (Figure 1.20) with both facies displaying dark-gray to black coloration, high concentrations of carbon, silica and radioactive nuclides providing gamma-ray intensity readings greater than 160 API (Cardott and Lambert, 1985; Roberts and Mitterer, 1992). Lewan (1983) described the Woodford shale as a very fine-grained rock classifying it as a quartzose claystone. The Woodford shale varies in composition; quartz is the most abundant mineral with minor amounts of calcite, dolomite, illite, kaolinite, pyrite present and trace amounts of potassium feldspar and apatite (Lewan, 1983; Kirkland et al., 1992; Cardott, 2007). Quartz was found to compose 29-96 wt% with dolomite composing greater than 50 wt% of some samples (Kirkland et al., 1992). The clay-content of the Woodford shale is low, with none of the 10 samples analyzed by Kirkland et al. (1992) containing greater than 50 wt% of clay (illite plus kaolinite).

---

[3] 1 Bubnoff (B) is defined as 1 μm/year = 1 mm/ thousand years = 1 m/million years. Fischer (1969) proposed the Bubnoff in order to standardize the many ways used to express the rates of geologic processes.

Quartz can be derived from detrital sources or from siliceous microorganisms such as radiolarians (Kirkland et al., 1992). Grains of quartz are more common on the northwestern shelf and the northwestern part of the Anadarko basin, areas closer to detrital sources (Comer, 2008). Biogenic quartz, represented by chert, increases the further from land deposition occurred (Comer, 2008). The presence of microfossils in the chert, some of which are well preserved displaying delicate spines and a lacy wall-structure, suggests a primary origin for the cherts rather than being a result of diagenesis (Kirkland et al., 1992; Roberts and Mitterer, 1992). Lenses of microcrystalline quartz and fibrous chalcedony are interpreted to be the crushed remains of radiolarian tests (Kirkland et al., 1992).

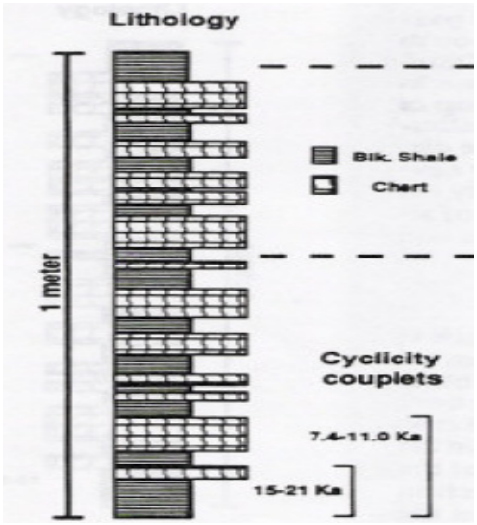

Figure 1.20- Interbedded black shale and chert over a 1-m section in the Woodford shale. This section is from an outcrop on the southern flank of the Arbuckle Mountains. Cyclicity couplets are shown at the bottom (from Roberts and Mitterer, 1992).

The total amount of quartz from silt, preserved radiolarian tests and quartz lenses when combined does not equal the amount of quartz indicated by X-ray diffraction (Kirkland et al., 1992). Dissolution of biogenic opal forming cryptocrystalline quartz cement likely makes up the balance (Kirkland et al., 1992).

1.5.3 Organic Matter

Organic matter found in the Woodford shale is classified into two types based on solubility in organic solvents (Cardott, 1989). Kerogen is organic matter that is insoluble in organic solvents while bitumen is organic matter that is soluble in organic solvents and results from thermal maturation of kerogen (Cardott, 1989). Four types of kerogen have been defined: type I is sourced from lacustrine algae (i.e. *Botryococus*) and marine algae (i.e. *Tasmanites*); type II is sourced from marine phytoplankton, zooplankton and various other microorganisms including bacteria and terrestrial herbaceous organic matter; type III is sourced from woody tissues of terrestrial plants (stems, bark, roots and leaves of vascular plants); type IV is oxidized, reworked organic matter or high-gray vitrinite (Cardott, 1989).

The Woodford shale is unique in Southern Oklahoma in that it is the oldest rock that contains vitrinite (Ham et al., 1973; Cardott and Lambert, 1985). Lewan (1983) found amorphous type-II kerogen to represent greater than 90% of vitrinite within the Woodford shale, structured type-III and palyniferous type-I kerogen represented the remaining kerogen. The type III vitrinite was derived from the woody tissues of plants which first successfully colonized land during Devonian time (Sullivan, 1985; Cardott, 1989).

The chief source of organic matter for the Woodford shale was fecal pellets from zooplankton (Kirkland et al., 1992). Kirkland et al. (1992) proposed three factors that led to the preservation of the organic matter- 1) the small particle size of the clay and radiolarian tests helped preserve organic matter. These small particles increased tortuosity thereby decreasing the ability of sulfate anions to diffuse through the sediment. Clay particles also sorbed organic matter. 2) Anoxic waters helped preserve organic matter. Metazoans which feed on organic matter on the sea floor cannot live in oxygen poor water. These microbes not only feed on

organic matter but also stir up the seabed further exposing the organic matter to oxygen and microbes. 3) Under anoxic conditions part of the organic matter cannot be metabolized by bacteria. These large organic molecules are stable and act as "trellis-work" for smaller hydrogen rich molecules. These molecules are bound to each other by condensation reactions becoming resistant to anaerobic oxidation.

The total organic content of the Woodford shale ranges from 0.3 to 25 wt%, with many measured values greater than 1.0 wt% (Cardott and Lambert, 1985; Kirkland et al., 1992). The organic content of the rhythmically interbedded shales and cherts of the Woodford shale are not uniform, chert displays lower organic content than the shales (Roberts and Mitterer, 1992). The lower organic content of the chert is most likely the result of deposition occurring over a relatively short period of time during which production of silica was high resulting in organic carbon-rich siliceous oozes (Roberts and Mitterer, 1992). Comparatively, the organic carbon-rich shale was deposited over longer time intervals during lower production of silica oozes resulting in higher concentrations of organic carbon within the shales (Roberts and Mitterer, 1992). The chert may have accumulated at a rate 2.5 times faster than a comparable section of shale (Roberts and Mitterer, 1992).

1.5.4 Thermal Maturity

The vitrinite found in the Woodford shale may be used to assess the thermal maturity and the lack of older sources of vitrinite which may contribute recycled or high-gray type IV vitrinite, allow greater confidence in measured VR_o (Cardott and Lambert, 1985; Cardott, 1989). Studies measuring the thermal maturity of the Woodford shale found thermal maturity corresponded to orogenic belts and stratigraphic age (Figure 1.21) (Houseknecht and Mathews, 1985; Comer, 2005). Areas displaying the highest maturity or VR_o occurred in deep basins and

orogenic belts, i.e. greater than 2.0% in the Anadarko Basin, while structural highs displayed the lowest maturity, i.e. less than 0.5% on the northeastern shelf (Hester and Schmoker, 1993; Comer, 2005). The Ouachitas found in Oklahoma, display increasing thermal maturity with increasing stratigraphic age (Houseknecht and Mathews, 1985). Comparison of older strata on upthrown faultblocks to younger strata on downthrown faultblocks shows that the older strata are more thermally mature (Houseknecht and Mathews, 1985).

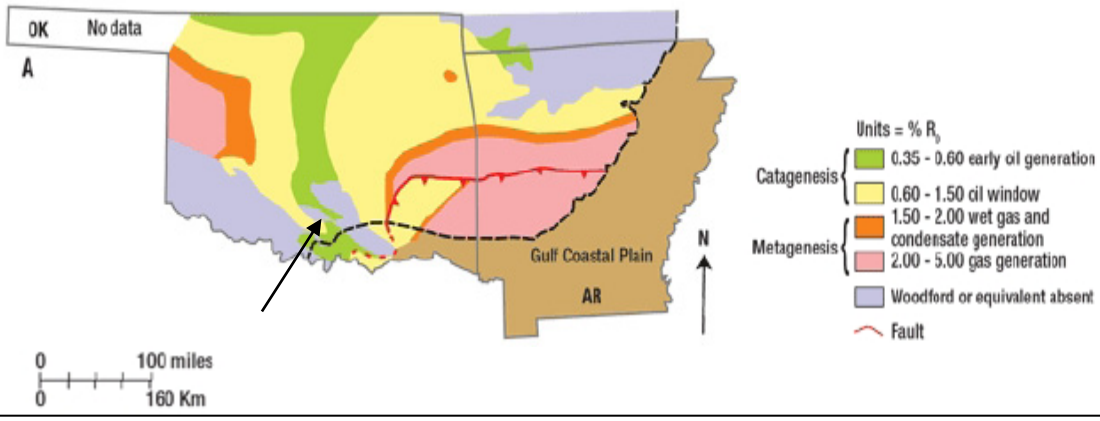

Figure 1.21- Map of thermal maturity, based on VR_o, of the Woodford Shale and age equivalents across Oklahoma and Arkansas (from Comer, 2008). Arrow points to approximate sample locations.

Lewan (1985) found VR_o values within the Woodford shale to likely be suppressed. Suppression of VR_o occurs when the maturation state of hydrogen-rich kerogen is lower than would be expected of other kerogen (Lee and Deming, 1999). VR_o values <2.0% exhibit the greatest degree of suppression and suppression increases when thermal maturation occurs under relatively high concentrations of hydrogen (Lo, 1993; Lee and Deming, 1999).

1.5.5 The Three Members of the Woodford Shale

The Woodford shale has been shown to vary vertically and can show distinctive variations when analyzed with gamma ray, formation-density and resistivity logs (Hester and

Schmoker, 1993). Hester et al. (1988) described three members, referred to as the Upper, Middle and Lower Woodford shale, which can be correlated across Oklahoma.

The upper and lower Woodford shale display similar log signatures while the middle Woodford shale is less dense, more radioactive and generally more resistive (Figure 1.22) (Hester and Schmoker, 1993). The Middle Woodford shale displays different log signatures because of a higher average total organic carbon than the Lower or Upper, 5.5 wt% vs. 2.7 and 3.2 wt% respectively (Hester et al., 1990; Hester and Schmoker, 1993).

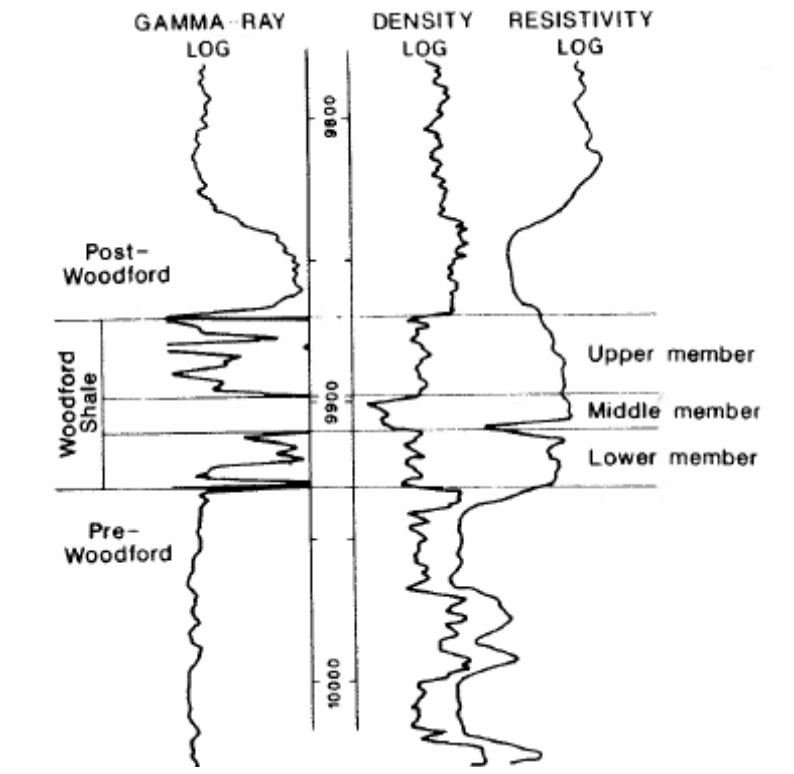

Figure 1.22- Results from logs showing characteristic log signatures of Upper, Middle and Lower Woodford (from Hester et al., 1992).

Microfossils may also be used to differentiate the three members. Using the presence of spores, *Hystrichospaerid* and the distribution of *Tasmanites*, Urban (1960) was able to divide the Woodford shale into three members (Table 1.1). The Lower Woodford was characterized by the

presence of spore tetrads which may indicate a depositional environment relatively close to shore (Urban, 1960). The Middle Woodford was found to have little to no *Hystrichosphaerids* present with *Tasmanites* dominating the microfossil record during this time (Urban, 1960). Urban (1960) suggests this may indicate a more marine depositional environment relative to the Lower and Upper Woodford members. Spores and *Hystrichosphaerids* reappear in the Upper Woodford and suggest the depositional environment had returned to a near-shore environment (Urban, 1960).

Table 1.1- Abundance and distribution of Palynomorphs found in the Buckhorn Creek section of the Woodford Shale (modified from Urban, 1960).

	Tasmanites	Leisphaeridia	Hystrichospaerid
Upper Zone	few present	diameters of 30 to 50 microns w/ maximum diameter of 80 microns	large number and variety present
Middle Zone	large number and variety present	diameters average between 70 and 100 microns	little or none reported
Lower Zone	very few present	diameters range between 40 and 70 microns	small number present

A positive paleotopographic feature divided Oklahoma into two depocenters, the southwest and northeast (Figure 1.23) (Hester et al., 1992). The feature represented a hinge line separating the two depocenters due to regional basement flexure and subsidence (Hester et al., 1992). The three members of the Woodford shale thicken to the southwest from the feature due to either the subsidence of the Oklahoma aulacogen or the compaction of older Paleozoic sediment (Schmoker and Gautier, 1989; Hester et al., 1992). The Lower and Middle Woodford

shale deposited in the northeastern depocenter show near uniform thickness due to deposition on a stable shelf while the Upper Woodford shale thickens to the north due to down-warping (Hester et al., 1992). The Lower and Middle Woodford shale dominate the thickness of the southwestern depocenter due to the flexure or subsidence of the Oklahoma aulacogen while down-warping caused the Upper Woodford shale to dominate the thickness of the northeastern depocenter (Hester et al., 1992).

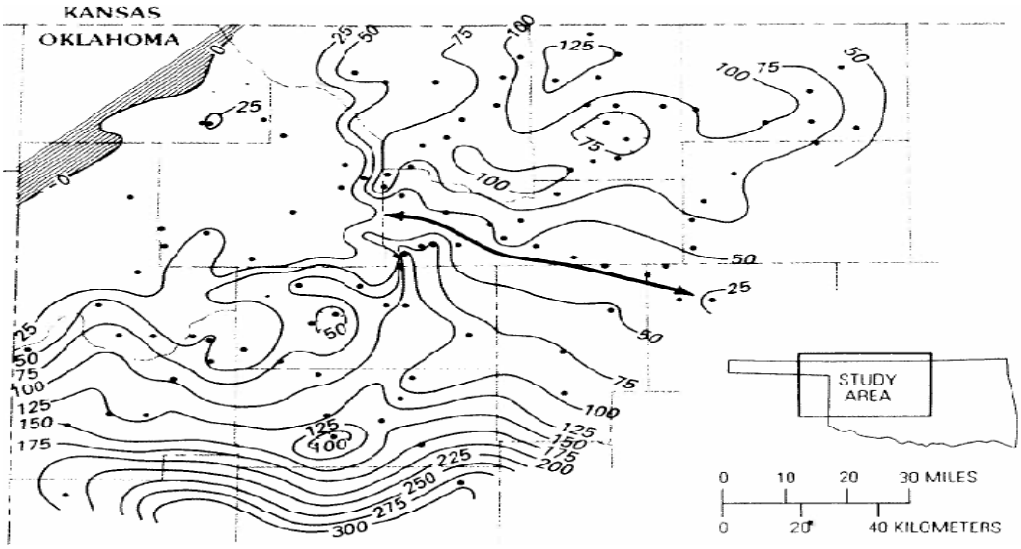

Figure 1.23- Isopach map of the Woodford shale. Contours showing the thickness with 25 ft. intervals. Dark line represents the positive topographic feature dividing the northeast and southwest depocenters due to regional basement flexure and subsidence (from Hester et al., 1992).

1.5.6 Summary

The Woodford shale was deposited during Late Devonian to Early Mississippian time based upon studies of conodonts. Deposition within the Oklahoma basin and aulacogen occurred upon a regional unconformity. An euxinic sea stretching across most of North America promoted the preservation of type-II kerogen sourced from fecal pellets of zooplankton. Three members can be identified within the Woodford shale due to changes in depositional

environments. These members can be identified by differences in gamma ray, formation-density and resistivity logs, total organic content and the microfossils present.

Cycles of alternating shale and chert form the Woodford shale, both exhibit the same black to blackish-brown coloration and high carbon content. Quartz is the main mineral found in the Woodford with calcite, dolomite, illite, kaolinite and others also present. Quartz can be sourced from radiolarian tests, some of which have been preserved while others have been compacted forming lenses of microcrystalline quartz. Additional silica may be sourced from biogenic dissolution of opal which releases quartz forming cryptocrystalline quartz cement.

During Pennsylvanian time the Ouachita orogeny transformed the Oklahoma aulacogen and basin by uplifting blocks and isolating basins. These basins were filled by sediment sourced from the uplifted blocks. Rocks within the basins and those that composed the adjacent structural highs experienced the greatest thermal maturity. Areas such as the northeastern shelf, unaffected by the Ouachita orogeny display low thermal maturity. By Permian time erosion had resulted in almost the complete loss of topography across Oklahoma. Since this time the geology of Oklahoma has been relatively unchanged.

CHAPTER 2- METHODS

2.1 Samples

Dr. Elmore and students collected samples for paleo-magnetic study from surface outcrops of the Woodford shale along the southern and northern flanks of the Arbuckle Mountains (Figure 2.1 and Table 2.1). Five of these samples were studied to determine the clay mineralogy and compared for this thesis. These five samples were collected from 3 outcrops. The Hass A samples, identified as QE, QW, CN and CS, are from a single location with 2 outcrops of the Woodford shale present. The other outcrop is located within the Lake Classen Spillway and the sample is identified as LC.

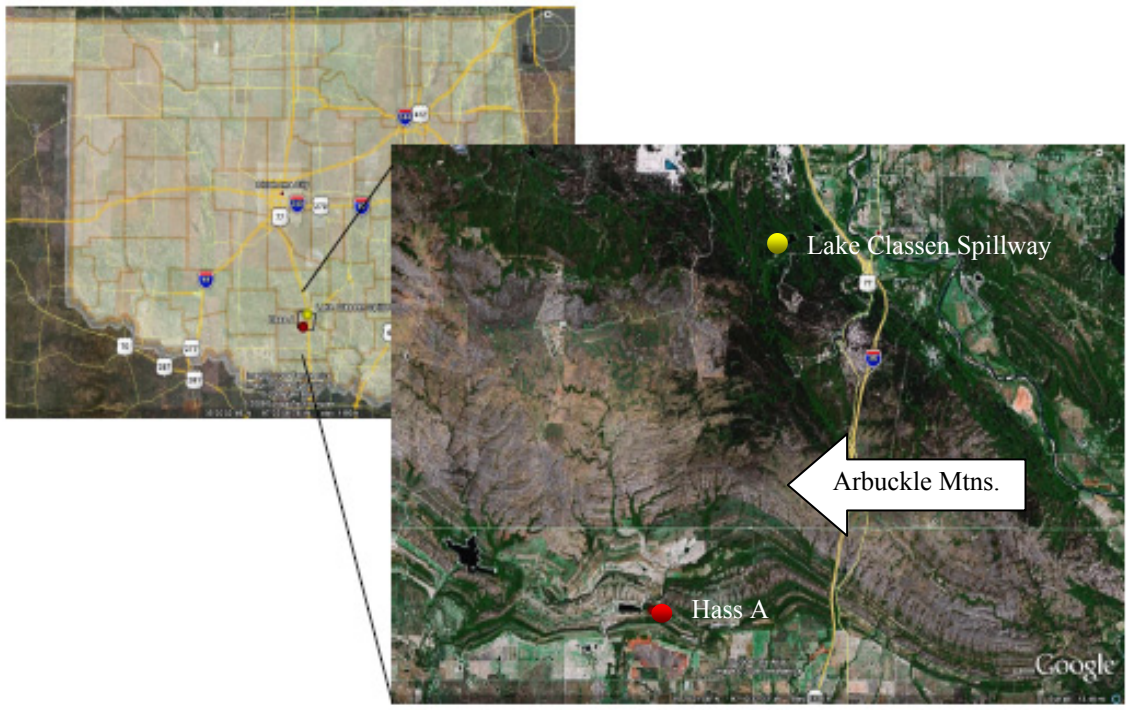

Figure 2.1: Locations of the samples. Locations of Lake Classen Spillway samples are represented by the yellow and the Hass A samples by the red points. The samples are separated by the Arbuckle Mountains. Locations provided by Dr. Elmore. Images from Google Earth, 1/19/09.

Table 2.1- Summary of sample information.

Sample	Location	County	Stratigraphic Location	Latitude	Longitude
QE	Hass A (AKA-Henry House Creek)	Carter	Middle to Upper	N 34° 21'	W 97° 13'
QW	Hass A (AKA-Henry House Creek)	Carter	Middle to Upper	N 34° 21'	W 97° 13'
CS	Hass A (AKA-Henry House Creek)	Carter	Middle to Upper	N 34° 21'	W 97° 13'
CN	Hass A (AKA-Henry House Creek)	Carter	Middle to Upper	N 34° 21'	W 97° 13'
LC	Lake Classen Spillway	Murray	Lower to Middle	N 34° 27' 30"	W 97° 10'

Samples arrived as chips and pieces of paleo-magnetic cores in labeled bags. Each sample underwent several treatments and was separated into different size fractions in order to determine the clay mineralogy by XRD as discussed in the following sections.

2.2 Preparation of Sample and Size Separation

Approximately 30 grams of each sample were separated, weighed and placed in de-ionized water to soak for a week. Using a mortar and pestle, the core chips and pieces were gently broken and disaggregated. Special care was taken not to overly reduce the samples, breaking the detrital illite into smaller fractions making future dating and analysis less accurate. Crushing of approximately 20 grams of each sample yielded what appeared to be a sufficient clay fraction. The remaining ten grams of sample were returned to soak in de-ionized water. A slide was prepared from the silt and clay fractions of each sample in order to determine the preliminary mineralogy. Preliminary XRD patterns displayed an abundance of quartz and dolomite with no discernable phyllosilicates present (Appendix A).

After disaggregation the samples were allowed to settle; excess water was removed and replaced with approximately 125 mL of 1 M sodium acetate-acetic acid buffer (NaAc-HAC buffer, pH=4.5). The samples were then placed in a water bath set at 50°C and allowed to react overnight. The supernatant of samples CS and LC were clear while samples CN, QW and QE had an orange hue to variable extents, with CN being the lightest orange hue and QE the strongest orange hue. The presence of ferroan dolomite may explain the hue or supernatant coloration. The supernatant was siphoned off and 100 mL of 1 M NaAc-HAC buffer, pH=4.5, was added to each sample. Each sample was returned to the warm water bath set at 50°C for one more night.

Organics were the second cementing material to be removed. The samples were divided in half and placed in centrifuge bottles. Samples were washed in approximately 10 mL of 1 M NaAc-HAC buffer to saturate exchangeable surfaces again with Na and to promote flocculation. Then the buffer and water solution were removed and 10 mL H_2O_2 was added and mixed into the samples. The samples were allowed to react for 30 minutes at room temperature. Following the first 30 minutes another 10 ml of 30% H_2O_2 was added for a total of 20 mL and the reaction was allowed to proceed for another 30 minutes. Next the samples were placed in a water bath set at 50°C where the reaction was monitored over the course of four hours.

The removal of both coatings of and crystalline iron oxides constitutes the third treatment. The removal of these iron oxides and cementing phases promote the parallel orientation of aluminosilicates as they dry on the slides and also increase the basal diffraction intensity for X-ray diffraction scans (Jackson, 1985). The samples that were divided for the removal of organics were washed with approximately ten mL of 1 M NaAc-HAC buffer to aid in flocculation, placed in the centrifuge and spun to speed the flocculation of the sample (1300 rpm

for 8 minutes), followed by the removal of the supernatant. Due to the labor intensive nature of the citrate-bicarbonate-dithionate (CBD) treatment used to remove both Fe-oxide coatings and crystalline Fe-oxides, only two samples were treated at a time (Jackson, 1985). The CBD treatment as follows is from Jackson (1985). Forty mL of Na-Citrate, used as a chelating or complexing agent for Fe^{2+} and Fe^{3+}, and five mL of bi-Carbonate (pH 7.3), used as a buffer, were placed in each centrifuge bottle, then each bottle was transferred to a water bath set at 50°C. One gram of sodium hydrosulfite, used for the reduction, was added to a sample and stirred constantly for one minute followed by four minutes of rest. This was repeated twice more for a total of three grams of sodium hydrosulfite.

With treatments finished, the samples were ready to be separated into different size fractions following Jackson's (1985) procedure (Table 2.2). Separating the samples into three fractions for silt and clay is done based upon the abundance and importance of these fractions (Jackson, 1985). These fractions represent simple mixtures which will provide as few diffraction peaks as possible when analyzed with X-ray diffraction easing mineral identification (Jackson, 1985).

Table 2.2- Designated size fractions and settling times.

Fraction	Size (μm)*	Settling Time/cm of water	Time of Centrifugation @ 900 rpm for sample height of 1 cm
Sand	> 50	4 sec/ 1 cm	
Coarse Silt	20 - 50	25 sec/ 1 cm	
Medium Silt	5 - 20	400 sec/ 1 cm	
Fine Silt	2 - 5	42 min/1 cm	
Coarse Clay	1 - 2		13 min/ 1 cm of sample
Medium Clay	0.25 - 1		211 min/ 1 cm of sample
Fine Clay	<0.25		

* Size corresponds to equivalent spherical diameter

Separation of clay fractions >2 μm were done utilizing Stokes' settling velocity. Jackson (1985) defines the variables within Stokes' Law- D is the particle diameter in centimeters, v is the settling velocity measured in cm/sec, and n is the viscosity in poises, the differential in specific gravity (mineral solid versus liquid) is represented by $\Delta s = s_p - s_l$, and g is the gravitational constant (980 cm/sec^2),

$$v = \frac{g(s_p - s_l)D^2}{18n}$$

Because v = h/t, where h is the height of the water in cm and t is the time in seconds, therefore,

$$t = \frac{18nh}{g(s_p - s_l)D^2}$$

The samples were transferred from the centrifuge bottles where the previous treatments were performed to beakers. Five mL of dilute (5%) sodium metaphosphate was added to aid in suspension. The height of the water was noted, then the sample was stirred vigorously, suspending all sediment and then the sample was allowed to settle at a rate of four seconds per one centimeter of water to remove the sand fraction. After the calculated amount of time had elapsed the natant was decanted and more de-ionized water was added. This procedure was repeated at least three times to ensure satisfactory separation. The settled sediment was then marked as "Sand >50 μm" and stored.

This procedure is repeated for coarse, medium and fine silt with settling rates of 25 seconds, 400 seconds and 42 minutes per one centimeter of water, respectively. The first settling time for the separation of the fine silt fraction from the clay fraction was extended by one and a half, to ensure no silt was added to the clay fraction during decantation.

The separation of the clay fraction into coarse, medium and fine clays was done by centrifugation necessitating the transfer of the samples from the one liter beakers, where previous

separations were done, to centrifuge bottles. Approximately ten mL of $CaCl_2$ was added to each beaker to flocculate the clay and the resultant supernatant was siphoned off. The samples were then transferred from their respective beakers to centrifuge bottles. The samples were spun to remove the clay from suspension and then washed with de-ionized water until the clay began to re-suspend thus indicating the removal of the $CaCl_2$. The sediment level was measured and noted followed by the addition of de-ionized water to a height of ten centimeters. The clay was then re-suspended by stirring with a plastic rod. Centrifugation time was calculated using the following equation provided by Jackson (1985):

$$t_{(minutes)} = \frac{\left[63.0 \times 10^8 \, \eta \, \log_{10}\left(\frac{R}{S}\right)\right]}{\left[(N_m)^2 \left(D_{\mu m}\right)^2 (\Delta s)\right]}$$

R is the radius in cm to the top of the sediment in the centrifuge tube, S is the height of the water in the centrifuge bottle (a constant ten cm), η is the viscosity in poises, N_m is the rotation rate in RPS, and Δs is the difference in specific gravity between the solvated particle and the suspension liquid. The procedure was repeated three times for each size fraction to ensure a sufficiently separated sample. The accumulated size fraction was then transferred to a plastic Nalgene® bottle with a minimal amount of water so that the sample was not unduly diluted.

Samples were allowed to settle within the bottles and excess water was removed leaving approximately ten mL of water thereby concentrating the samples. Oriented slides were created for the fine silt fraction and each clay fraction by removing approximately four mL from each bottle with a fresh eyedropper then dropping the sample on to a clean X-ray diffraction slide. The slides were allowed to dry overnight. Due to the high silica content of the samples some samples rolled making analysis by X-ray diffraction impossible.

The slides were analyzed in a Phillips Model 12045 X-ray diffractometer with a Bragg-Brentano geometry connected to a MDI Databox®. The first sample ran was LC from 2-32°, stepping 0.02 for one second. The resulting pattern showed only small diffraction peaks. The computer froze so we were unable to save this pattern. When Dr. Elliott and I reran the sample we extended the count time from one second to three seconds producing a better pattern. The three second count time was adopted for all future analysis.

The subsequent patterns had large amorphous humps starting at 15° 2θ and extending to 30° 2θ. In an effort to minimize this and to remove the background noise we increased the kilovolts from 35 to 40 and the milliamperes from 15 to 20, subjecting the sample to 800 watts of power rather than the typical 525 watts (35 KV, 15mA). The diffraction pattern did not improve dramatically.

The high background noise coupled with the large amorphous hump displayed within the patterns led to the decision to retreat the fine clay fraction with 30% H_2O_2. The samples were transferred to centrifuge bottles, removed from suspension by the addition of 1 M NaAc-HAC buffer and centrifugation and then washed with de-ionized water. Great care was taken during cleaning to not lose much of the small amount of black, fine clay which constituted each sample. The supernatant was removed and five mL of 30% H_2O_2 was added to each sample with no visible reaction. After ten minutes, ten mL of 30% H_2O_2 was added and samples QE and LC started reacting. Ten minutes elapsed before the samples were added to a water bath set at 50°C. Five mL of 30% H_2O_2 was added to the samples bringing the total amount of 30% H_2O_2 to 20 mL. Samples QW and CN did not start to react until placed into the water bath while CS did not start to react visibly for one and a half hours had elapsed. The samples were allowed to react overnight.

The next day samples QW, QE, CN and LC were very light in color indicating that the remaining carbon had been removed. Sample CS did not have the same light coloration therefore 20 mL of 30% H_2O_2 was added and the reaction was allowed to continue until a light coloration was achieved, an additional two days. 20 mL of 1 M NaAc-HAC buffer was added to each sample to saturate exchangeable surfaces with Na and to aid in flocculation and then spun in the centrifuge to speed flocculation. When the samples were removed from the centrifuge, the small amount of black fine clay which was present before the second organic treatment had been transformed into a smaller amount of white fine clay.

The supernatant was removed from the samples and each sample was carefully washed with de-ionized water until the clays began to re-suspend. Cleaning by dialysis was not attempted due to the small sample size. The clean samples were then transferred to new storage bottles with only the smallest amount of water possible. Oriented slides were prepared and diffraction patterns were obtained. The resultant patterns displayed illite, kaolinite and quartz peaks along with peaks associated with the NaAc-HAC buffer indicating that efforts to clean the samples of the NaAc-HAC buffer were unsuccessful. A conservative approach for cleaning the samples was necessitated due to the small amount and this approach proved to be insufficient at removing the NaAc-HAC buffer.

The significant change in coloration of the samples when treated with 30% H_2O_2 for extended amounts of time indicated that the standard four hours of organic treatment was insufficient. The high carbon content of the Woodford shale, ranging from 0.3 to 25 wt%, necessitated longer treatment times compared to traditional soils and rocks (Cardott and Lambert, 1985; Kirkland et al., 1992). With this knowledge Dr. Elliott and I determined to prepare the reserve samples following the preparation steps laid out previously with the

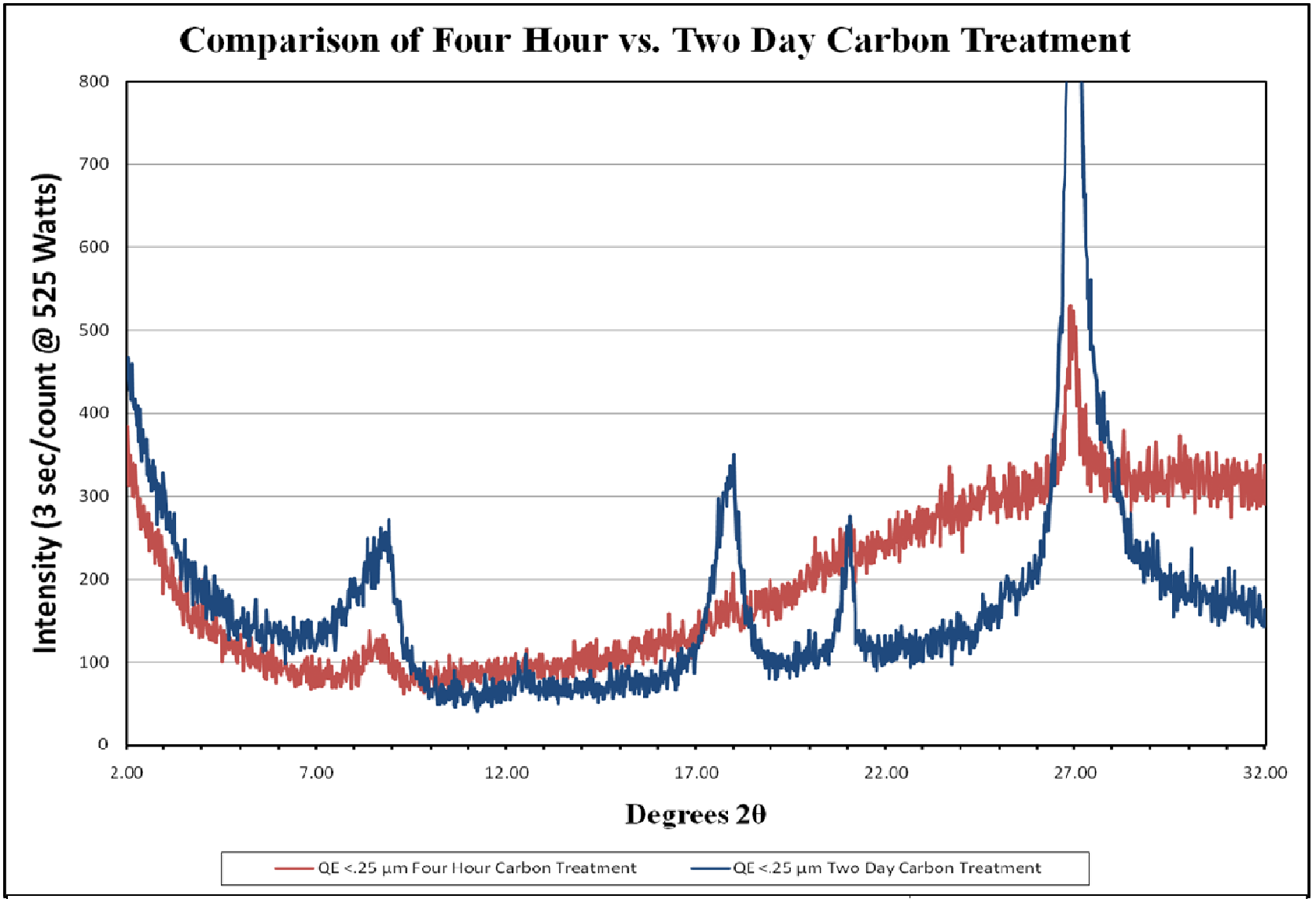

Figure 2.2- Comparison of four hour versus two day carbon treatment.

exception of the organic treatment. The organic treatment was extended for the bulk samples from four hours to two days (Figure 2.2).

After separation of the clay fractions into course, medium and fine, each fraction was analyzed. The organic treatment for the bulk sample removed sufficient carbon from the fine clay fraction to allow accurate X-ray diffraction with insignificant background or the amorphous hump from 15-30° 2θ previously discussed. The organic treatment for the bulk sample was insufficient in the removal of carbon from the coarse and medium clay fractions. These fractions underwent an additional carbon removal treatment of two days. The resulting clays allowed for accurate X-ray diffraction without significant background or the amorphous hump from 15-30° 2θ.

2.3 X-Ray Diffraction

The identification of clay minerals is done by analyzing an oriented slide and scanning with Cu K_α X-rays creating a diffraction pattern (Moore and Reynolds, 1997). The oriented slides promote the diffraction of basal or 00*l* reflections for phyllosilicates which is more diagnostic than either the a or b dimensions (Moore and Reynolds, 1997). X-rays penetrate the lattice structure and are scattered by the atoms creating constructive and destructive interference (Moore and Reynolds, 1997). Constructive interference occurs when two or more rays are in phase and destructive interference occurs when the rays are out of phase (Moore and Reynolds, 1997). When the atoms are not evenly spaced within the lattice then constructive interference cannot occur and therefore no diffraction takes place (Moore and Reynolds, 1997). Rows of atoms in the c direction, evenly spaced, will constructively scatter X-rays at specific angles satisfying Bragg's law:

$$2d \sin\theta = n\lambda$$

λ is the wavelength of the X-rays, Cu K_α= 1.54 Å is used here, θ is the angle of incidence, n equals the order of reflections, typically n=1 and d is the spacing of the atoms within the crystal lattice in the c direction.

The clay mineralogy of each sample was determined by X-ray diffraction under three different circumstances. The first analysis was an air-dried oriented slide. The pattern produced provided an initial interpretation of the clay mineralogy. The pattern also is used as a reference with which to compare the next two X-ray diffraction patterns. Next the slide was placed in a bath of ethylene glycol vapors for 24 hours and then analyzed immediately by X-ray diffraction, this results in the expansion of all expandable interlayers. The ethylene glycol X-ray diffraction pattern is the most diagnostic when interpreting the presence of mixed layer illite/smectite, estimating the percentage of illite layers in mixed layer illite/smectite and for the presence of discreet smectite (Moore and Reynolds, 1997). The expandability of smectite is dependent on the ambient humidity, resulting in a d-spacing ranging from 10-17Å in air-dried sample patterns. Smectite when saturated with ethylene glycol will swell to a characteristic d-spacing of 17Å. Illite, which is not expandable, does not swell when saturated by ethylene glycol. This swelling will change the diffraction pattern helping to diagnose the presence of smectite.

The final X-ray diffraction pattern is produced after heating the sample for one hour at 550°C. The addition of heat to an oriented slide is useful in diagnosing the presence of smectite and kaolinite. If smectite is present the hydrated interlayers, which had expanded to 17Å due to ethylene glycol, will collapse to 10Å and mirror the reflections of illite. Any kaolinite present will become amorphous when heated to 550°C removing it from the diffraction pattern because amorphous material cannot be diffracted.

2.4 Analysis of XRD Patterns

The X-ray patterns were interpreted for clay mineralogy using data from Moore and Reynolds (1997) and Hoffman and Hower (1979). Relative abundances of the minerals found in each sample were quantified using the intensities of the illite (001), kaolinite (002), quartz (100) and dolomite (100) peaks normalized against %100 (Spötl et al., 1993). These values are not intended as accurate quantitative estimates but as relative indicators of changes in mineralogy (Spötl et al., 1993).

$$Relative\ abundance\ of\ illite = \frac{intensity\ of\ illite\ (001) peak}{intensity\ of\ illite\ (001) + \ kaolinite\ (002) + \ quartz\ (100) + \ dolomite\ (100)\ peaks}$$

The degree of illite expandability was determined by comparing the d-spacing of the (001) and (002) peak of illite presented by Jackson (1977):

$$relative\ expandability = \frac{d - spacing\ of\ (001)}{d - spacing\ of\ (002)}$$

Largely illitic or pure illitic clays will display an (I001) peak with a d-spacing of 10Å and an (I002) peak of 5Å yielding a ratio of 2. Clays that are slightly expandable will display an (I001) peak with d-spacings >10Å and an (I002) peak ≥5Å yielding a ratio >2.

Illite crystallinity was determined four ways. The Kübler index is defined as the width of the 10Å peak at one-half the maximum peak height; this index decreases as illite crystallinity increases (Figure 2.3) (Kübler, 1968). The narrowness of the (I001) peak relates to the crystallinity of the illite (Kübler, 1968). A broad peak suggests interstratification of expandable clays, interlayer hydration and small crystal size. A sharp peak indicates an increase in illite crystallinity where the collapse of interlayers and the conversion of smectite to illite under increased temperature and pressure, decreases the scattering domain of illite (Weaver, 1961; Kübler, 1968). Kübler (1968) related the (I001) peak sharpness to increased metamorphic

conditions, diagenesis equates to a sharpness >0.42° 2θ. The anchizone marks the limit of diagenesis, the appearance of chloritoids minerals and precedes the epizone, ranging from 0.42-0.25° 2θ (Kübler, 1968). The epizone or low grade metamorphism is represented by values <0.25° 2θ (Kübler, 1968).

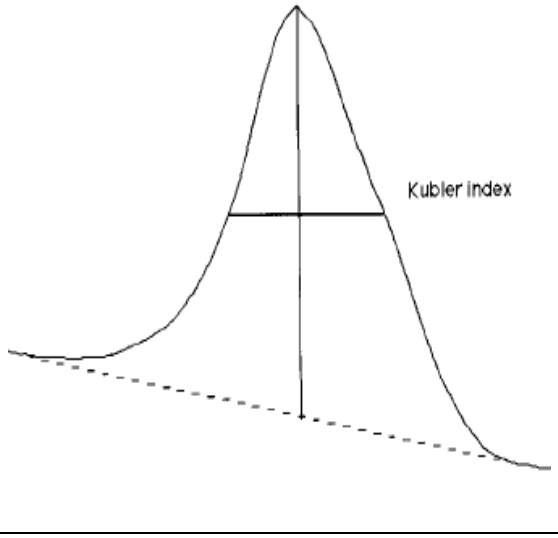

Figure 2.3- Example of how the Kübler Index is determined (Eberl and Velde, 1989).

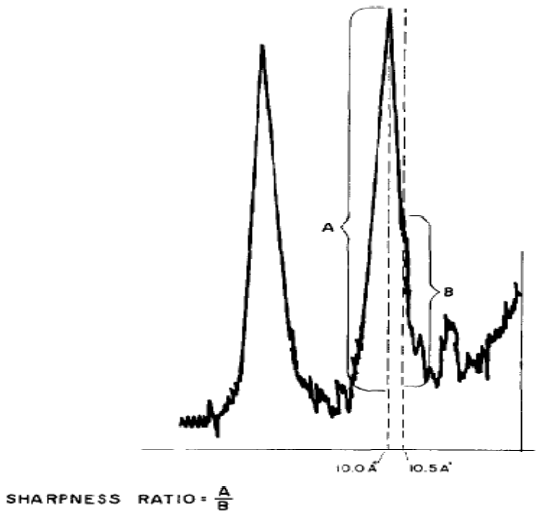

Figure 2.4- Determination of Weaver's Sharpness Ratio (Weaver, 1960).

Table 2.3- Comparison of degree of metamorphism and corresponding Sharpness Ratio (Flawn et al., 1960; Weaver, 1960).

Degree of Metamorphism	Sharpness Ratio
Low-grade metamorphism	12.1
Weak to very weak metamorphism	6.3
Incipient to weak metamorphism	4.5
Incipient metamorphism	2.3
Unmetamorphosed Stanley shale	2.3
Unmetamorphosed Atoka Formation	1.8

Weaver (1960) proposed a Sharpness Ratio which is the intensity of the peak height at 10.0 Å divided by the intensity of the illite peak at 10.5 Å, the value of this ratio increases as illite crystallinity increases (Figure 2.4). See Table 2.3 for representative illite Sharpness Ratio measurements for various illites. The Sharpness Ratio is defined as follows per Weaver (1960):

$$Sharpness\ Ratio = \frac{Peak\ Height\ at\ 10.0\ \text{Å}}{Peak\ height\ at\ 10.5\ \text{Å}}$$

Środoń's Intensity Ratio is defined as the intensity of the (001) to (003) illite peaks for air dried samples versus the same ratio for ethylene glycol solvated samples. This is a very sensitive measurement for small amounts of expandable layers (typically <10% smectite layers) in mixed layer illite/smectite. The Intensity Ratio is defined as follows per Środoń (1984):

$$Intensity\ Ratio = \frac{(I\ 001)/(I003)\ Air\ Dry}{(I001)/(I003)\ Ethylene\ Glycol}$$

The Intensity Ratio decreases and approaches one as illite crystallinity increases. The presence of quartz precludes the applicability of this ratio due to the overlap of the quartz (101) reflection overlapping the illite (003) reflection.

Lastly, the increase in crystallinity measured by the above indices and ratios is largely controlled by crystal thickness which increases as illite experiences progressive diagenetic conditions (Jaboyedoff et al., 2001). The crystal thickness and the percentage of smectite layers in mixed layer illite/smectite can be determined by plotting the values of the air dried and ethylene glycol solvated Kübler Indices on models by Jaboyedoff et al. (2001). Jaboyedoff et al. (2001) presented several models for random (R=0), ordered (R≥1) and long range ordered (R≥3) stacking orders for I/S (Figure 2.5).

The Jaboyedoff et al. (2001) models are based on X-ray diffraction patterns created by the computer program NEWMOD with the assumption of two swelling layers of water or ethylene glycol. The percentage of smectite and N layers can be related:

$$\frac{\%S}{100} = \frac{k}{N}$$

where *k* is a constant limited to values of 0-3.

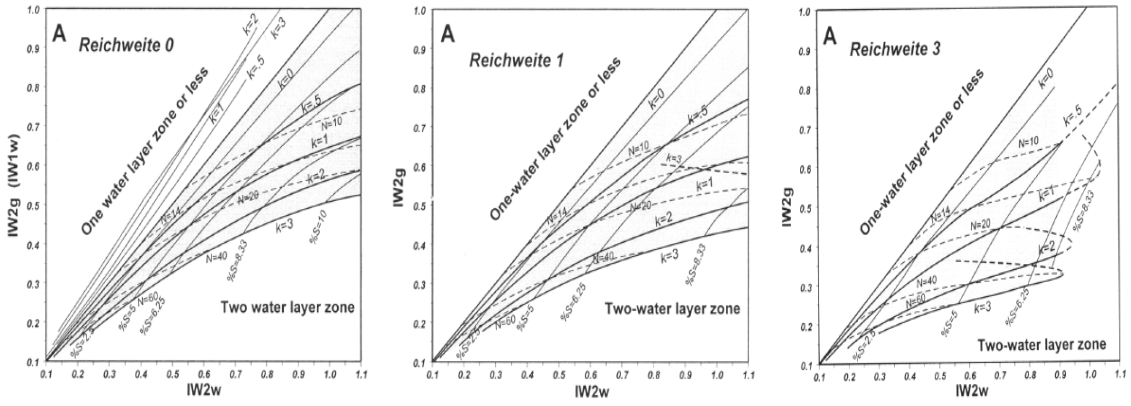

Figure 2.5- Examples of Jaboyedoff et al. (2001) models for ordering R=0, R≥1 and R≥3. The models created by NEWMOD plot the ethylene glycol solvated Kübler Index (IW2g) versus the air dried Kübler Index (IW2w).

When Fe^{2+} and/or Mg^{2+} is substituted for Al^{3+} in the octahedral sheet three divalent cations are necessary for electrical neutrality compared to only two for Al^{3+} , transforming the illite from a dioctahedral clay mineral to a trioctahedral clay mineral (Moore and Reynolds, 1997). The substitution of Fe^{2+} and/or Mg^{2+} for Al^{3+} in the octahedral layer likely occurs during low grade metamorphism and the presence of Fe and/or Mg rich illite would likely indicate a detrital source rather than a diagenetic source for the illite (Esquevin, 1969, Gingele, 1996).

The presence of dioctahedral Al rich illite versus trioctahedral Fe and/or Mg rich illite may be estimated by analyzing the intensity ratio of the 5Å and 10Å. A high content of Mg and Fe is indicated with a ratio <.03 while a ratio >0.3 indicates a high content of Al (Esquevin,

1969). If the ratio is >.03, dioctahedral Al rich illite is present and is likely the result of diagenesis, allowing the illite to be used as a geothermometer (Esquevin, 1969, Gingele, 1996).

$$Illite\ peak\ ratio = \frac{(I002)}{(I001)}$$

A more precise determination of dioctahedral versus trioctahedral illite can be done using the illite (060) reflection from randomly oriented slides (Moore and Reynolds, 1997). Scanning the randomly oriented slides for count times of >4 seconds allow the weak peaks of dioctahedral and trioctahedral clays to be differentiated (Moore and Reynolds, 1997). Due to time constraints this analysis was not attempted.

Illite polytypes were determined by preparing random mounts of each sample and scanning these mounts from 28° to 36° 2θ with a count time of forty five seconds per step. Both kaolinite and dolomite interfere with polytype determination due to overlapping reflections, therefore kaolinite was removed by heating and residual dolomite was removed using the carbonate removal treatment previously described. Random orientation of the samples was promoted during preparation with each sample backfilled into the sample holder (Moore and Reynolds, 1997). This method minimizes the interaction of the sample with the preparer where a preferred orientation may be induced.

The resultant patterns were analyzed to determine the percentage of the $2M_1$ (detrital) illite polytype present in the clay fractions of the Woodford shale. The percentages of the $2M_1$ polytype were quantified by the following equation from Maxwell and Hower (1967):

$$\%2M_1 = 100 \text{ x } \left(\frac{2m_1\ polytype\ peak\ area\ (3.00\text{Å})}{total\ polytype\ peak\ area\ (2.58\text{Å})}\right)$$

The 3.00Å peak is unique to the $2M_1$ polytype while the 2.58Å peak is representative of all polytypes and is the least affected by preferential orientation.

If the weak peaks of the $1M_d$ illite polytype were able to be identified and separated from the $1M$, then the percentage of the $2M_1$ polytype can be determined with the following equations from Grathoff and Moore (1996):

$$\%2M_1 = 3.25 + 335\left[\frac{2m_1\ polytype\ peak\ area\ (3.00\text{Å})}{total\ polytype\ peak\ area\ (2.58\text{Å})}\right]$$

$$\%1M = 3.40 + 132\left(\frac{1M\ polytype\ peak\ area\ (3.07\text{Å})}{total\ polytype\ peak\ area\ (2.58\text{Å})}\right)$$

$$\%1M_d = 100 - (\%1M + \%2M_1)$$

Deconvolution of the ethylene glycol solvated illite (001) peak was done using PeakFit v4.12. This program allowed for the decomposition of X-ray diffraction patterns helping to identify and characterize the three different illite sub-populations: mixed layer illite/smectite, poorly crystallized illite and well crystallized illite. The size of the individual peak was used as a proxy for the relative abundance of the three sub-populations. The peak position was used to determine mixed layer illite/smectite from poorly crystallized illite from well crystallized illite. Mixed layer illite/smectite contains expandable layers causing the peak to display variable and higher d-spacings. Poorly crystallized illite is not expandable but will not display a d-spacing of 10 Å due to crystalline defects. Well crystallized illite will display 10 Å d-spacing.

First, the section of d-spacings from 9.5-11.5Å was isolated from the overall diffraction pattern. Next the pattern was smoothed by Gaussian convolution and a baseline was subtracted from the data. Deconvolution was carried out by the AutoFit Peaks III Deconvolution function with three individual Gaussian peaks of varying widths. To achieve the best fit the amplitude and area of each peak was manually refined until $r^2 = 0.99$ and the standard error was minimized. The r^2 value is the regression coefficient. The value of r^2 is an indicator of how good a predictor the model is for the observed peak, the closer to 1 the r^2 value, the better the modeled illite (001)

peak. The standard error (SE) is a measure for how close the modeled illite (001) peak represents the observed peak where the lower the standard error the greater the agreement between the two peaks.

CHAPTER 3- RESULTS

3.1 Clay Mineralogy and Illite Crystallinity

The clay mineralogy of the Woodford shale found on the northern and southern flanks of the Arbuckle Mountains consists of kaolinite and long range ordered, R≥3, mixed layered illite/smectite. Their relative abundances along with quartz and dolomite are presented in Table 3.1 and XRD patterns can be found in Appendix B. Mixed layer illite/smectite was present in all samples of all size fractions and the relative abundance decreases as the size fraction increased. Kaolinite was present in all samples of all size fractions and was confirmed by heating as described in the previous chapter. As the size fractions decreased the relative abundance of kaolinite generally decreased.

Table 3.1- Relative abundances of minerals found in the clay size fraction.

Sample	Size Fraction (μm)	% mixed layer illite/smectite	% Kaolinite	% Quartz	% Dolomite
CN	1-2	5%	6%	18%	71%
CN	.25-1	19%	21%	60%	0%
CN	<.25	32%	31%	37%	0%
CS	1-2	15%	20%	51%	14%
CS	.25-1	19%	21%	47%	14%
CS	<.25	41%	33%	26%	0%
LC	1-2	9%	6%	20%	66%
LC	.25-1	30%	19%	21%	30%
LC	<.25	72%	28%	0%	0%
QE	1-2	20%	11%	69%	0%
QE	.25-1	27%	12%	46%	16%
QE	<.25	48%	11%	41%	0%
QW	1-2	7%	5%	39%	48%
QW	.25-1	15%	10%	50%	25%
QW	<.25	49%	11%	40%	0%

Other minerals found within the Woodford shale included quartz and dolomite. Sample LC <0.25 μm, was the only sample in the clay size fraction that did not show the presence of quartz. The relative abundance of quartz and dolomite combined accounted for a large portion of each sample. Dolomite, a cement which we attempted to remove during the preparation of the samples, was found in all the samples of the 1-2 μm fraction except QE and in every sample of the 0.25-1 μm fraction except CN.

The diffraction patterns of each sample after soaking in ethylene glycol vapors for 24 hours showed no discernable expandability or the presence of discreet smectite. The expandability was quantified roughly from the diffraction pattern by dividing the d-spacing of the illite (001) peak by the d-spacing of the illite (002) peak. This ratio ranged from 1.98-2.01.

Illite crystallinity was determined from the patterns of samples soaked in ethylene glycol vapors for 24 hours by the Kübler Index, Weaver's Sharpness Ratio and Środoń's Intensity Ratio (Table 3.2). Most samples demonstrated a Kübler Index within the diagenetic range, >0.42. Two of the coarse fraction (1-2 μm) samples displayed anchizone indices. The Kübler Index exhibited a decreasing trend with increasing size fraction, ranging from 0.70-0.85 for the <0.25 μm fraction to 0.41-0.50 for the 1-2 μm fraction.

Weaver's Sharpness Ratio resulted in values ranging from 1.58-2.74 for the <0.25 μm fraction up to 3.71-9.60 for the 1-2 μm fraction, these values denote unmetamorphosed to weakly metamorphosed conditions. Guthrie et al. (1986) correlated a linear relationship between the Sharpness Ratio and the Kübler Index on a log-log plot demonstrating the consistency between the methods. The Sharpness Ratio and the Kübler Index of the Woodford shale display the same correlation (Figure 3.2). Środoń's Intensity Ratio was determined for the one sample that did not contain any quartz, LC <0.25 μm, and a value of 1.79 was determined.

Table 3.2- Results for illite crystallinity, Al vs. Fe & Mg chemical composition and expandability for ethylene glycol slides.

Sample	Size Fraction (μm)	Kübler Index	Weaver's Sharpness Ratio	Środoń's Intensity Ratio*	I(002) / I(001)	(001) Spacing (Å)	(002) Spacing (Å)	(001) Spacing / (002) Spacing
CN	<0.25	0.74	1.58		0.86	9.99	5.03	1.98
CN	0.25-1	0.73	2.68		0.85	9.93	4.99	1.99
CN	1-2	0.43	9.60		1.04	9.88	4.99	1.99
CS	<0.25	0.85	2.11		0.96	10.05	4.98	2.01
CS	0.25-1	0.73	3.06		0.82	10.04	4.99	2.01
CS	1-2	0.49	5.85		0.67	9.88	4.99	1.98
LC	<0.25	0.71	2.74	1.79	0.70	9.93	4.98	1.99
LC	0.25-1	0.72	3.27		0.68	9.93	4.98	1.99
LC	1-2	0.41	6.00		0.78	9.88	4.96	1.99
QE	<0.25	0.70	1.86		0.88	9.99	4.98	2.00
QE	0.25-1	0.70	2.97		0.75	9.93	4.99	1.99
QE	1-2	0.41	6.40		1.39	9.88	4.98	1.98
QW	<0.25	0.82	1.74		0.79	9.99	5.03	1.98
QW	0.25-1	0.70	2.04		0.99	9.93	4.96	2.00
QW	1-2	0.50	3.71		1.04	9.99	4.98	2.00

*- All samples but LC <0.25 μm contained quartz making the Środoń's Intensity Ratio not accurate.

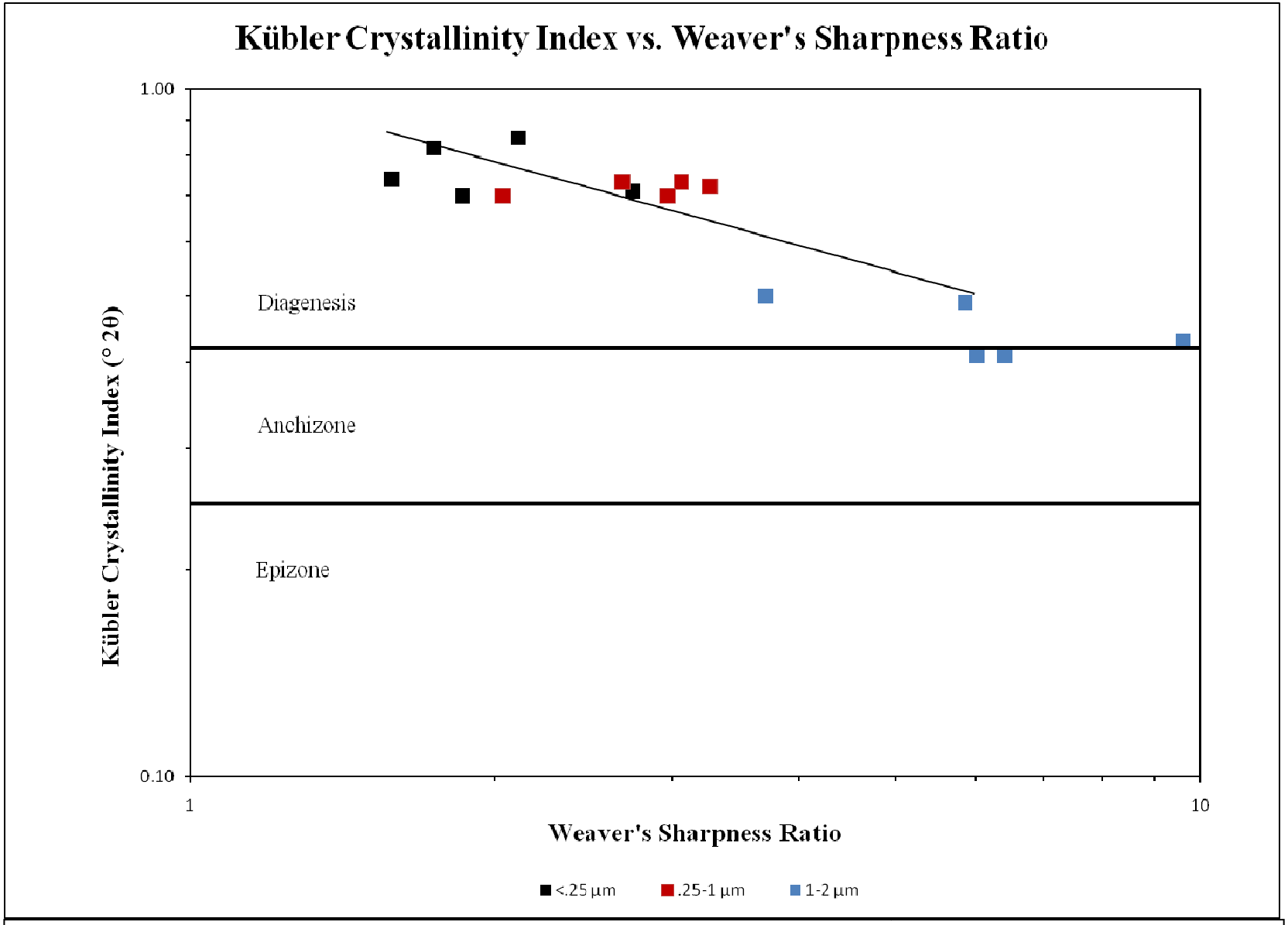

Figure 3.1- Kübler Crystallinity Index vs. Weaver's Sharpness Ratio for the Woodford shale.

An estimated chemical content was determined from the (I002)/(I001) peak ratio. All samples display a value, >.3, indicating a higher Al^{3+} content than Mg^{2+} or Fe^{2+}.

3.2 Modeling Results

The Kübler Indices of air dried and ethylene glycol slides were plotted on the models presented by Jaboyedoff et al. (2001) for the long range stacking order (R≥3). Most samples in the <0.25 µm and 0.25-1 µm fractions plotted in the field of the model where it was possible to derive a percentage of smectite in the mixed layer illite/smectite (Figure 3.2). The percentage of smectite layers in mixed layer illite/smectite ranges from nearly 0-5% based on this model. The model estimated the number of illite layers to be <10 for the <0.25 µm and 0.25-1 µm fractions and ~14-20 layers for the 1-2 µm fraction.

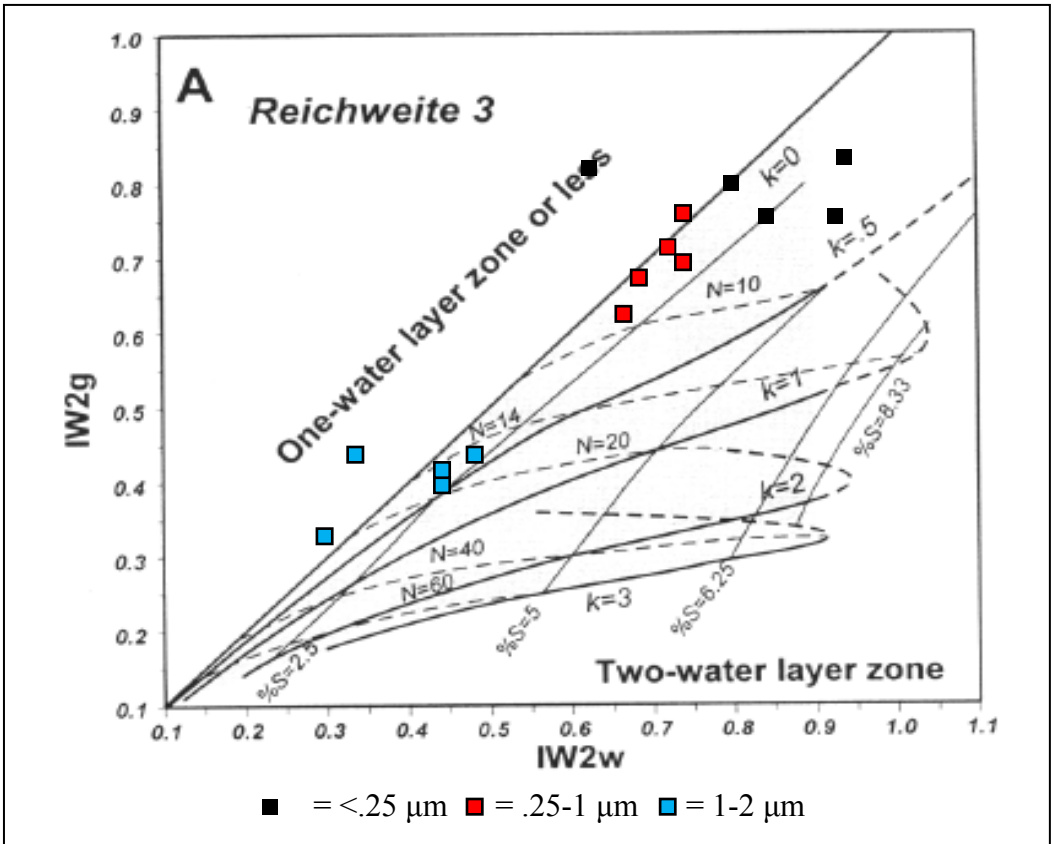

Figure 3.2. – Jaboyedoff et al. (2001) model results. %S and n layers of illite. Illite Width of the glycol (001) peak vs. the Illite Width of the air dried (001) peak (from Jaboyedoff et al., 2001).

In a cross plot of Środoń's Intensity Ratio versus the Kübler Index proposed by Eberl and Velde (1989), only one sample could be plotted: LC <0.25 μm. The percentage of smectite in mixed layer illite/smectite was estimated to be 5% with n ~15 layers (Figure 3.3).

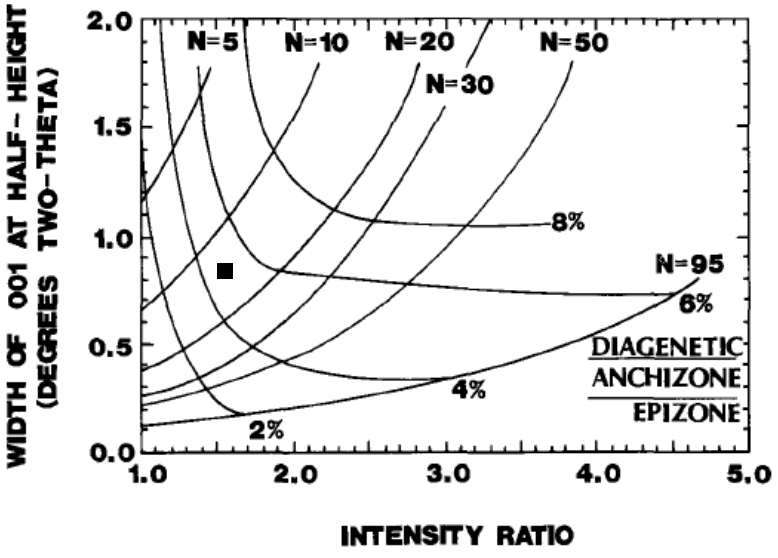

Figure 3.3 – Kübler Index versus Środoń's Intensity Ratio (Eberl and Velde, 1989).

3.3 Illite Polytypes

Illite polytypes are useful in estimating the percentage detrital illite present in clay fractions. The XRD diffraction patterns yielded no separate and discernable $1M_d$ polytype peaks making quantification of all polytype sub-populations not possible using equations by Grathoff and Moore (1996). The percentage of the $2M_1$ polytypes were thus determined by the ratio of the 3.00Å and 2.58Å peaks (Maxwell and Hower, 1967). Polytype XRD patterns can be found in Appendix C. The Woodford shale contains detrital illite, $2M_1$ polytype, in all samples (Table 3.3). The percentage of the $2M_1$ polytype increases with increasing clay size fraction from 13-27% for the smallest size fraction, <0.25 μm increasing to 27-33% for largest clay size fraction, 1-2 μm.

Table 3.3- Percentage of the $2M_1$ polytype.

Sample	Size Fraction (μm)	%$2M_1$
CN	<0.25	18%
CN	0.25-1	20%
CN	1-2	27%
CS	<0.25	*
CS	0.25-1	27%
CS	1-2	27%
LC	<0.25	27%
LC	0.25-1	30%
LC	1-2	26%
QE	<0.25	27%
QE	0.25-1	16%
QE	1-2	33%
QW	<0.25	13%
QW	0.25-1	16%
QW	1-2	23%

*-Insufficient sample remained for polytype analysis.

3.4 Illite (001) Peak Deconvolution

Deconvolution of the illite (001) peak showed three sub-populations of illite in each sample: mixed layer illite/smectite, poorly crystallized illite and well crystallized illite. The use of three peaks to deconvolute the illite (001) peak was necessary to most accurately model the illite (001) peak. No illite (001) peak could accurately be deconvoluted using less than three peaks. The deconvoluted peaks are shown in Appendix D.

From the peak deconvolution data, the relative abundance and peak position of each sub-population by size fraction is presented here. The relative abundance of the sub-population mixed layer illite/smectite present within the <0.25 μm clay fraction ranged from ~4.5-19% and the peak position ranged from ~10.3-10.8Å. For the 0.25-1 μm clay fraction the relative abundance of mixed layer illite/smectite ranged from ~7-23% and the peak ranged from ~10.3-

10.5Å. For the 1-2 μm clay fraction the relative abundance of mixed layer illite/smectite ranged from ~3-11% and the peak ranged from 10.0-10.3Å. The relative abundance and expandability, based upon peak position, of the mixed layer illite/smectite decreased with increasing clay size fraction.

The relative abundance of the sub-population of poorly crystallized illite within the <0.25 μm clay fraction ranged from ~17.7-36.0% and the peak position from ~10.0-10.5Å. For the 0.25-1 μm clay fraction the abundance of poorly crystallized illite ranged from ~6-43% and the peak position ranged from ~10.0-10.2Å. For the 1-2 μm clay fraction the abundance of poorly crystallized illite ranged from ~21.0-33.6% and the peak ranged from 9.95-10.14Å.

The relative abundance of the sub-population of well crystallized illite within the <0.25 μm clay fraction ranged from ~54-68% and the peak position ranged from ~9.89-10.05Å. For the 0.25-1 μm clay fraction the abundance of well crystallized illite ranged from ~49-88% and the peak ranged from ~9.90-9.98Å. For the 1-2 μm clay fraction the abundance of well crystallized illite ranged from ~61-73% and the peak ranged from 9.88-9.95Å.

In Figures 3.4-3.6, the relative abundances of each sub-population of illite (mixed layer illite/smectite, poorly crystallized illite and well crystallized illite) are shown against the d-spacing of the peak position for each size fraction of each sample. A trend of increasing relative abundance and decreasing d-spacing is observed from mixed layer illite/smectite to well crystallized illite. For all clay size fractions, mixed layer illite/smectite is the least abundant illite sub-population in these Woodford shale samples. Well crystallized illite is the most abundant illite sub-population in these Woodford shale samples.

Table 3.4- Deconvolution of illite (001) peak results.

	Size Fraction (μm)	Peak Position of I/S (Å)	Area of I/S (%)	Peak Position of PCI (Å)	Area of PCI (%)	Peak Position of WCI (Å)	Area of WCI (%)
CN	<.25	10.49	13	10.21	30	9.96	57
CN	.25-1	10.33	23	10.08	28	9.95	49
CN	1-2	10.29	5	10.14	34	9.90	61
CS	<.25	10.76	12	10.45	20	10.05	68
CS	.25-1	10.49	8	10.16	38	9.98	54
CS	1-2	10.15	8	9.98	21	9.92	71
LC	<.25	10.28	4	10.00	36	9.90	60
LC	.25-1	10.31	7	10.04	5	9.93	88
LC	1-2	10.05	11	9.95	27	9.88	62
QE	<.25	10.55	14	10.25	18	9.91	68
QE	.25-1	10.28	8	10.04	43	9.90	50
QE	1-2	10.04	3	9.96	33	9.93	63
QW	<.25	10.63	19	10.17	26	9.94	55
QW	.25-1	10.49	18	10.18	24	9.92	57
QW	1-2	10.11	6	10.04	21	9.95	73

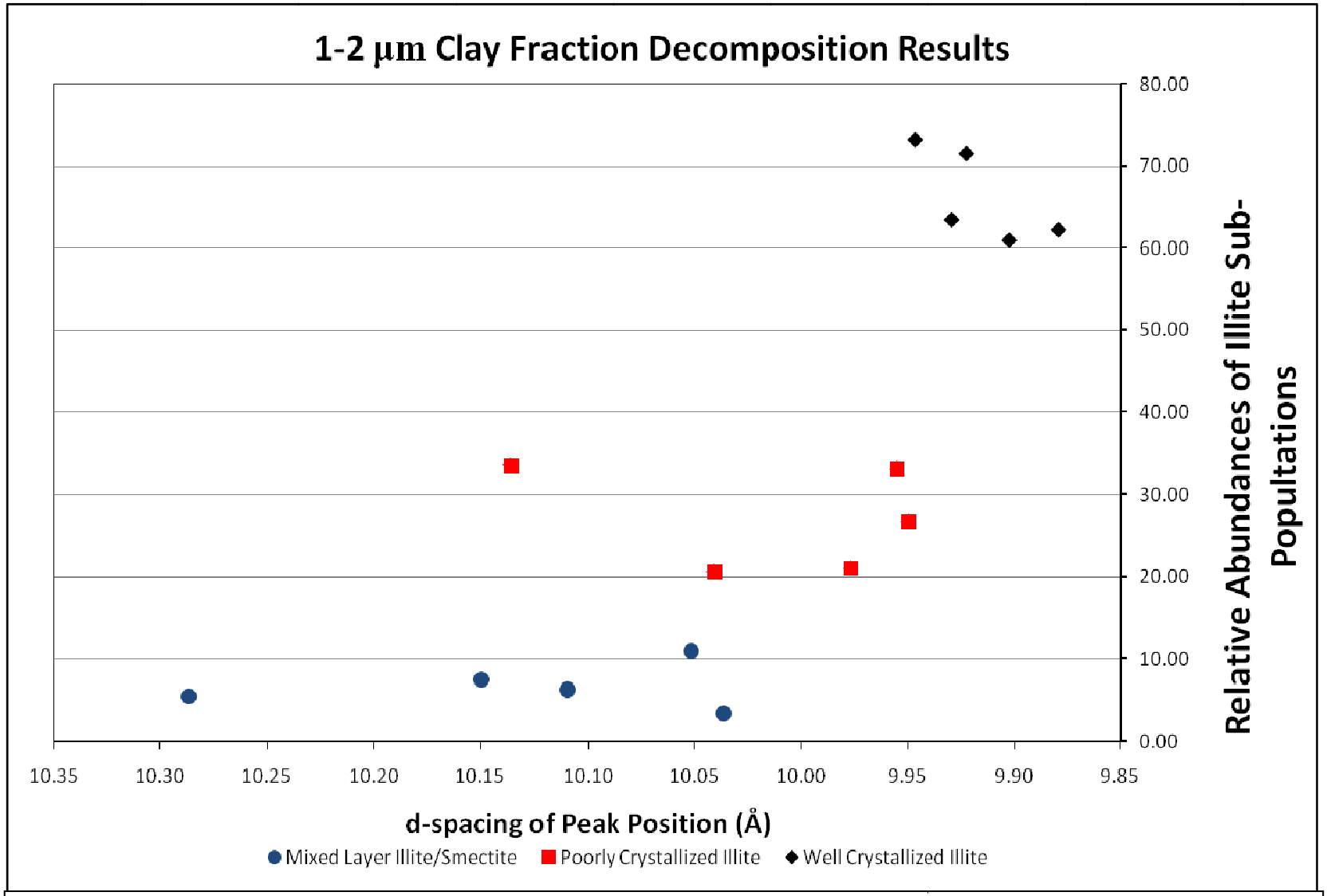

Figure 3.4- Comparison of 1-2 µm clay fraction decomposition results.

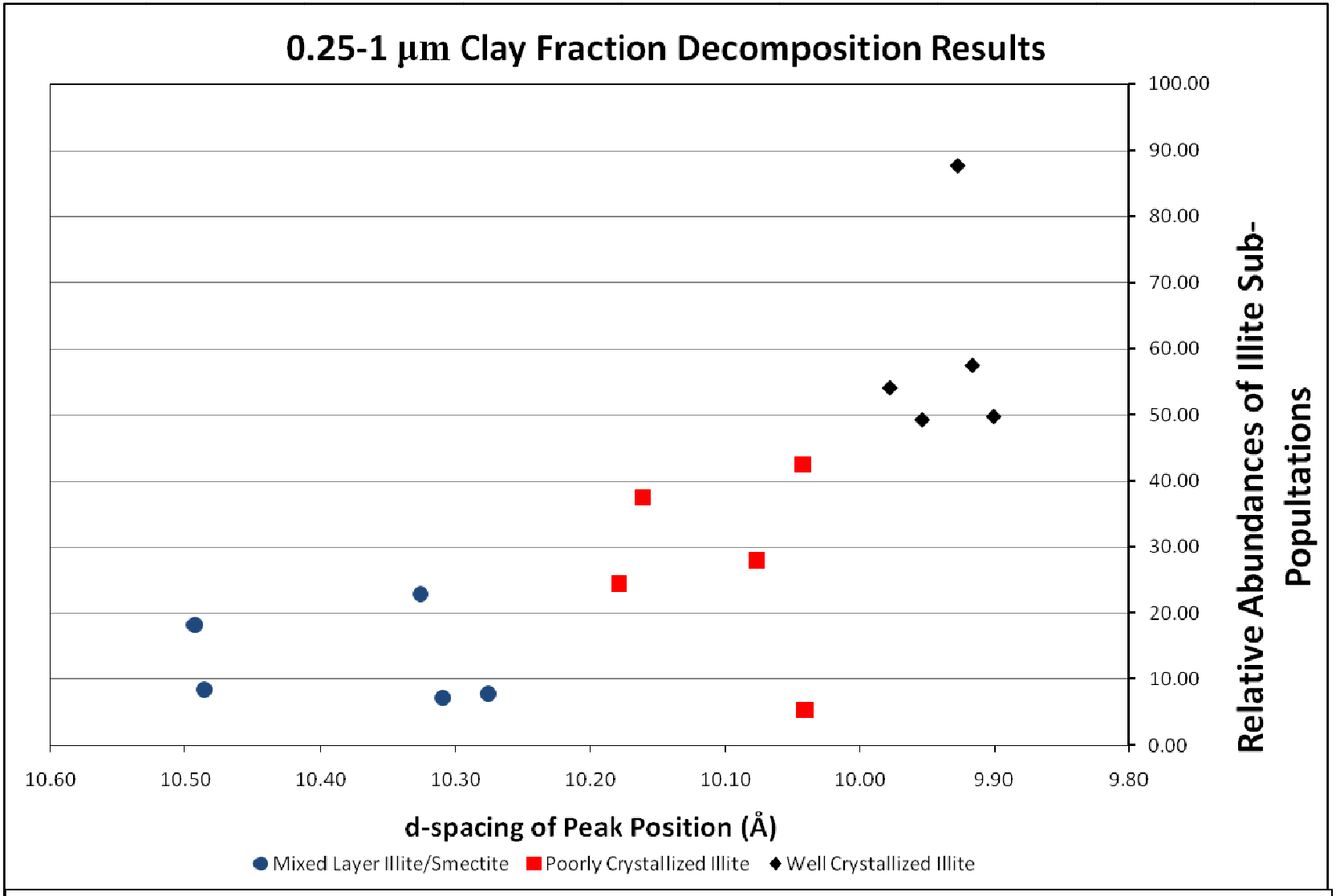

Figure 3.5- Comparison of 0.25-1 µm clay fraction decomposition results.

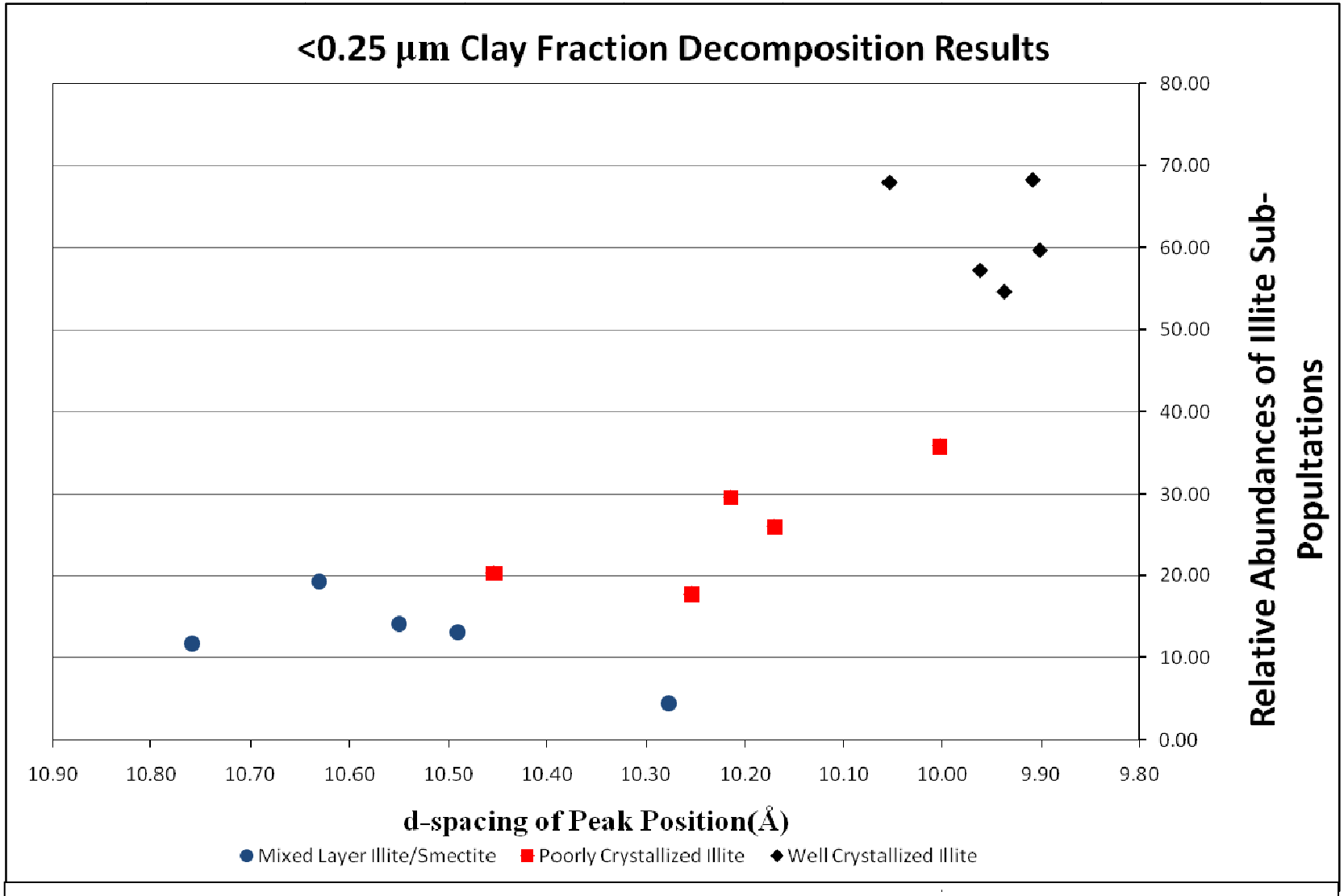

Figure 3.6- Comparison of <0.25 µm clay fraction decomposition results.

CHAPTER 4- DISCUSSION

4.1 Comparison of Samples

Four of the samples (CN, CS, QE and QW) studied came from two outcrops on the southern flank of the Arbuckle Mountain uplift and one (LC) from the northern flank. The samples do not differ appreciably in mineralogy or in the presence of illite polytype, though they were deposited in stratigraphically different sections. The southern samples were deposited in the middle to upper Woodford shale and the northern sample in the lower to middle Woodford shale. A constant source and/or a similar depositional environment from the time of deposition of the northern samples through the deposition of the southern samples may explain these findings. The period of time represented by this interval may be small due to the overlap of the estimated stratigraphic positions.

Analysis of illite crystallinity shows no difference between the samples. The Kübler Index, Weaver's Sharpness Ratio, smectite content and deconvolution of the illite (001) peak show the same degree of illitization and crystallinity for both sample locations.

4.2 Clay Mineralogy and Illite Crystallinity

Minerals found in the clay fraction of the Woodford shale included quartz, dolomite, kaolinite and mixed layer illite/smectite. The presence of kaolinite may be due to diagenesis or detrital input. The data set for this study is not broad enough to characterize the kaolinite and presents an opportunity for further study. The presence of both quartz and dolomite in the clay fraction supports previous studies characterizing quartz and dolomite as the dominant minerals of the Woodford shale (Lewan, 1983; Kirkland et al., 1992; Cardott, 2007).

The quartz may have been derived from detrital sources, microfossils, diagenetic sources (dissolution of biogenic opal), the conversion of smectite to illite and/or sample preparation error

during disaggregation (Kirkland et al., 1992; Elliott and Matisoff, 1996). Sample preparation for this study necessitated the use of a mortar and pestle in order to disaggregate the sample into different size fractions. It is possible quartz present in the silt fraction was incorporated into the clay fraction. Likewise, coarse grained illite may have been incorporated into finer fractions through the disaggregation process.

Interpretation of the XRD patterns suggests that the illite present is a long-range ordered, R≥3, mixed layer illite/smectite. R≥3 ordering contains little smectite and the lack of an observable "shoulder" on the higher d-spacing arm suggests a conservative estimate of the smectite content to be less than 5% (Hower, 1981). Comparison of the d-spacings for the (001)/(002) illite peaks of diffraction patterns suggest little to no expandability.

With models developed by Eberl and Velde (1989) and Jaboyedoff et al. (2001), more detailed percentages of smectite layers in mixed layer illite/smectite were derived. The one sample that could be modeled with Eberl and Velde (1989) found a smectite content of ~5% in mixed layer illite/smectite. The Jaboyedoff et al. (2001) model suggested a similar smectite content in mixed layer illite/smectite of <5% in some samples and <2.5% in most samples. The lack of expandability in the Woodford shale suggests a high thermal maturity of 150-200°C (Hoffman and Hower, 1979).

The illite in the Woodford shale is Al rich, suggesting a diagenetic origin increasing the accuracy when used as an indicator of thermal maturity (Esquevin, 1969, Gingele, 1996). Values for both Weaver's Sharpness Ratio and the Kübler Index, measures of illite crystallinity, show the Woodford shale has undergone increased temperatures and pressures suggestive of diagenesis. Comparison of the thermal maturity of the samples by both measures of crystallinity display similar trends. Illite within the smallest clay fraction (<0.25 μm) has the lowest

crystallinity representative of diagenesis and incipient metamorphism for the Kübler Index and Weaver's Sharpness Ratio respectively. The medium clay fraction (0.25-1 μm) trended towards higher crystallinity and the coarsest clay fraction (1-2 μm) displays the greatest crystallinity. Weaver's Sharpness Ratio corresponds to weak to very weak metamorphism for all but one sample which has a value that corresponded to incipient metamorphism. Values for the Kübler Index indicate a high degree of diagenesis with two samples within the anchizone (Kübler, 1968).

The parameters which control the observed crystallinity include the presence of expandable minerals, defects or disorder in the crystal structure, crystal thickness and detrital illite. The presence of expandable minerals has been determined to be minimal with total percentage of smectite present in mixed layer illite/smectite being <5%. Defects or disorder in the structure of the illite may be due to strain upon the crystal lattice and thus cause variations in measured d-spacings but not enough research has been done to understand this relationship and apply it to this study (Jaboyedoff, 2001).

The greatest control on illite crystallinity is crystal thickness (Jaboyedoff, 2001). The crystal thickness of the illite in the Woodford shale samples was determined using models by Eberl and Velde (1989) and Jaboyedoff et al. (2001). These models found the number of n layers of illite to range from <10 to ~20 with the number of layers increasing with an increase in clay size fraction. This is not unexpected because illite is always more coarse grained than mixed layer illite/smectite, accumulating in coarser fractions (Środoń, 1984). The accumulation of illite in coarser fractions may be due to lower energy barriers of nucleation during crystal growth (Altaner and Ylagan, 1997). Nucleation of illite on pre-existing crystals is favored over

new crystal growth, thus promoting illite crystallinity by increasing crystal thickness (Altaner and Ylagan, 1997).

The results of the Jaboyedoff et al. (2001) model characterize the illite layers of the Woodford shale but do not quantify them. This is due to differences in how the Kübler Index is measured. Jaboyedoff et al. (2001) removed instrument effects and based the axes of their model on "illite width" measurements. Jaboyedoff et al. (2001) removed instrument effects because they may cause peak broadening, resulting in lower crystallinity measurements. The Kübler Indexes of this study contain instrumental effects and do not correlate directly to axes of the model. The goal of this study is to characterize the illite present in the Woodford shale and this model allows a conservative characterization to occur, but with less accurate results. If the "illite width" were to be determined for the samples studied, the model would likely yield a greater number of n layers suggesting greater crystallinity.

The thickness of the crystals may not be a result of crystal growth during diagenesis but of metamorphism represented by detrital illite present in the Woodford shale. The presence of detrital illite is an important parameter to recognize because detrital illite sharpens the diffraction peaks. Pevear (1999) found the percentage of detrital illite, $2M_1$ polytype, to increase with increasing size fraction. Data from the quantification of $2M_1$ polytype suggests not all samples in the Woodford shale exhibit an increase in the percentage of the $2M_1$ polytype as the clay size fraction increases. Two samples CN and QW followed the trend suggested by Pevear (1999), the percentage of $2M_1$ polytype increased as the clay size fraction increased from12%→20%→27% and 13%→16%→23% respectively. Detrital input appears to be relatively homogeneous across the clay size fractions for samples CS and LC. The percentage of $2M_1$ polytype present in sample CS was 27% for both the 0.25-1 μm and the 1-2 μm size fractions (the <0.25μm did not

contain enough sample to determine the percentage of $2M_1$ polytype present. Size fractions for sample LC <0.25 μm, 0.25-1 μm and 1-2 μm contained 27%, 20% and 26% $2M_1$ polytype, respectively . Sample QE displayed no discernable trend.

The percentage of detrital illite in the Woodford shale samples ranged from 13-33% based on polytype quantification as described above. The presence of detrital illite will have an effect on the diffraction patterns and its presence is noted, but the overall trend of high illite crystallinity for the Woodford shale remains and is likely the product of diagenesis.

The low percentages of detrital illite present in the Woodford shale from this study is in contrast to the findings of Carr (1987) who found detrital illite representing a significant portion of the clay fraction of the Chattanooga shale. As noted previously the Chattanooga shale was deposited at the same time as the Woodford shale. The Woodford shale is referred to as the Chattanooga in Arkansas. This slippage in naming can result in the names being used interchangeably in the Arkoma basin which spans eastern Oklahoma and western Arkansas. Carr (1987) studied a transect of the Chattanooga shale along the Oklahoma and Arkansas border and found illite crystallinity, as measured by the Kübler Index, was not affected by burial depth. The measured values for the transect, ranged from 0.4-0.7° 2θ. The platform of the Arkoma basin displayed similar values as the basin, unlike VR_o which increased with burial depth. The crystallinity values were interpreted to be poor indicators of thermal maturity and to be heavily influenced by detrital illite. Unfortunately no polytype information was reported to confirm the presence of detrital, $2M_1$, illite.

If detrital illite dominated the observed polytypes and its presence increased with increased size fraction, the ratio of the (I002)/(I001) peaks, the Weaver's Sharpness Ratio and Kübler's Crystallinity Index observed in the Woodford shale would be different (Figure 4.1 and

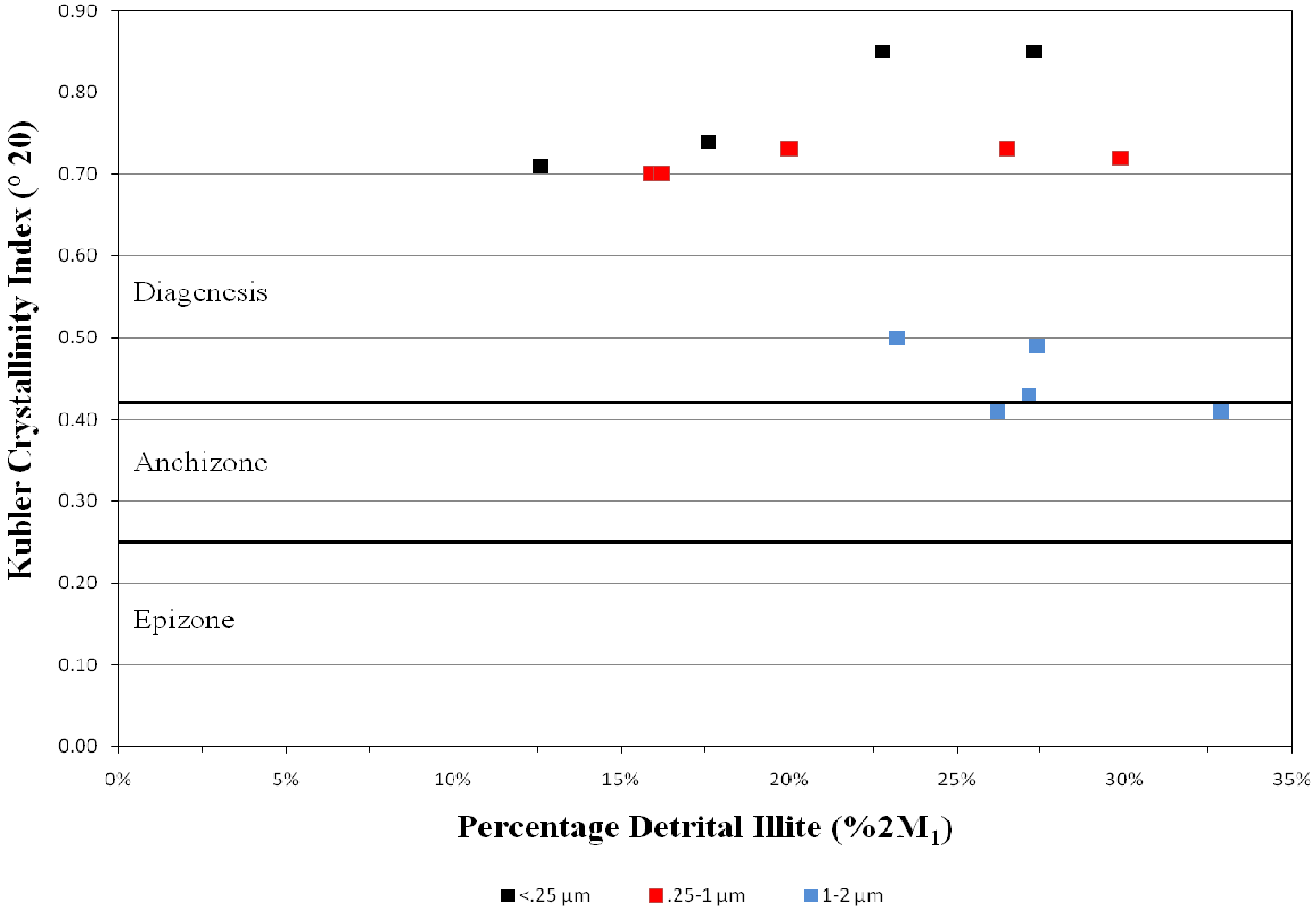

Figure 4.1- Comparison of Kübler Crystallinity Index to the percentage detrital illite ($2M_1$).

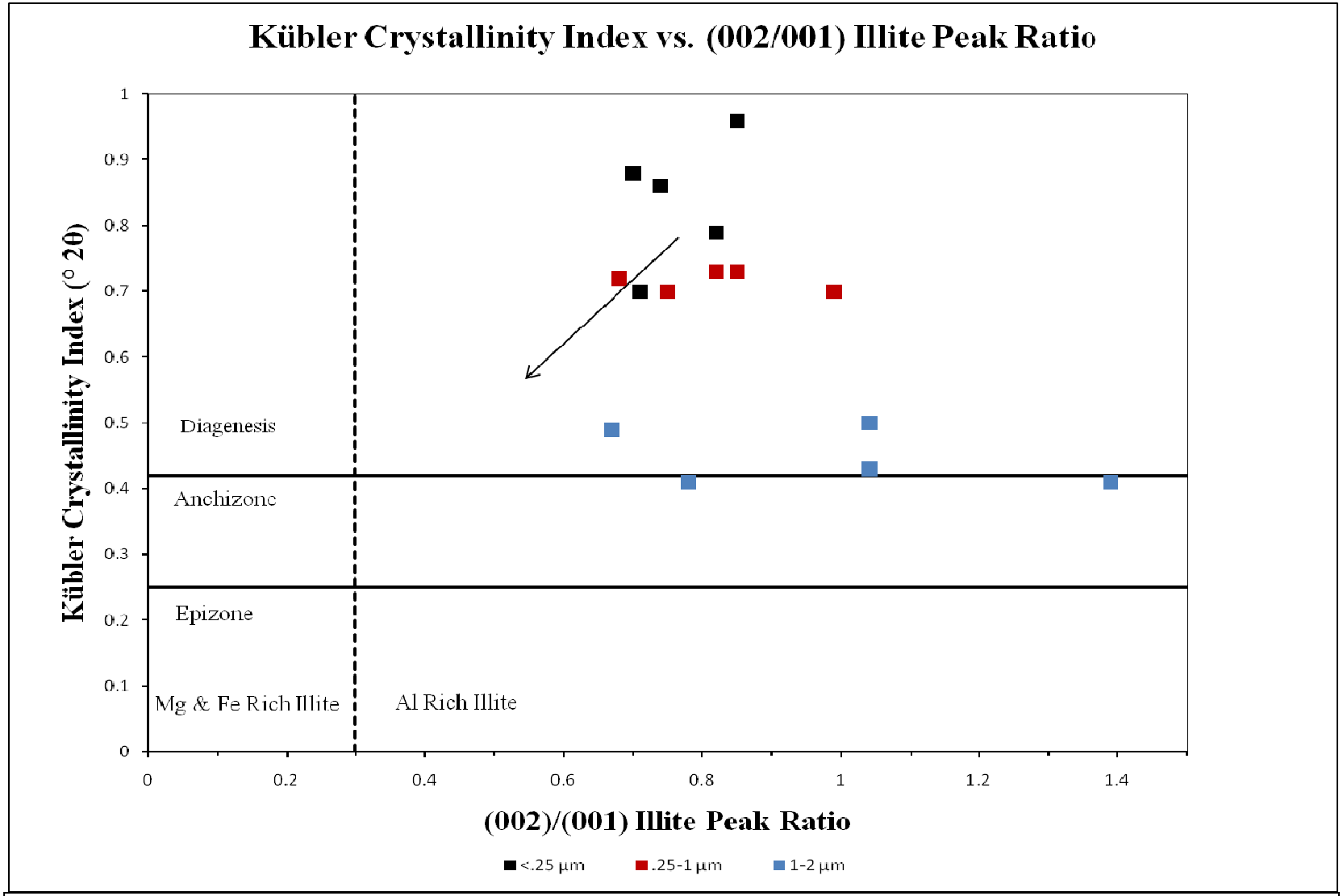

Figure 4.2- Comparison of Kübler Crystallinity Index to the (002)/(001) Illite Peak Ratio. Black arrow suggests trend if detrital illite dominated the clay mineral assemblage of the Woodford shale.

4.2). Figure 4.1 illustrates the lack of influence the percentage of detrital illite has on the observed Kübler Crystallinity Index where samples with a greater detrital content do not display a higher crystallinity value. The observed Kübler Crystallinity Indexes are generally constant for each clay size fraction.

Detrital illite is likely sourced from metamorphic rocks formed under conditions where Fe^{2+} and Mg^{2+} may have substituted for Al^{3+} in the octahedral layer forming trioctahedral illite. The presence of detrital illite, with higher concentrations of Fe^{2+} and Mg^{2+} in the octahedral layer, would cause the ratio of the (I002)/(I001) peaks to trend closer to the 0.3 demarcation of Fe^{2+} and Mg^{2+} rich illite. This trend is not found in figure 4.2.

In addition, the observed Weaver's Sharpness Ratio and Kübler's Index would suggest an environment of greater temperature and pressure than those observed, likely deep in the anchizone or epizone range. None of these parameters appear to be influenced in such a manner.

4.3 Decomposition of Illite (001) Peaks

The high crystallinity of the Woodford shale has been established by means of Weaver's Sharpness Ratio and the Kübler Index. Illite crystallinity is the by product of the mixed layer illite/smectite sub-population decreasing in abundance during diagenesis and poorly or well crystallized illite sub-populations increasing in abundance. The greater the well crystallized illite sub-population the larger the number of layers of illite and the fewer the defects found in the crystal lattice resulting in greater crystallinity.

The evolution of mixed layer illite/smectite to well-crystallized illite is documented in the deconvolution of the illite (001) peak. The deconvolution of the illite (001) peak for each size fraction of each sample showed all samples contain three subpopulations: mixed layer illite/smectite, poorly crystallized illite and well crystallized illite.

The relative abundance of the mixed layer illite/smectite ranges from an average of ~12.5% for the <0.25 μm clay fraction to ~6.7% of the 1-2 μm clay fraction. The sub-population of mixed layer illite/smectite exerts the largest influence, indicated by relative abundance and variability in peak position, on the shape of the <0.25 μm illite (001) peak increasing the a-symmetry of the (I001) peak. The relative abundance and variability of peak positions decreases as the clay size fraction increases, indicating the crystallinity of the larger clay fractions is greater than the smaller clay fractions.

Poorly crystallized illite constitutes a minor part of the deconvoluted illite (001) peak of ~26-27.5% of relative abundances on average. Defects in the crystal lattice of poorly crystallized illite cause the peak position to be located at greater d-spacings than well crystallized illite. The lack of expandable layers in the clay causes little expansion by ethylene glycol as evidenced by a consistent d-spacing of peak positions for clay fractions 0.25-1 μm and 1-2 μm. The <0.25 μm clay fraction displayed less consistent d-spacing of peak positions possibly due to the larger influence small lattice defects have on smaller crystals.

Well crystallized illite accounts for the majority of the sub-population of the deconvoluted illite (001) peak. No expandability is displayed by any sample of all clay size fractions with consistent d-spacing for the observed peak position. The progression of diagenesis has caused well crystallized illite to become more prominent at the expense of mixed layer illite/smectite and poorly crystallized illite.

Deconvolution of the illite (001) peak supports the interpretations of the XRD patterns. Three peaks were necessary to deconvolve each peak because of the asymmetrical shape formed by slightly interstratified smectite. Mixed layer illite/smectite represents a small sub-population

after deconvolution supporting the interpretation of XRD patterns that the percentage of smectite in mixed layer illite/smectite is very low.

The crystallinity of the Woodford shale, as interpreted from the XRD patterns, correlated mostly with conditions found during diagenesis. The use of three peaks necessary to deconvolve the asymmetrical peak and the large sub-population of well-crystallized illite support a diagenetic interpretation. Rocks of anchizone or epizone crystallinity display sharp, symmetrical diffraction peaks requiring one or two deconvolution peaks rather than the three peaks necessary for rocks that have experienced diagenesis. If the Woodford shale displayed higher thermal maturity, indicative of epizone conditions, more deconvolutions would have had results similar to the sample LC 0.25-1 μm. The processed peak contained minimal amounts of illite/smectite and poorly-crystallized illite, ~7 and 5% of the relative abundances respectively and 88% of the relative abundances were well crystallized illite. None of the other parameters studied for this sample indicate a thermal maturity of this degree and most likely, the results are an anomaly.

4.4 Possible Thermal Maturation History of the Woodford Shale

Interpretation of the illite data for the Woodford shale suggests it is diagenetic and can be used as a semi-quantitative geothermometer. Using previous studies of the conversion of smectite to illite, the geologic history of the Woodford shale and the present study on illite crystallinity and thermal maturity pose one possible explanation for the thermal maturation of the Woodford shale is presented here. This interpretation is only one of many possible explanations of the thermal history for the Woodford shale sample due to their likely deposition within the Oklahoma aulacogen, an area with an imprecisely known burial history.

Uplift of the Arbuckle Mountains by the Ouachita orogeny, led to the erosion of >3 km of sediment, representing strata from Early Cambrian to Mississippian. The erosion of the

Arbuckle Mountains buried both its northern and southern flanks exposing both sample locations to increased pressure and temperature.

The detrital smectite of the Woodford shale, sourced possibly from the craton or from the devitrification of volcanic glass, experienced increased temperature, pressure and K^+ content and underwent illitization as erosion buried the flanks of the Arbuckle Mountains. The illitization was likely aided by the high organic content of the Woodford shale and the movement of water through the formation due to the increase of temperature and pressure. During the thermal maturation of the organic matter, organic acids and CO_2 created chemical disequilibrium causing dissolution of potassium feldspar, kaolinite and smectite. These three minerals were sources for K^+ and Al^{3+}, which illite was a sink for, as well as Si^{4+} and Fe^{2+} which are likely precipitated in pore spaces as silica cement and magnetite, respectively.

The presence of CO_2 and organic acids affect the dissolution of source minerals differently. Harrison and Thyne (1991) found CO_2 dissolved potassium feldspar while the presence of organic acids enhanced the rate of reaction. Slightly acidic environments (pH 4-6.5) aid illitization by helping transport cations, i.e. oxalic acid, a difunctional organic acid, is the preferred complexing agent with Al^{3+} in this pH interval.

The illitization of smectite may have occurred by solid state transformation, dissolution and precipitation, Oswald ripening or a combination of the three processes. These processes likely began with the onset of the Ouachita Orogeny during Early Pennsylvanian continuing until erosion caused little relief to remain in the Oklahoma region in Early Permian time. The increase in temperature and pressure during ~32 million years of burial resulted in a highly illitic Woodford shale with little expandability/smectite content.

The high crystallinity and long range ordering, R≥3, exhibited by the mixed layer illite/smectite of the Woodford shale suggests a higher thermal maturity than observed VR_o. VR_o suggests the formation of oil and/or biogenic natural gas while illite crystallinity and stacking order suggests the formation of thermogenic gas indicating different thermal maturities. The disconnect between the two indicators of thermal maturation is interesting and needs further study in order to better understand the thermal history of the Woodford shale.

CHAPTER 5- CONCLUSIONS

5.1 Summary of Conclusions

From the study of three different outcrops of the Woodford shale located on both the northern and southern flanks of the Arbuckle Mountains several conclusions can be made-

1) The clay mineralogy of the Woodford shale displays consistency both spatially and stratigraphically. Kaolinite and mixed layer illite/smectite are the phyllosilicate minerals found in all clay fractions for all samples.
2) No discreet smectite is present. Smectite can only be found interlayered in long range ordered illite/smectite. The expandability of illite was not discernable from ethylene glycol solvated XRD patterns by inspection or the comparison of d-spacings of (I001) and (I002) peak locations. The percentage of smectite layers in mixed layer illite smectite was characterized using models by Jaboyedoff et al. (2001) and Velde and Lanson (1989) to be present but in very low amounts, <5% and commonly <2.5%. This was confirmed by deconvolution of the illite (001) peak finding mixed layer illite/smectite represented only a small sub-population of the illite (001) peak.
3) The Woodford shale contains highly ordered illite, R≥3. The crystallinity of the illite corresponds to conditions associated with diagenesis and suggests the Woodford shale is thermally mature. Highly ordered illite, R≥3, suggests the Woodford shale has experienced burial temperatures ranging from 150-200° C, conditions under which thermogenic gas would have been produced. Previous studies using VR_o found the Woodford shale to be less thermally mature than indicated in this study suggesting the formation of oil and biogenic gas (VR_o = 0.3-1.5). Organic acids within the Woodford

shale may have promoted illitization or the VR_o measurements may have been suppressed.

4) Detrital illite is present but does not exert a large influence on crystallinity measurements. The measured Kübler Crystallinity Index values do not suggest increased thermal maturity with increasing detrital content nor does the ratio of the (I002)/(I001) peaks suggesting Fe and/or Mg rich illite. If detrital illite influenced the crystallinity of the Woodford shale we would expect to see these parameters change with increasing detrital content.
5) Deconvolution of the illite (001) peak found well-crystallized illite constituted the largest sub-population of illite crystals. Deconvolution shows the Woodford shale has undergone diagenesis where the sub-population of illite/smectite has undergone illitization becoming poorly-crystallized illite with crystal lattice defects to well-crystallized illite of greater thickness and fewer lattice defects. The use of three peaks to deconvolute the illite (001) peak combined with the large sub-population of well crystallized illite supports the assessment the Woodford shale has undergone diagenesis.

5.2 Future Studies

This study focused on the use of phyllosilicates and their use as a geothermometer indicating thermal maturity of the Woodford shale adjacent to the Arbuckle Mountains. Additional information for these outcrops concerning thermal maturity may be found by studying the VR_o and the coloration of conodonts found in the Woodford shale. Geochemical analysis of the Woodford shale found on the flanks of the Arbuckle Mountains for the presence of biogeneic gas or thermogenic gas may also help to explain the thermal maturity.

Future studies of the phyllosilicate minerals could use Transmission Electron Microscopy to study the illite sub-populations. Chemical composition analysis of the phyllosilicates may also prove useful from the study of the illite (060) peak or by a different method. If K-Ar or Ar-Ar dating is attempted consideration for detrital illite must be taken.

From this study the origin of kaolinite cannot be determined. Further study of how diagenesis affects the kaolinite through the stratigraphic column as well as the study of kaolinite polymorphs and fabric can be used to determine its origin.

REFERENCES

Abid, I. and R. Hesse (2007) Illitizing fluids as precursors of hydrocarbon migration along transfer and boundary faults of the Jeanne d'Arc Basin offshore Newfoundland, Canada: Marine and Petroleum Geology 24(4): 237-245.

Ahn, J. H. and D. R. Peacor (1986) Transmission and analytical electron microscopy of the smectite-to-illite transition: Clays and Clay Minerals 34: 165-179.

Aplin, A. C. (2003) Influence of mechanical compaction and chemical diagenesis on the microfabric and fluid flow properties of Gulf of Mexico mudstones. Journal of Geochemical Exploration. I. F. Matenaar and B. van der Pluijm. International, Elsevier : Amsterdam-New York, International. 78-79: 449-451.

Altaner, S. P. (1989) Calculation of K diffusional rates in bentonite beds: Geochimica et Cosmochimica Acta 53(4): 923-931.

Altaner, S. P. and R. F. Ylagan (1997) Comparison of structural models of mixed-layer illite/smectite and reaction mechanisms of smectite illitization: Clays and Clay Minerals 45: 533-517.

Amsden, T.W. (1973) Stop 3: Late Ordovician, Silurian, and early Devonian strata, *in* Ham, W.E. (ed.), Regional geology of the Arbuckle Mountains, Oklahoma: Geological Society of America Guidebook for Field Trip 5, p. 39-43.

Amsden, T.W. (1975) Hunton Group (Late Ordovician, Silurian, and Early Devonian) in the Anadarko basin of Oklahoma: OGS Bulletin 121, 214 p.

Bell, T. E. (1986) Microstructure in mixed-layer illite/smectite and its relationship to the reaction of smectite to illite: Clays and Clay Minerals 34: 154-146.

Berger, G., J.C. Lacharpagne, B. Velde, D. Beaufort and B. Lanson (1997) Kinetic constraints on illitization reactions and the effects of organic diagenesis in sandstone/shale sequences: Applied Geochemistry 12(1): 23-35.

Boles, J.R. and S.G. Franks (1979) Clay diagenesis in Wilcox sandstones of Southwest Texas: Implications of smectite diagenesis on sandstone cementation. Journal of Sedimentary Petrology 49, 55-70.

Burgess, W.J. (1976) Geological evolution of the mid-continent and Gulf Coast areas-a plate tectonics view: Transactions: Gulf Coast Association of Geological Societies, v. 26, p.132-143.

Byrnes, A. P. and G. Lawyer (1999) Burial, maturation, and petroleum generation history of the Arkoma Basin and Ouachita Foldbelt, Oklahoma and Arkansas: Natural Resources Research 8: 3-6.

Capuano, R. M. (1990) Hydrochemical constraints on fluid-mineral equilibria during compaction diagenesis of kerogen-rich geopressured sediments: Geochimica et Cosmochimica Acta 54(5): 1283-1299.

Cardott, B.J., and M.W. Lambert (1985) Thermal maturation by vitrinite reflectance of Woodford Shale, Anadarko basin, Oklahoma: AAPG Bulletin, v. 69, p. 1982-1998.

Cardott, B.J. (1989) Thermal maturation of the Woodford Shale in the Anadarko basin, *in* K.S. Johnson, ed., Anadarko basin symposium, 1988: OGS Circular 90, p. 32-46.

Cardott, B.J. (2007) Overview of Woodford gas-shale play in Oklahoma: OGS, Woodford Gas Shale Conference, May 23, 2007, PowerPoint presentation. http://www.ogs.ou.edu/pdf/WoodfordOverview.pdf.

Carter, L.S., S.A. Kelley, D.D. Blackwell, and N.D. Naeser (1998) Heat flow and thermal history of the Anadarko basin, Oklahoma: AAPG Bulletin, v. 82, p. 291-316.

Charpentier, D., R. H. Worden, C. G. Dillon and A. C. Aplin (2003) Fabric development and the smectite to illite transition in Gulf of Mexico mudstones; an image analysis approach: Journal of Geochemical Exploration 78-79: 463-459.

Carr, J.L., III (1987) The thermal maturity and clay mineralogy of the Chattanooga Formation along a transect from the Ozark Uplift to the Arkoma Basin: Fayetteville, University of Arkansas, unpublished M.S. thesis, 76 p.

Comer, J.B. (2005) Facies distribution and hydrocarbon production potential of Woodford Shale in the southern Midcontinent, *in* B.J. Cardott, ed., Unconventional energy resources in the southern Midcontinent, 2004 symposium: Oklahoma Geological Survey Circular 110, p. 51-62.

Comer, J.B. (2008) Reservoir characteristics and production potential of the Woodford Shale. World Oil® Magazine, v. 229:8, p. 83-89.

Conant, L. C. and V. E. Swanson (1961) Chattanooga Shale and related rocks of central Tennessee and nearby areas. U. S. Geological Survey Professional Paper. United States, U. S. Geological Survey: Reston, VA, United States.

Cuadros, J. (2006) Modeling of smectite illitization in burial diagenesis environments: Geochimica et Cosmochimica Acta 70: 4181-4195.

Denison, R. E. (1982) Geologic cross section from the Arbuckle mountains to the Meunster arch, southern Oklahoma and Texas: Geological Society of America Map and Chart Series MC 28-R, 8p.

Denison, R.E., E.G. Lidiak, M.E. Bickford and E.B. Kisvarsanyi (1984) Geology and geochronology of the Precambrian rocks in the central region of the United States. U.S. Geol. Surv. Prof. Pap. 1241-C.

Dong, H., C. M. Hall, D. R. Peacor, A. N. Halliday and D. R. Pevear (2000) Thermal 40Ar/39Ar separation of diagenetic from detrital illitic clays in Gulf Coast shales: Earth and Planetary Science Letters 175(3-4): 309-325.

Eberl, D. D. and J. Środoń (1988) Ostwald ripening and interparticle-diffraction effects for illite crystals: American Mineralogist 73: 1345-1335.

Elliott, W.C. and J.L. Aronson (1987) Alleghanian episode of K-bentonite illitization in the southern Appalachian Basin, Geological Society of America: Geology [Boulder], Volume 15: p. 735-739.

Elliott, W. C., J. L. Aronson, G. Matisoff and D. L. Gautier (1991) Kinetics of the smectite to illite transformation in the Denver Basin; clay mineral, K-Ar data, and mathematical model results: AAPG Bulletin. 75: 462-436.

Elliott, W.C. and G. Matisoff (1996) Evaluation of kinetic models for the smectite to illite transformation, Clays and Clay Minerals, v 44: p. 77-87.

Elliott, W. C., S. G. Osborn, V. J. O'Brien, R. D. Elmore, M. H. Engel and J. M. Wampler (2006) On the timing and causes of illite formation and remagnetization in the Cretaceous Marias River Shale, Disturbed Belt, Montana: Journal of Geochemical Exploration 89(1-3): 92-95.

Esquevin, J. (1969) Influence de la composition chimique des illites sur leur cristallinité. Bull. Centre de Recherches de Pau (Soc. National des Pétroles d'Aquitaine), 3, 147-153.

Flawn, P.T., A. Goldstein, Jr., P.B. King and C.E.Weaver (1961) The Ouachita System: Bureau of Economic Geology, University of Texas Publication 6120, 401 p.

Fischer, A.G. (1969) Geological time-distance rates; The Bubnoff unit: Geological Society of America Bulletin, v. 80, p. 551-549.

Gallardo, J. D. and D. D. Blackwell (1999) Thermal structure of the Anadarko Basin: AAPG Bulletin 83: 333-361.

Gharrabi, M., B. Velde and J. P. Sagon (1998) The transformation of illite to muscovite in pelitic rocks; constraints from X-ray diffraction: Clays and Clay Minerals 46: 79-88.

Gilbert, M. C. (1983) Timing and chemistry of igneous events associated with the southern Oklahoma aulacogen: Tectonophysics, v.94, p. 439-455.

Gingele, F.X. (1996) Holocene climate optimum in southwest Africa- evidence from the marine clay mineral record. Palaeogeography, Palaeoclimatology, Palaeocology, 122, 77-87.

Graham, S. A., W. R. Dickinson and R. V. Ingersoll (1975) Himalayan-Bengal model for flysch dispersal in the Appalachian-Ouachita system: Geological Society of America Bulletin 86: 286-273.

Grathoff, G.H., and D.M. Moore, 1996, Illite polytype quantification using WILDFIRE calculated X-ray diffraction patterns: Clays and Clay Minerals, v. 44, p. 835-842.

Guthrie, J. M., D. W. Houseknecht and W. D. Johns (1986) Relationships among vitrinite reflectance, illite crystallinity, and organic geochemistry in Carboniferous strata, Ouachita Mountains, Oklahoma and Arkansas. AAPG Bulletin 70: 26-33.

Güven, N. (2001) Mica structure and fibrous growth of illite, Clays and Clay Minerals, v 49: p. 189-196.

Ham, W. E. and J. L. Wilson (1967) Paleozoic epeirogeny and orogeny in the central United States: American Journal of Science 265: 332-407.

Ham, W.E. (1969) Regional geology of the Arbuckle mountains, Oklahoma: Oklahoma Geologica Survey Guidebook 17, 52 p.

Ham, W.E., T.W. Amsden, R.E. Denison, J.R. Derby, R.O. Fay, A.A. Graffham, T.L. Rowland, R.L. Squires, J.H. Stitt and E.W.Wiltse (1973) Regional geology of the Arbuckle Mountains, Oklahoma: OGS Special Publication 73-3, 61 p.

Haq, B. U. and S. R. Schutter (2008) A chronology of Paleozoic sea-level changes. Science. American Association for the Advancement of Science: 322: 68-64.

Harrison, W. J. and G. D. Thyne (1992) Predictions of diagenetic reactions in the presence of organic acids. Geochimica et Cosmochimica Acta 56(2): 565-586.

Hatcher, R.D., Jr. (2002) Alleghanian (Appalachian) orogeny, a product of zipper tectonics: Rotational tranpressive continent-continent collision and closing of ancient oceans along irregular margins, *in* Martínez Catalán, J.R. Hatcher, R.D., Jr., Arenas, R., and Díaz García, F., eds., Variscan-Appalachian dynamics: The building of the late Paleozoic basement: Geological Society of America Special Paper 364, p. 199-208.

Hester, T.C., H.L. Sahl, and J.W. Schmoker (1988) Cross sections based on gamma-ray, density, and resistivity logs showing stratigraphic units of the Woodford Shale, Anadarko basin, Oklahoma: U.S. Geological Survey Miscellaneous Field Studies Map MF-2054, 2 sheets.

Hester, T.C., J.W. Schmoker, and H.L. Sahl (1990) Log-derived regional source-rock characteristics of the Woodford Shale, Anadarko basin, Oklahoma: U.S. Geological Survey Bulletin 1866-D, 38 p.

Hester, T.C., J.W. Schmoker, and H.L. Sahl (1992) Structural controls on sediment distribution and thermal maturation of the Woodford Shale, Anadarko basin, Oklahoma, in K.S. Johnson and B.J. Cardott, eds., Source rocks in the southern Midcontinent, 1990 symposium: OGS Circular 93, p. 321-326.

Hester, T.C., and J.W. Schmoker (1993) Regional geology of the Woodford Shale, Anadarko basin, Oklahoma—an overview of relevance to horizontal drilling, in K.S. Johnson and J.A. Campbell, eds., Petroleum-reservoir geology in the southern midcontinent, 1991 symposium: OGS Circular 95, p. 74-81.

Hoffman, J. and J. Hower (1979) Clay mineral assemblages as low grade metamorphic geothermometers: application to the thrust faulted disturbed belt of Montana, USA: Society of Economic Paleontologists and Mineralogists Special Publication 26: 55-79.

Houseknecht, D. W. and S. M. Matthews (1985) Thermal maturity of Carboniferous strata, Ouachita Mountains: AAPG Bulletin 69: 335-345.

Hower, J. and T. C. Mowatt (1966) The mineralogy of illites and mixed-layer illite/montmorillonites: American Mineralogist 51: 854-825.

Hower, J., E. Eslinger, M. E. Hower and E. A. Perry (1976) Mechanism of burial metamorphism of argillaceous sediment; 1, Mineralogical and chemical evidence: Geological Society of America Bulletin 87: 725-737.

Hower, J. (1981) X-ray diffraction identification of mixedlayer clay minerals: in Clays and the Resource Geologist, F. J. Longstaffe, ed., Mineral. Assoc. Canada, 39-59.

Huang, W.L., J. M. Longo and D. R. Pevear (1993) An experimentally derived kinetic model for smectite-to-illite conversion and its use as a geothermometer: Clays and Clay Minerals 41: 162-177.

Inoue, A., B. Velde, A. Meunier and G. Touchard (1988) Mechanism of illite formation during smectite-to-illite conversion in a hydrothermal system: American Mineralogist, 73: 1334-1325.

Jaboyedoff, M., F. Bussy, B. Kübler and P. Thelin (2001) Illite crystallinity revisited. Clays and Clay Minerals 49(2): 156-167.

Jackson, M. L. (1985) Soil Chemical Analysis- Advanced Course, Published by the author, Madison, Wis. 53705.

Jackson, T. A. (1977) A relationship between crystallographic properties of illite and chemical properties of extractable organic matter in pre-Phanerozoic and Phanerozoic sediments. Clays and Clay Minerals 25(3): 187-195.

Johnson, K.S. et al. (1988) Southern Midcontinent region, *in* L.L. Sloss, ed., Sedimentary cover—North America craton; U.S.: GSA, The Geology of North America, v. D-2, p. 307-359. (Reprinted as OGS Special Publication 89-2)

Johnson, Kenneth S. (1989) Geologic evolution of the Anadarko basin, *in* K. S. Johnson, ed., Anadarko basin symposium, 1988: OGS Circular 90, p. 3-12

Johnson, K.S., and B.J. Cardott (1992) Geologic framework and hydrocarbon source rocks of Oklahoma, in K.S. Johnson and B.J. Cardott, eds., Source rocks in the southern Midcontinent, 1990 symposium: OGS Circular 93, p. 21-37.

Jorgensen, Donald G. (1989) Paleohydrology of the Anadarko Basin, Central United States, *in* K. S. Johnson, ed., Anadarko basin symposium, 1988: OGS 90, p. 176-193.

Kharaka, Y. K., L. M. Law, W. W. Carothers and D. F. Goerlitz (1986) Role of organic species dissolved in formation waters from sedimentary basins in mineral diagenesis: Special Publication - Society of Economic Paleontologists and Mineralogists (SEPM) 38: 122-111.

Kirkland, D.W., R.E. Denison, D.M. Summers, and J.R. Gormly (1992) Geology and organic geochemistry of the Woodford Shale in the Criner Hills and western Arbuckle Mountains, in K.S. Johnson and B.J. Cardott, eds., Source rocks in the southern Midcontinent, 1990 symposium: OGS Circular 93, p. 38-69.

Kübler, B. (1968) Evaluation quantitative du metamorphisme par la cristallinite de l'illite; etat des progres realises ces dernieres annees. Quantitative evaluation of metamorphism using the crystallinity of illite; progress of the past few years 2: 385-397.

Lanson, B., B. Velde and A. Meunier (1998) Late-stage diagenesis of illitic clay minerals as seen by decomposition of X-ray diffraction patterns; contrasted behaviors of sedimentary basins with different burial histories: Clays and Clay Minerals 46: 69-78.

Lee, Y. and D. Deming (1999) Heat flow and thermal history of the Anadarko Basin and the western Oklahoma Platform: Tectonophysics 313(4): 399-410.

Lewan, M.D. (1983) Effects of thermal maturation on stable organic carbon isotopes as determined by hydrous pyrolysis of Woodford Shale: Geochimica et Cosmochimica Acta, v. 47, p. 1471-1479.

Lewan, M.D. (1985) Evaluation of petroleum generation by hydrous pyrolysis experimentation. Phylos. Trans. R. Soc. London, A315, 123-124.

Lewan, M. D. and T. E. Ruble (2002) Comparison of petroleum generation kinetics by isothermal hydrous and nonisothermal open-system pyrolysis: Organic Geochemistry 33: 1457-1475.

Lo, H.B. (1993) Correction criteria for the suppression of vitrinite reflectance in hydrogen-rich kerogens: preliminary guidelines. Organic Geochemistry 20, 653-657.

Lundegard, P. D. and Y. K. Kharaka (1990) Geochemistry of organic acids in subsurface waters; field data, experimental data, and models: ACS Symposium Series. American Chemical Society 416: 189-169.

Lynch, F. L., L. E. Mack and L. S. Land (1997) Burial diagenesis of illite/smectite in shales and the origins of authigenic quartz and secondary porosity in sandstones: Geochimica et Cosmochimica Acta 61: 1995-2006.

MacGowan, D. B. and R. C. Surdam (1990) Carboxylic acid anions in formation waters, San Joaquin Basin and Louisiana Gulf Coast, U.S.A.--Implications for clastic diagenesis: Applied Geochemistry 5(5-6): 687-701.

Meunier, A. and B. Velde (2004) Illite; origins, evolution and metamorphism. Federal Republic of Germany, Springer-Verlag : Berlin, Federal Republic of Germany.

Moore, D. M. and R. C. Reynolds (1997) X-ray diffraction and the identification and analysis of clay minerals. Oxford; New York, Oxford University Press.

Nadeau, P. H. and D. C. Bain (1986) Composition of some smectites and diagenetic illitic clays and implications for their origin. Clays and Clay Minerals 34: 455-464.

Nadeau, P. H., M. J. Wilson, W. J. McHardy and J. M. Tait (1984) Interstratified clays as fundamental particles: Science 225: 923-925.

Nance, R. D. and U. Linnemann (2008) The Rheic Ocean; origin, evolution, and significance: GSA Today 18: 12-4.

North, F. K. (1985) Petroleum Geology, Allen and Unwin.

Northcutt, R.A., K.S. Johnson, and G.C. Hinshaw (2001) Geology and petroleum reservoirs in Silurian, Devonian, and Mississippian rocks in Oklahoma, in K.S. Johnson, ed., Silurian, Devonian, and Mississippian geology and petroleum in the southern Midcontinent, 1999 symposium: OGS Circular 105, p. 1-15.

Oelkers, E. H. and J. Schott (1998) Does organic acid adsorption affect alkali-feldspar dissolution rates? Chemical Geology 151(1-4): 235-245.

Ohr, M., A. N. Halliday and D. R. Peacor (1991) Sr and Nd isotopic evidence for punctuated clay diagenesis, Texas Gulf Coast: Earth and Planetary Science Letters 105: 126-110.

Over, D. J. (1990) Conodont biostratigraphy of the Woodford Shale (Late Devonian-Early Carboniferous) in the Arbuckle Mountains, south-central Oklahoma: Abstract of Dissertation, Texas Tech University.

Palandri, J. L. and M. H. Reed (2001) Reconstruction of in situ composition of sedimentary formation waters: Geochimica et Cosmochimica Acta 65(11): 1741-1767.

Peltonen, C., O. Marcussen, K. Bjorlykke and J. Jahren (2008) Mineralogical control on mudstone compaction; a study of Late Cretaceous to early Tertiary mudstones of the Voring and More Basins, Norwegian Sea. Petroleum Geoscience. Geological Society Publishing House for EAGE (European Association of Geoscientists & Engineers): 14: 138-127.

Perry, E. and J. Hower (1970) Burial diagenesis in Gulf Coast pelitic sediments: Clays and Clay Minerals 18: 177-165.

Pevear, D. R., V. E. Williams and G. E. Mustoe (1980) Kaolinite, smectite, and K-rectorite in bentonites; relation to coal rank at Tulameen, British Columbia. Clays and Clay Minerals 28(4): 241-254.

Pevear, D. R. (1999) Illite and hydrocarbon exploration: Proceedings of the National Academy of Sciences 96(7): 3440-3446.

Pytte, A. M. and R. C. Reynolds (1989) The thermal transformation of smectite to illite: United States, Springer-Verlag: New York, NY, United States.

Ramseyer, K. and J. R. Boles (1986) Mixed-layer illite/smectite minerals in Tertiary sandstones and shales, San Joaquin Basin, California: Clays and Clay Minerals 34: 124-115.

Ransom, B. and H. C. Helgeson (1994) Estimation of the standard molal heat capacities, entropies, and volumes of 2:1 clay minerals: Geochimica et Cosmochimica Acta 58: 4547-4537.

Reynolds, R. J. (1968) The effect of particle size on apparent lattice spacings. Acta Crystallographica Section A 24(2): 319-320.

Roberts, C.T., and R.M. Mitterer (1992) Laminated black shale-bedded chert cyclicity in the Woodford Formation, southern Oklahoma, in K.S. Johnson and B.J. Cardott, eds., Source rocks in the southern Midcontinent, 1990 symposium: OGS Circular 93, p. 330-336.

Ross, R. J. and S. M. Bergstrom (1982) The Ordovician system in the United States : correlation chart and explanatory notes. [Paris], International Union of Geological Sciences, International Subcommission on Ordovician, Stratigraphy.

Saleemi, A. A. and Z. Ahmed (2000) Mineral and chemical composition of Karak Mudstone, Kohat Plateau, Pakistan; implications for smectite-illitization and provenance: Sedimentary Geology 130: 247-229.

Sass, B. M., P. E. Rosenberg and J. A. Kittrick (1987) The stability of illite/smectite during diagenesis: An experimental study: Geochimica et Cosmochimica Acta 51(8): 2103-2115.

Schmoker, J.W. and D.L. Gautier (1989) Compaction of basin sediments: modeling based on time-temperature history: Journal of Geophysical research, v. 94, p. 7379-7386.

Spöetl, C., D. W. Houseknecht and R. Jaques (1993) Clay mineralogy and illite crystallinity of the Atoka Formation, Arkoma Basin, and frontal Ouachita Mountains. Clays and Clay Minerals 41: 745-754.

Środoń, J. (1984) X-ray powder diffraction identification of illitic materials. Clays and Clay Minerals 32(5): 337-349.

Środoń, J. (1990) Illite-Smectite in the rock cycle: Lectures 6th Meet. European Clay Groups. Seville: 137-150.

Środoń J., Drits V.A. McCarty D.K., Hsieh J.C.C. and Eberl D.D (1999) Quantitative mineral analysis by powder X-ray diffraction from random preparations. Texaco Upstream Technology, Report 99-0134, 43 pp.

Sullivan, K.L. (1985) Organic facies variation of the Woodford Shale in western Oklahoma: Shale Shaker, v. 35, p. 76-89.

Urban, J.B. (1960) Microfossils of the Woodford Shale (Devonian) of Oklahoma: Norman, University of Oklahoma, unpublished M.S. thesis, 77 p.

Velde, B. (1980) Cell dimensions, polymorph type, and infrared spectra of synthetic white micas; the importance of ordering: American Mineralogist 65: 1282-1277.

Velde, B. and J. Hower (1963) Petrological significance of illite polymorphism in Paleozoic sedimentary rocks: American Mineralogist 48: 1239-1254.

Viele, G. W. (1982) Southern Appalachian-Ouachita dissimilarities: Abstracts with Programs - Geological Society of America 14: 93-93.

Wang, H. D. and R. P. Philp (1997) Geochemical study of potential source rocks and crude oils in the Anadarko Basin, Oklahoma: AAPG Bulletin 81: 249-275.

Waples, D. W. (June 1980) Time and temperature in petroleum formation; application of Lopatin's method to petroleum exploration: AAPG Bulletin 64(6): 916-926.

Warr, L.N. and A.H.N.Rice (1994) Interlaboratory standardization and calibration of clay mineral crystallinity and crystallite size data. Journal of Metamorphic Geology, 12, 141-152.

Weaver, C. E. (1958) The effects and geologic significance of potassium 'fixation' by expandable clay minerals derived from muscovite, biotite, chlorite, and volcanic material: American Mineralogist 43: 861-839.

Weaver, C. E. (1960) Possible uses of clay minerals in search for oil. AAPG Bulletin 44(9): 1505-1518.

Weaver, C. E. and B. R. Broekstra (1984) Illite-mica Developments in petrology: Netherlands, Elsevier: Amsterdam, Netherlands.

Whitney, G. and B. Velde (1993) Changes in particle morphology during illitization; an experimental study: Clays and Clay Minerals 41: 218-209.

Appendix A: Bulk Clay Mineralogy XRD Patterns

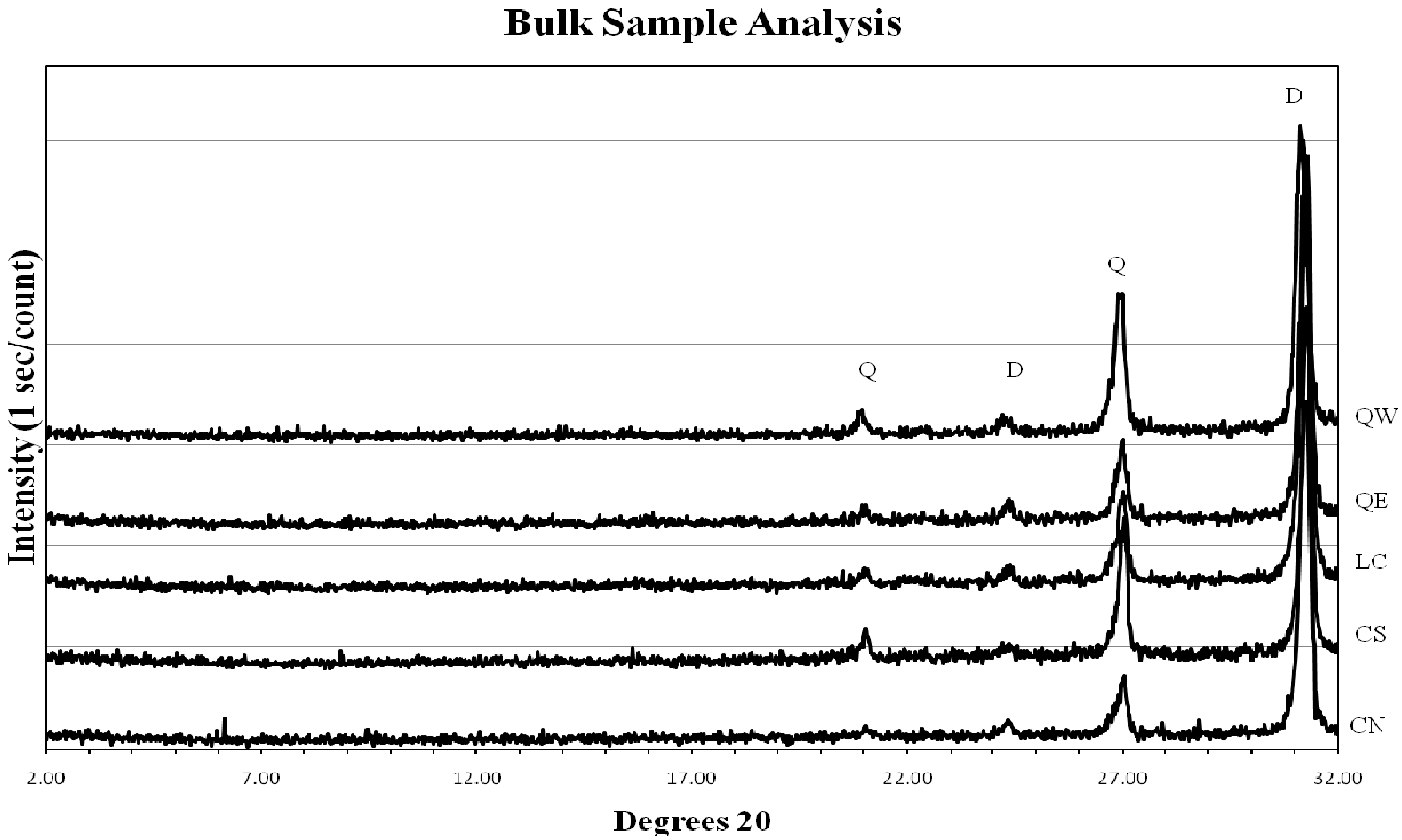

Figure A.1- Stacked XRD patterns for all samples displaying the bulk clay mineralogy.

Appendix B: Air Dry, Ethylene Glycol Solvated and Heated Sample Patterns

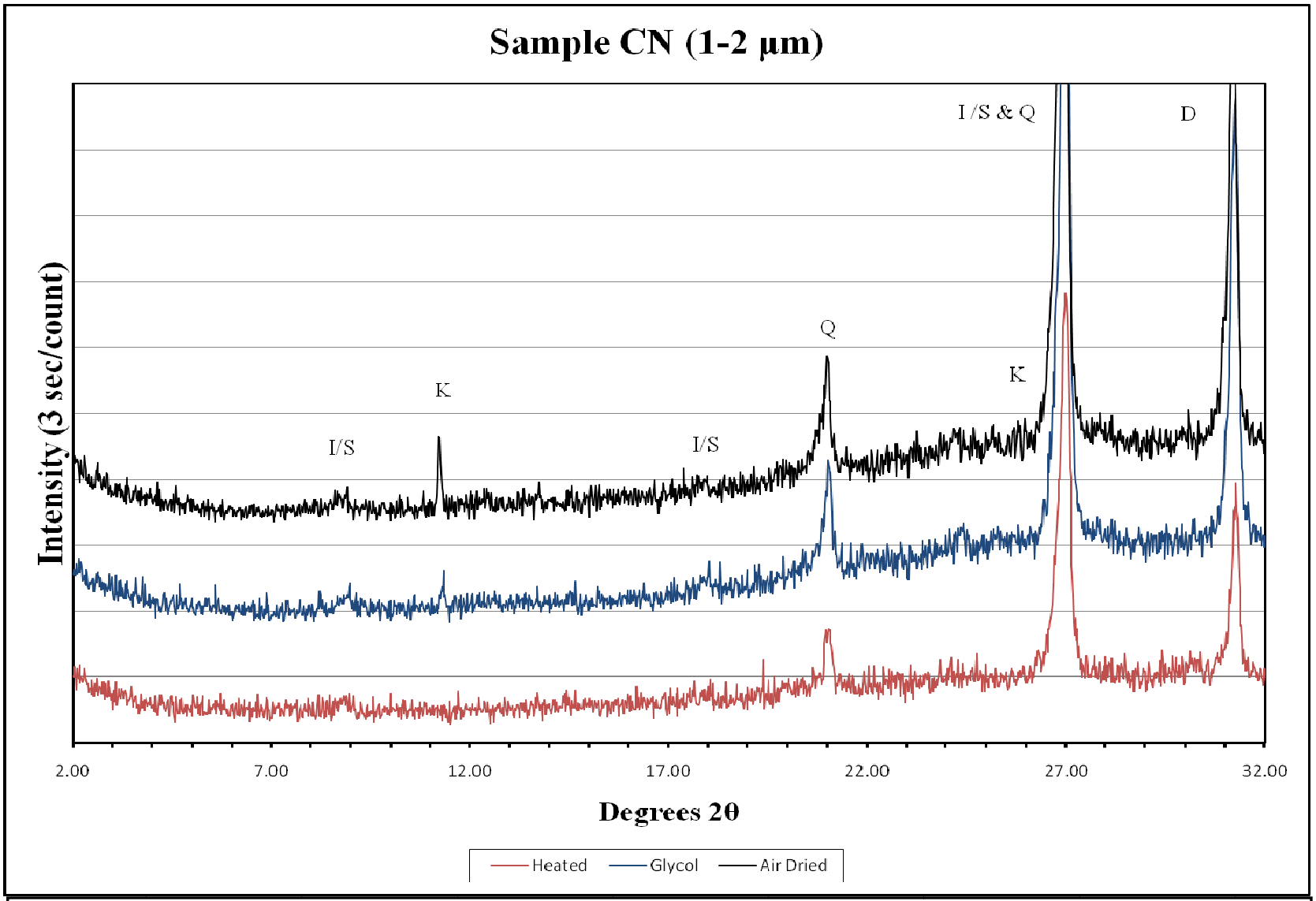

Figure B.1- Air-dried, ethylene glycol solvated and heated XRD patterns for sample CN (1-2 µm).

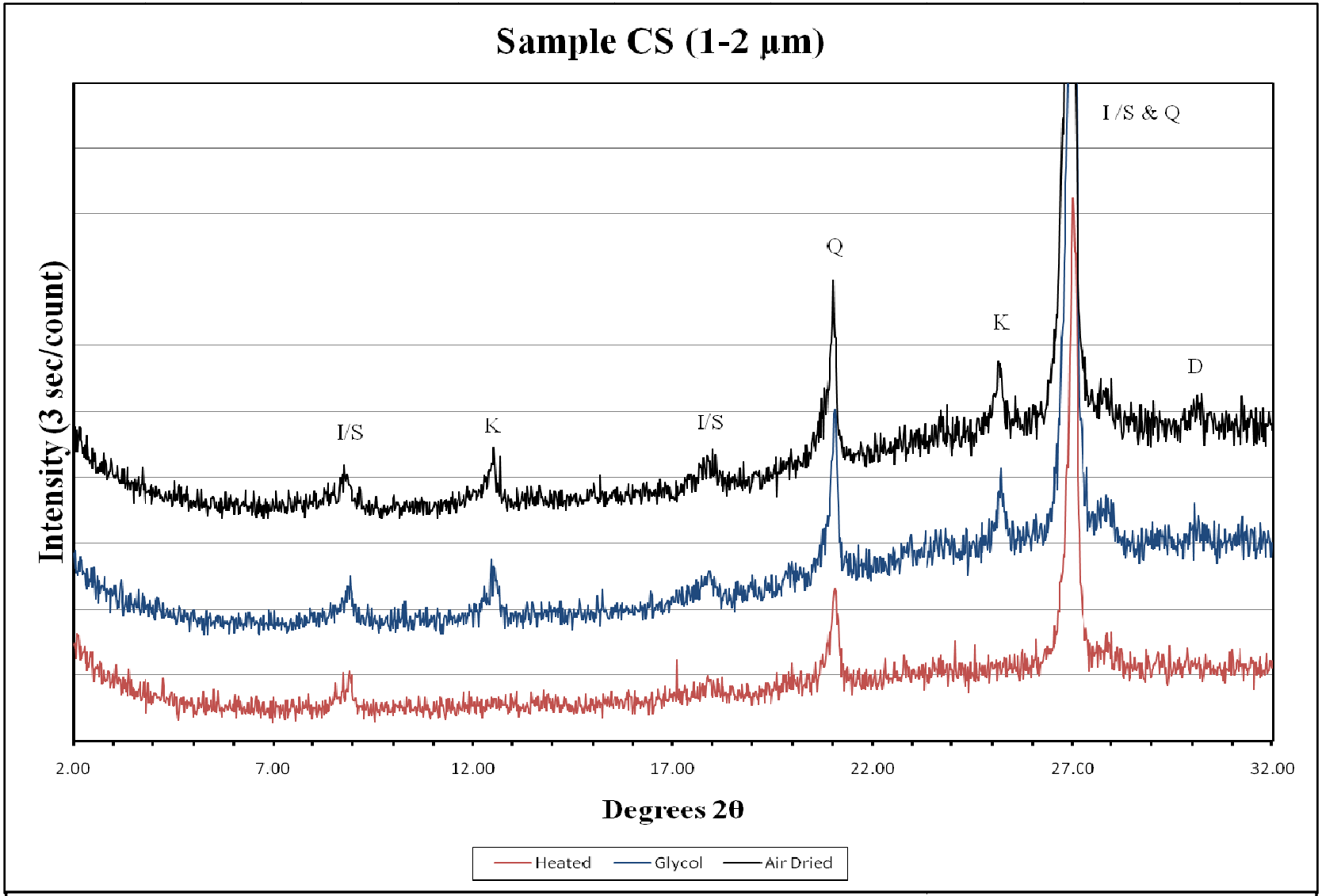

Figure B.2- Air-dried, ethylene glycol solvated and heated XRD patterns for sample CS (1-2 µm).

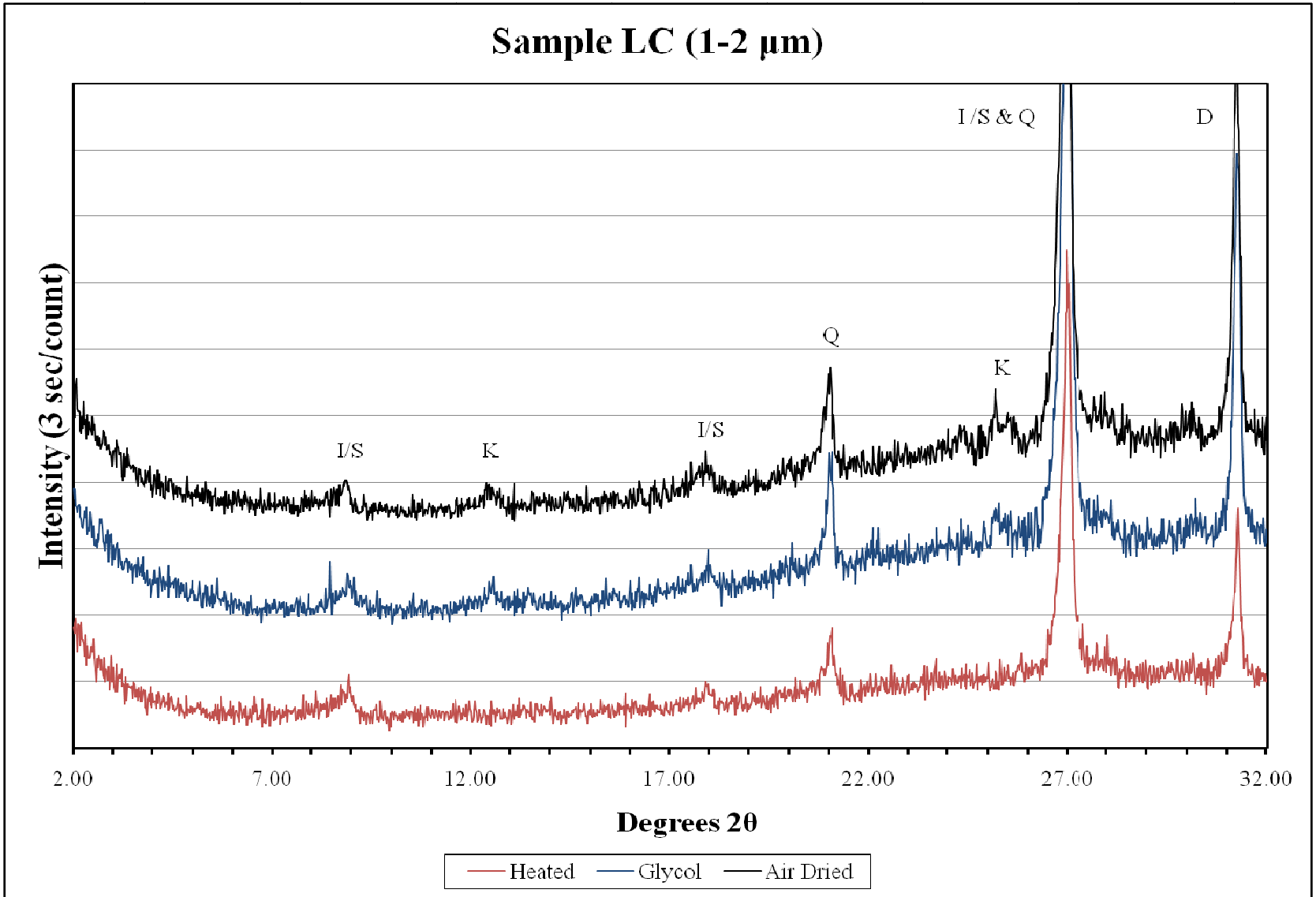

Figure B.3- Air-dried, ethylene glycol solvated and heated XRD patterns for sample LC (1-2 µm).

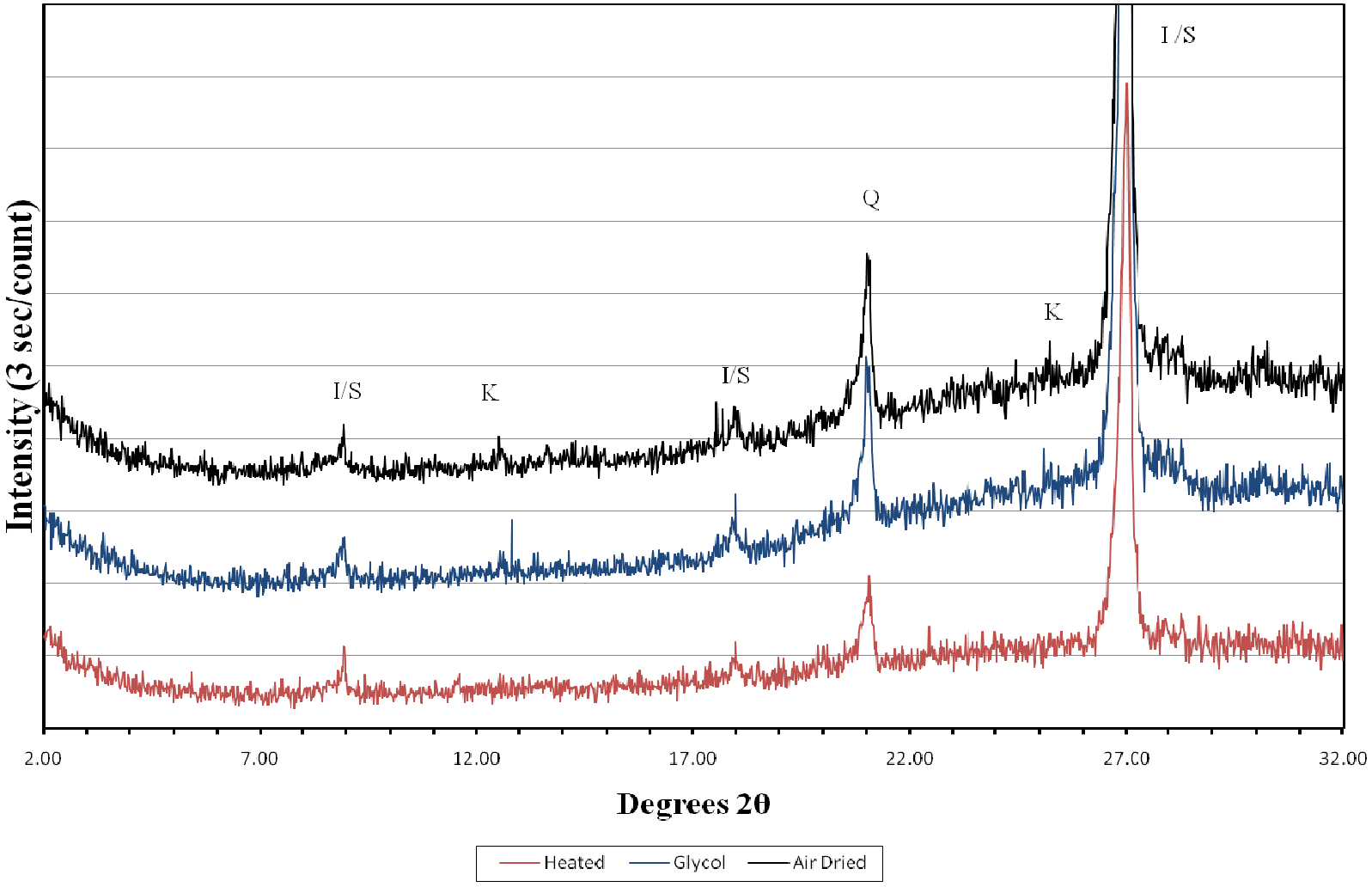

Figure B.4- Air-dried, ethylene glycol solvated and heated XRD patterns for sample QE (1-2 µm).

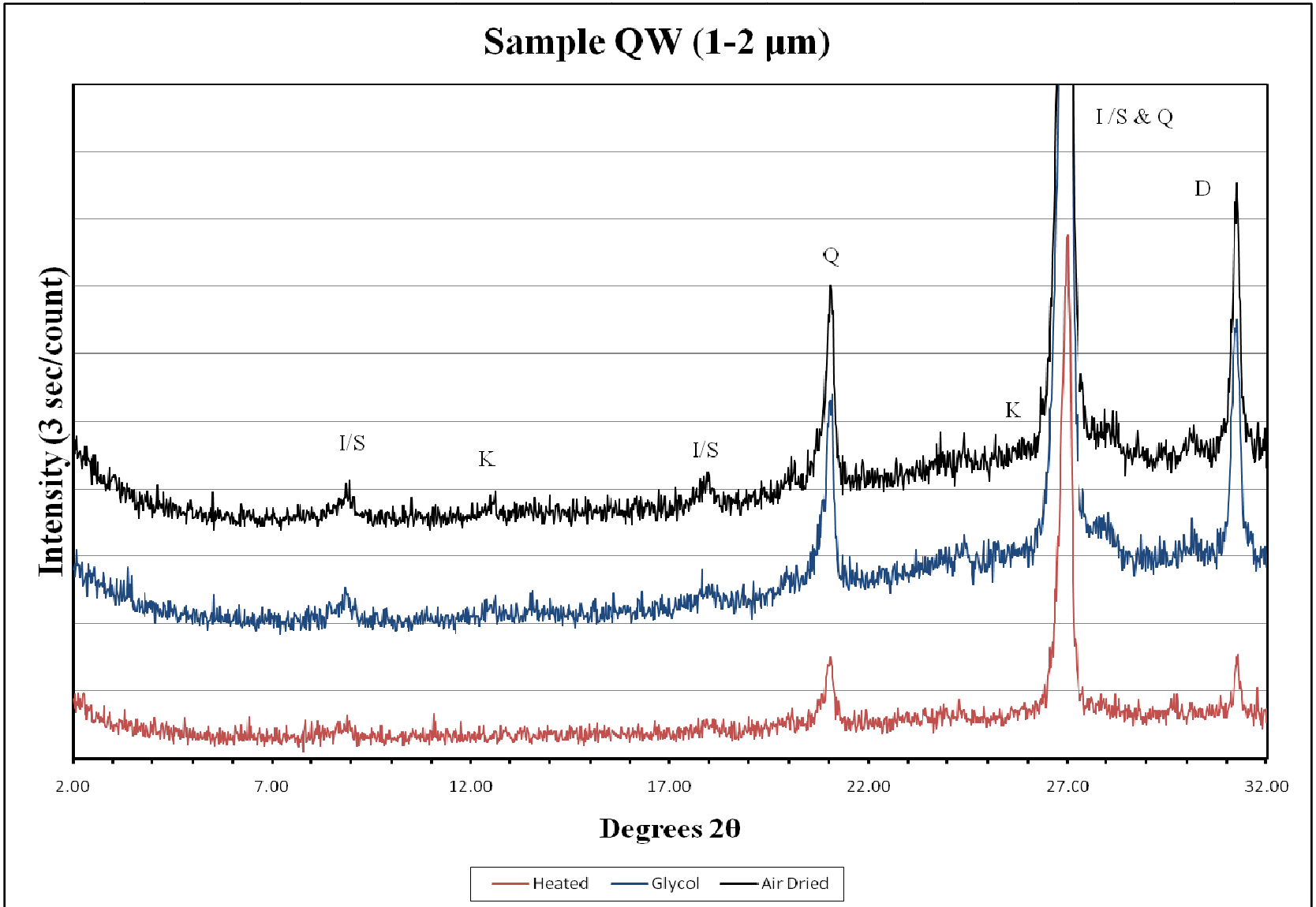

Figure B.5- Air-dried, ethylene glycol solvated and heated XRD patterns for sample QW (1-2 µm).

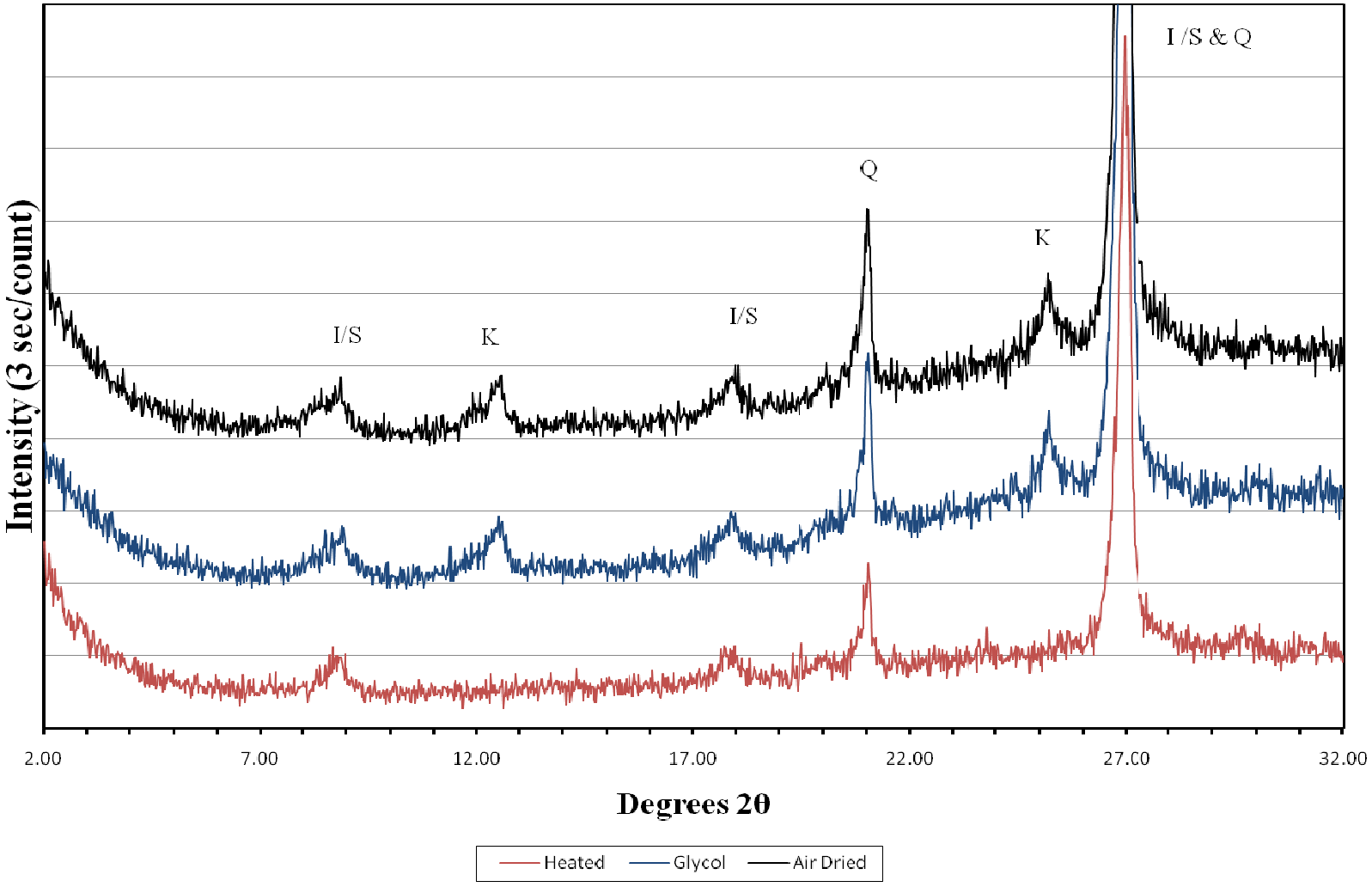

Figure B.6- Air-dried, ethylene glycol solvated and heated XRD patterns for sample CN (0.25-1 µm).

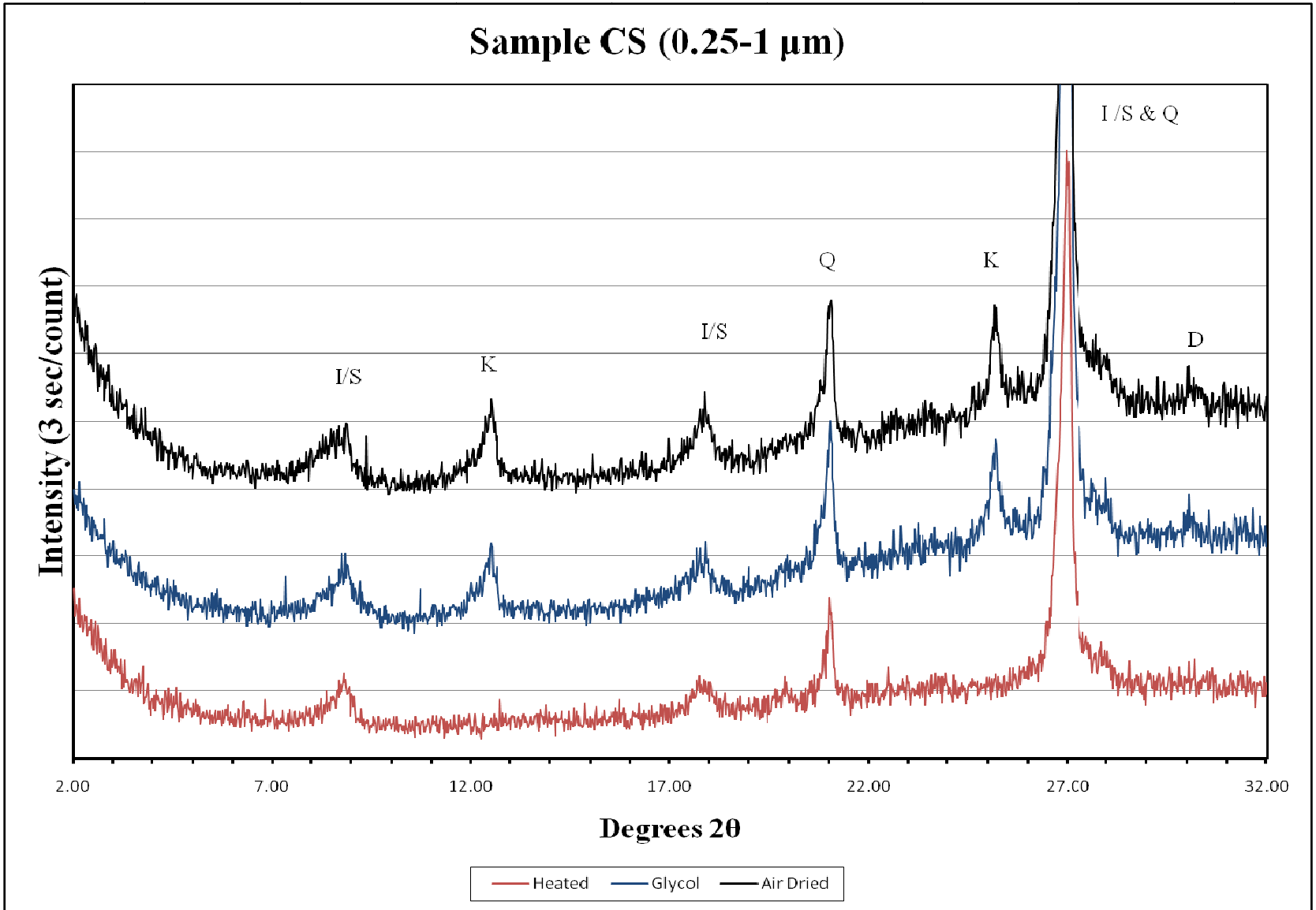

Figure B.7- Air-dried, ethylene glycol solvated and heated XRD patterns for sample CS (0.25-1 µm).

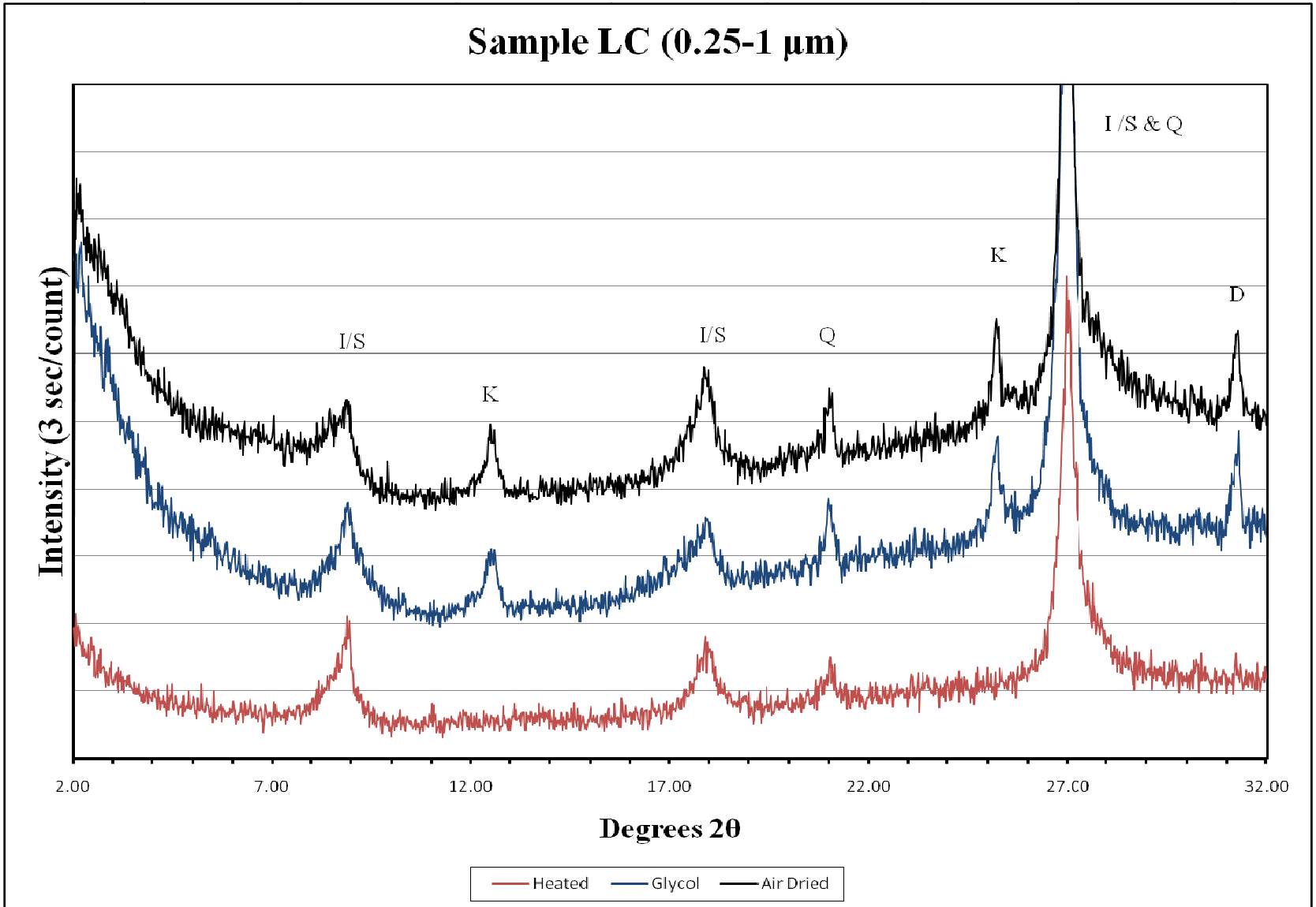

Figure B.8- Air-dried, ethylene glycol solvated and heated XRD patterns for sample LC (0.25-1 µm).

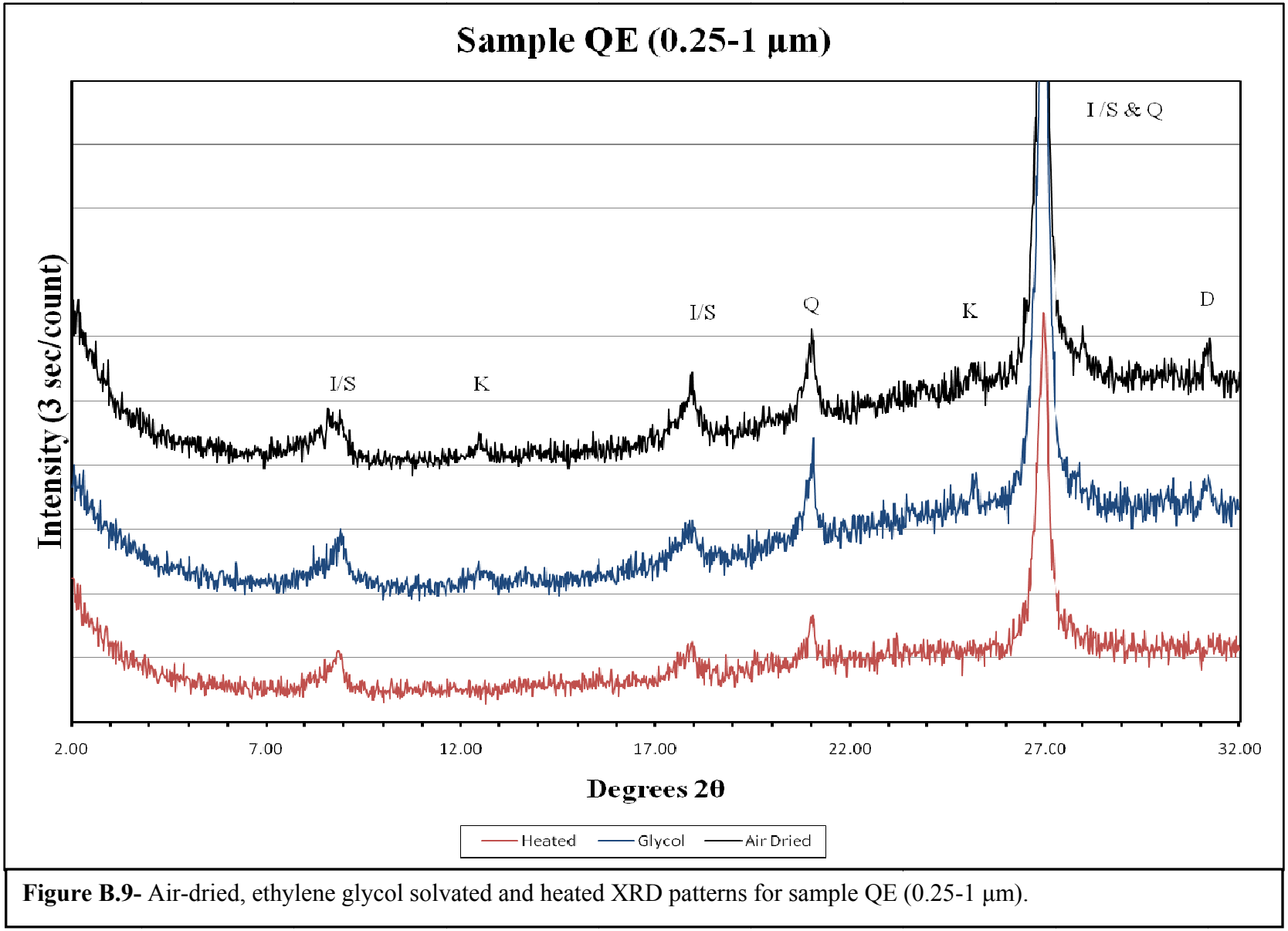

Figure B.9- Air-dried, ethylene glycol solvated and heated XRD patterns for sample QE (0.25-1 µm).

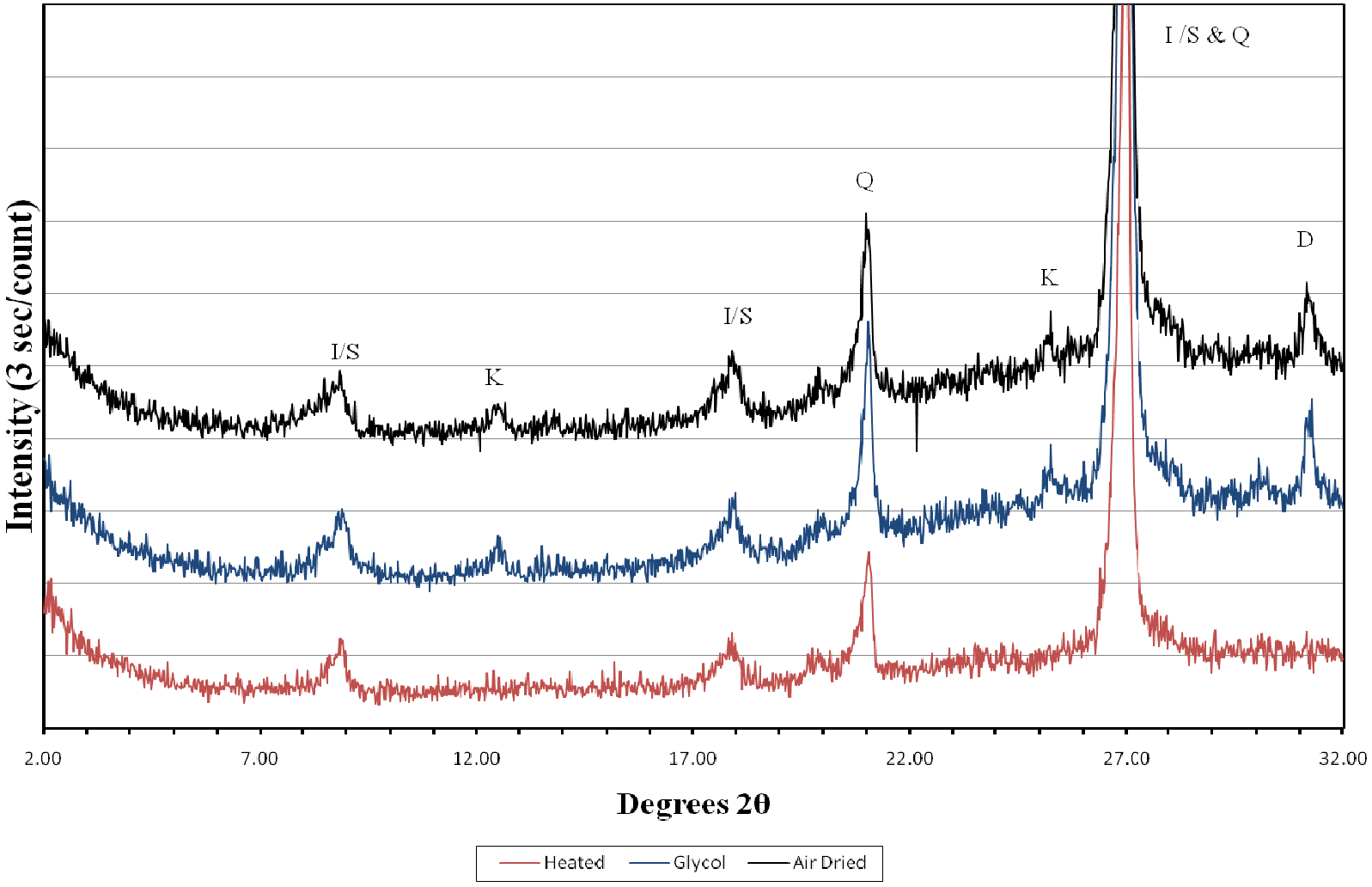

Figure B.10- Air-dried, ethylene glycol solvated and heated XRD patterns for sample QW (0.25-1 µm).

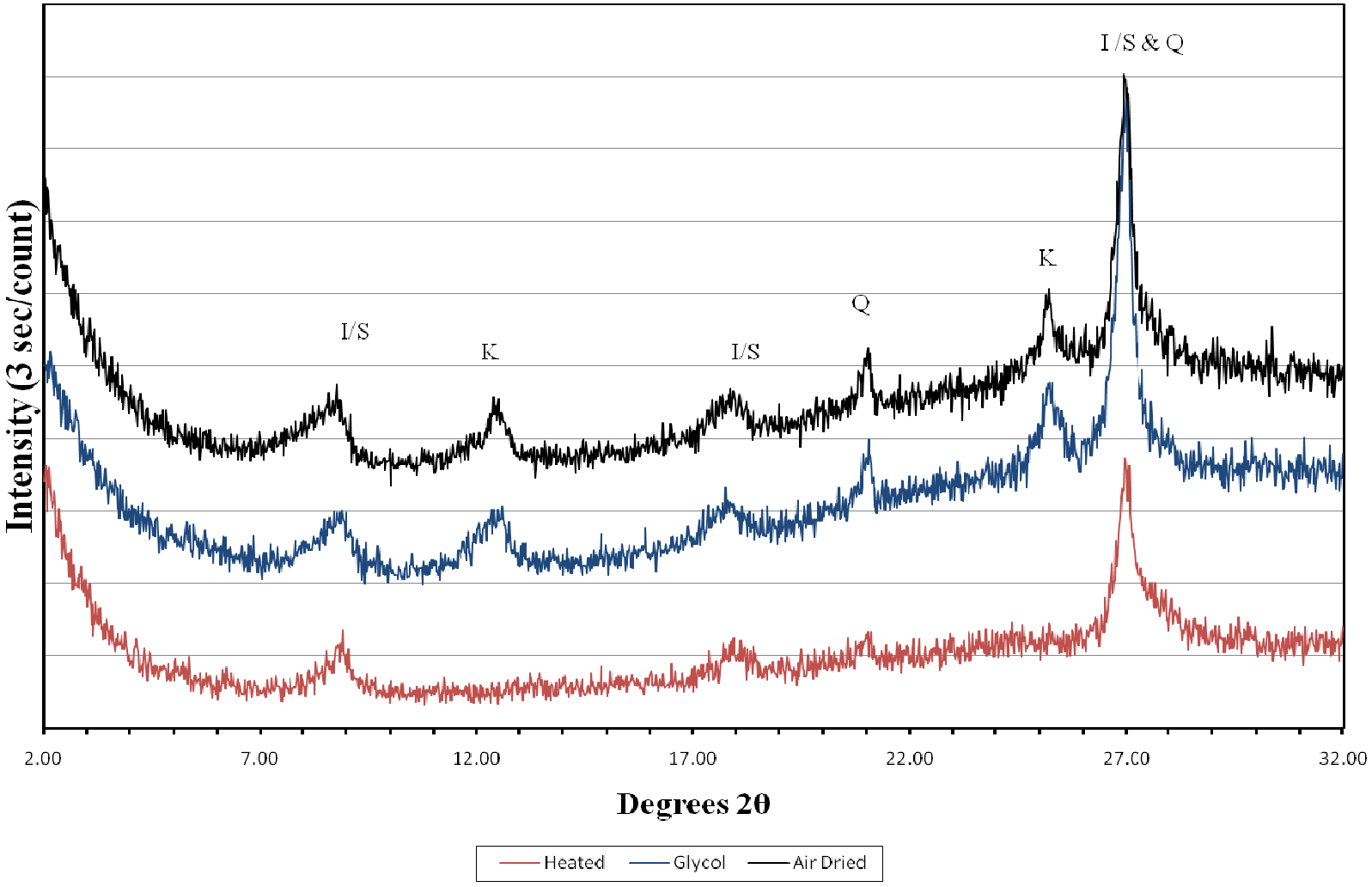

Figure B.11- Air-dried, ethylene glycol solvated and heated XRD patterns for sample CN (<0.25 µm).

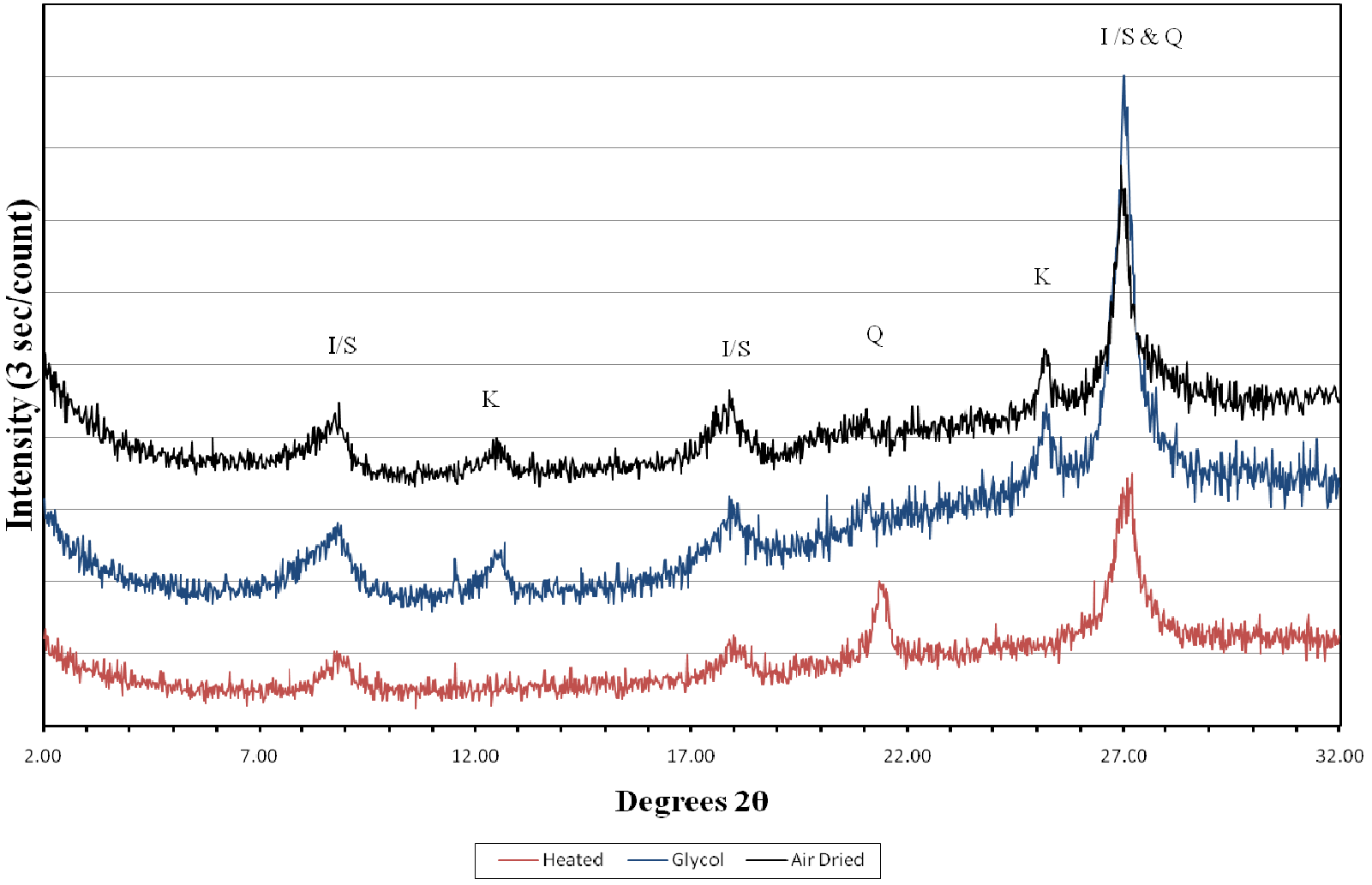

Figure B.12- Air-dried, ethylene glycol solvated and heated XRD patterns for sample CS (<0.25 µm).

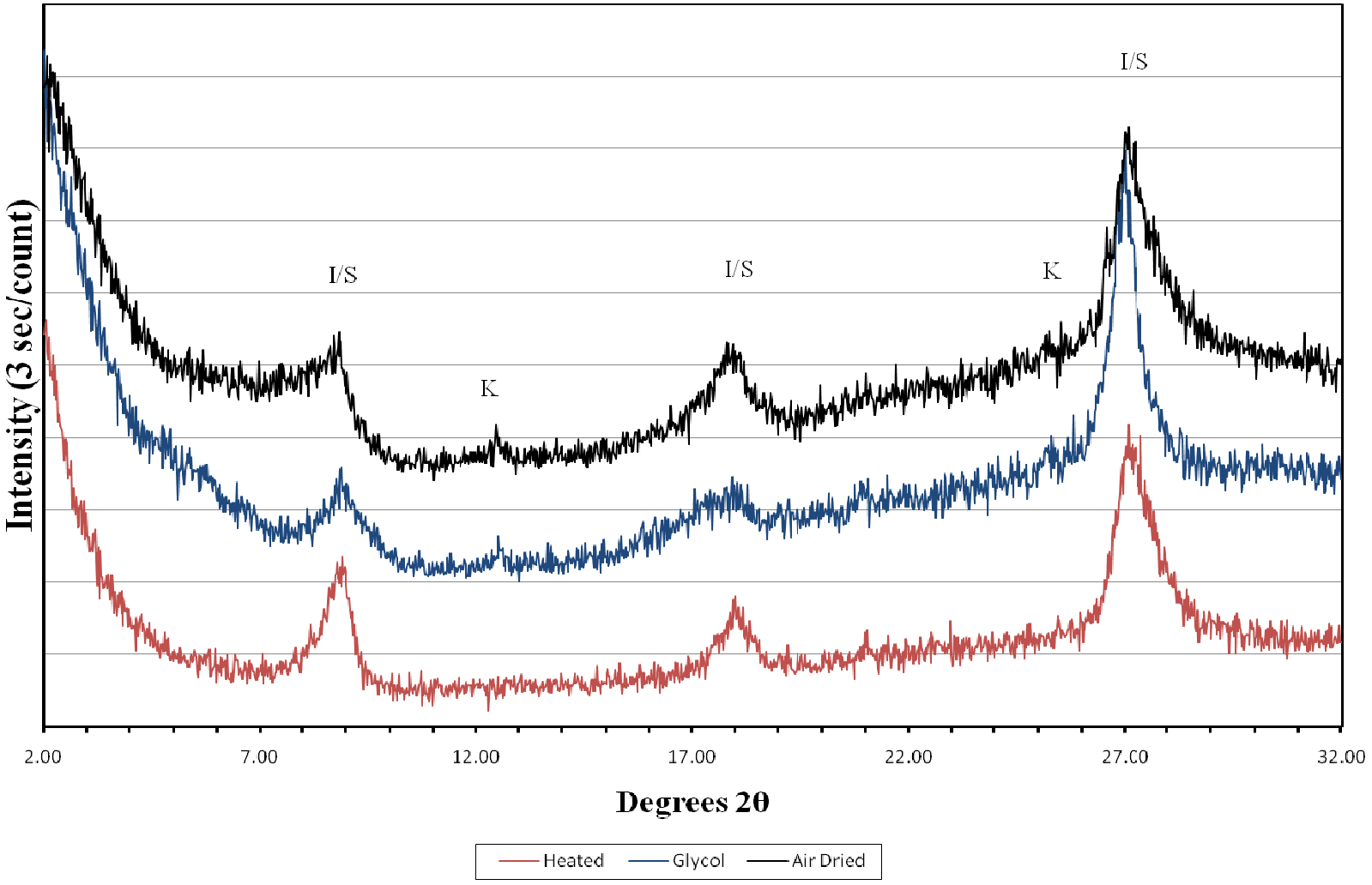

Figure B.13- Air-dried, ethylene glycol solvated and heated XRD patterns for sample LC (<0.25 µm).

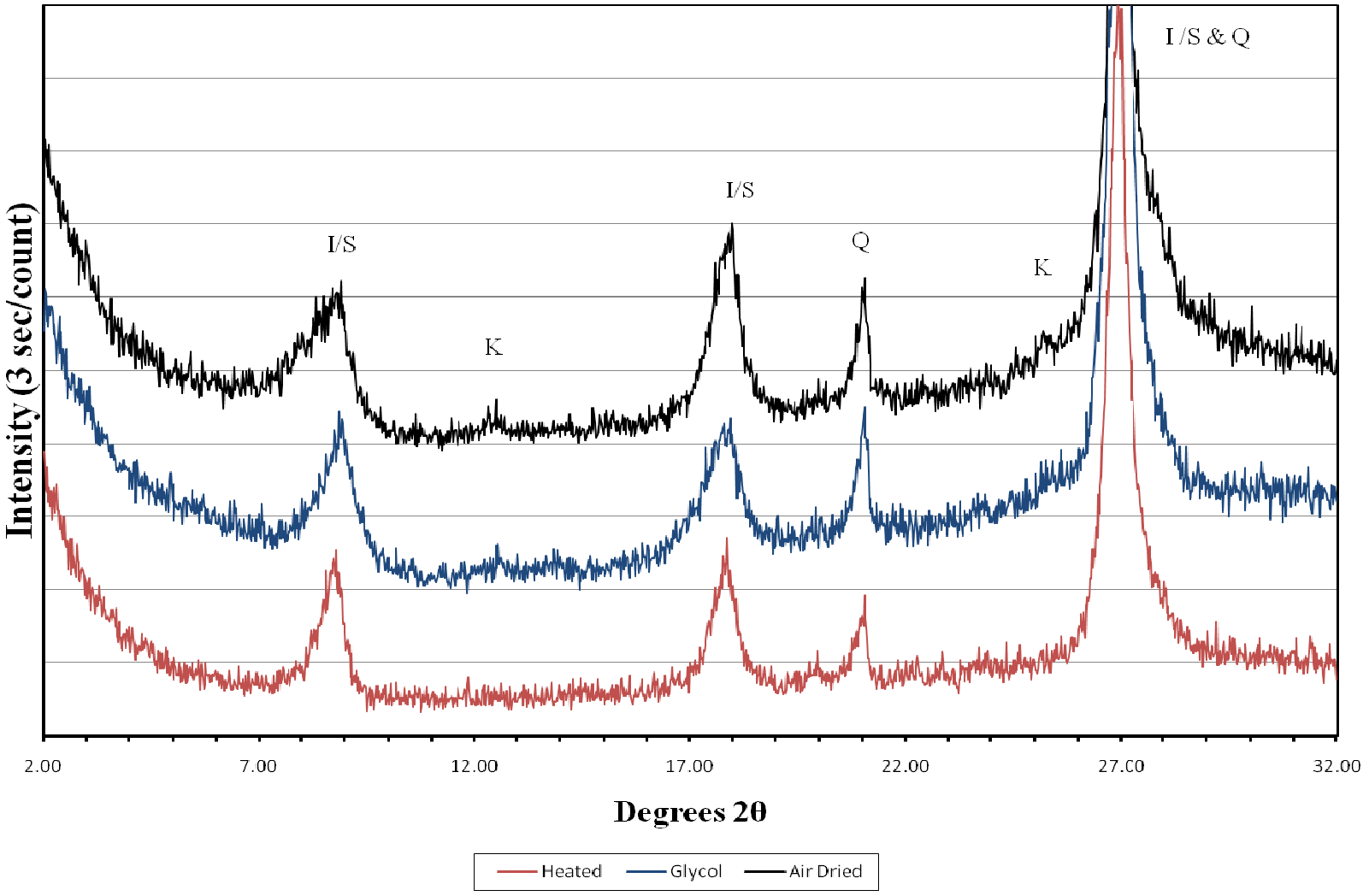

Figure B.14- Air-dried, ethylene glycol solvated and heated XRD patterns for sample QE (<0.25 µm).

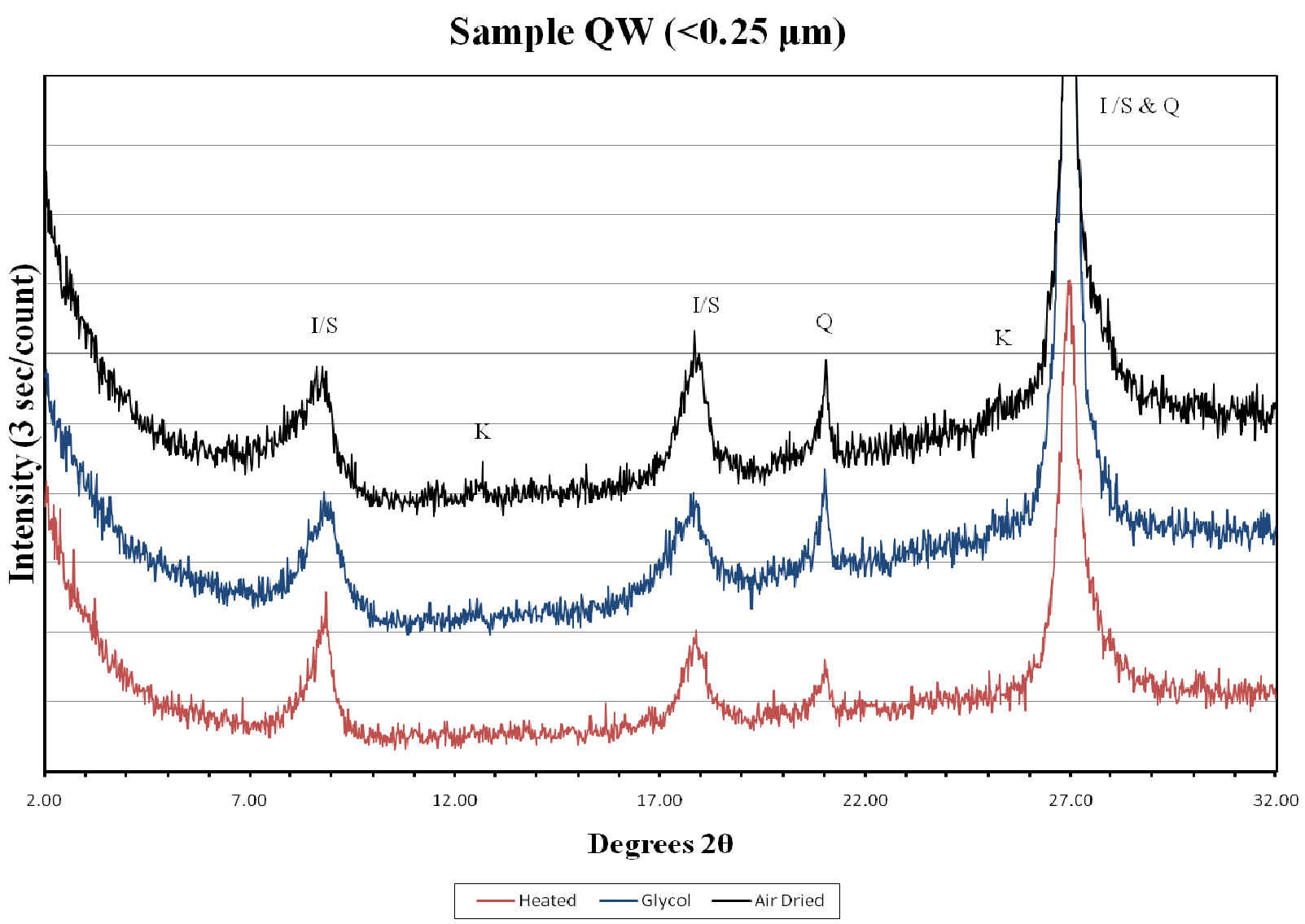

Figure B.15- Air-dried, ethylene glycol solvated and heated XRD patterns for sample QW (<0.25 µm).

Appendix C: Illite Polytype XRD Patterns

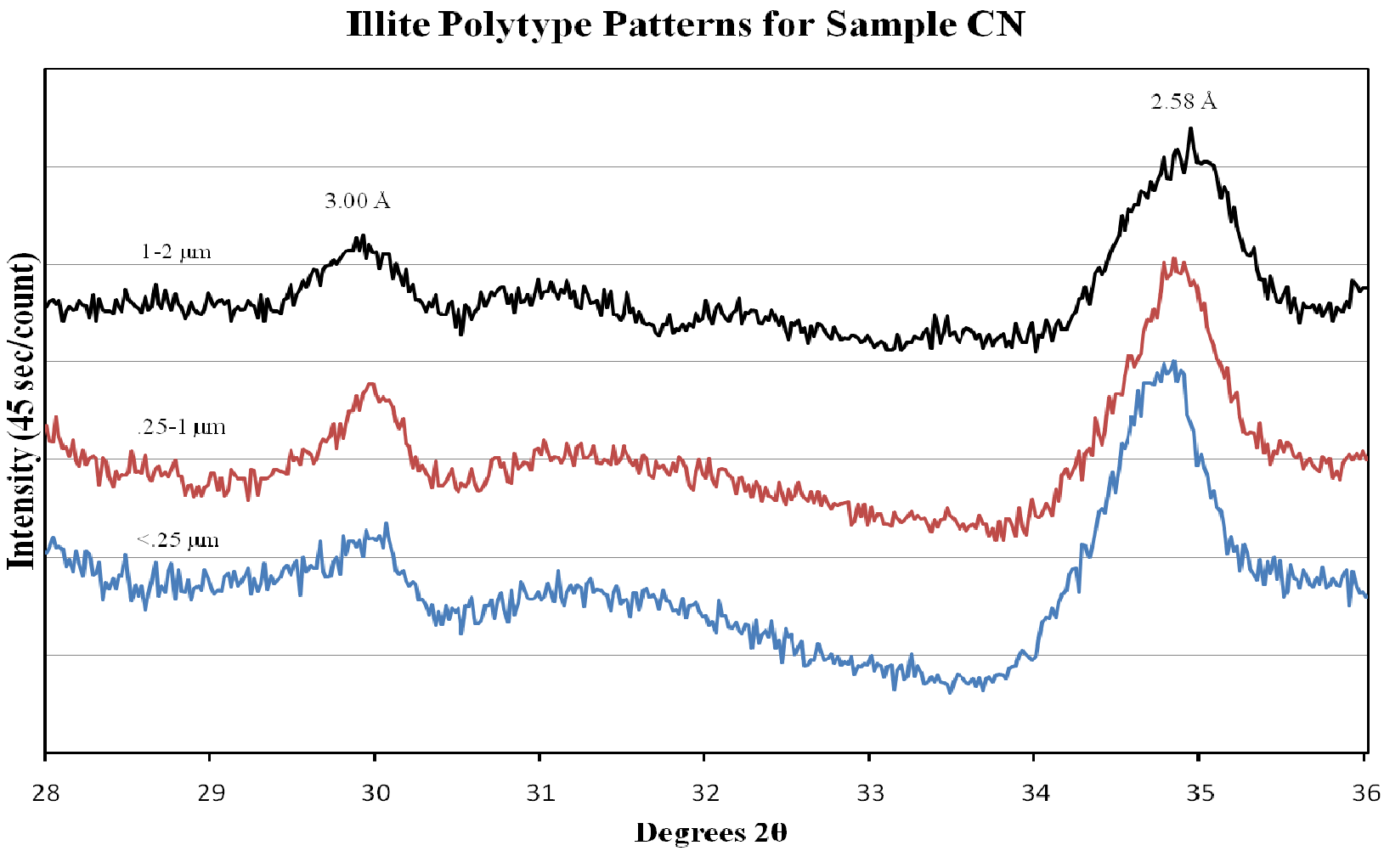

Figure C.1- Illite polytype patterns for sample CN.

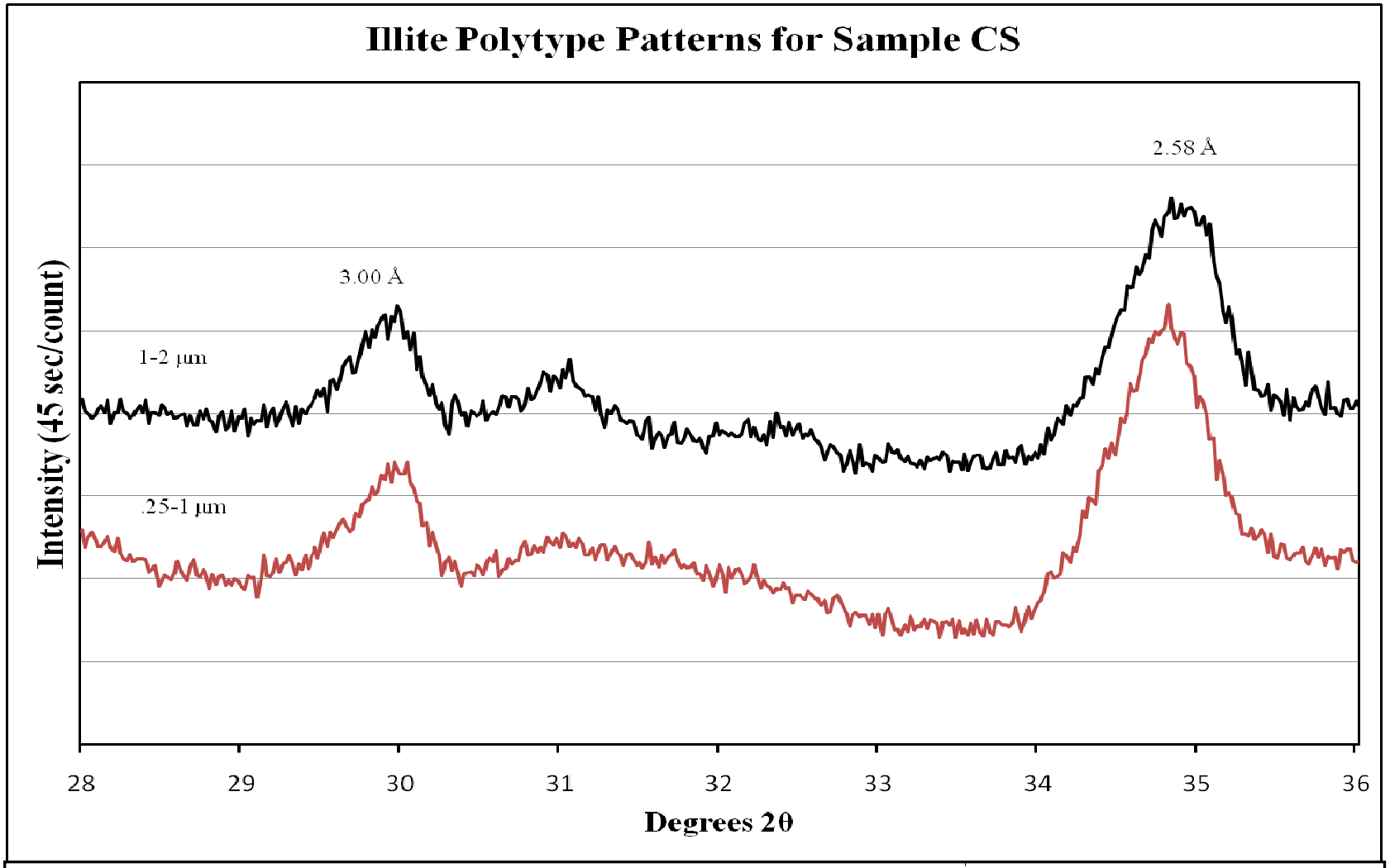

Figure C.2- Illite polytype patterns for sample CS.

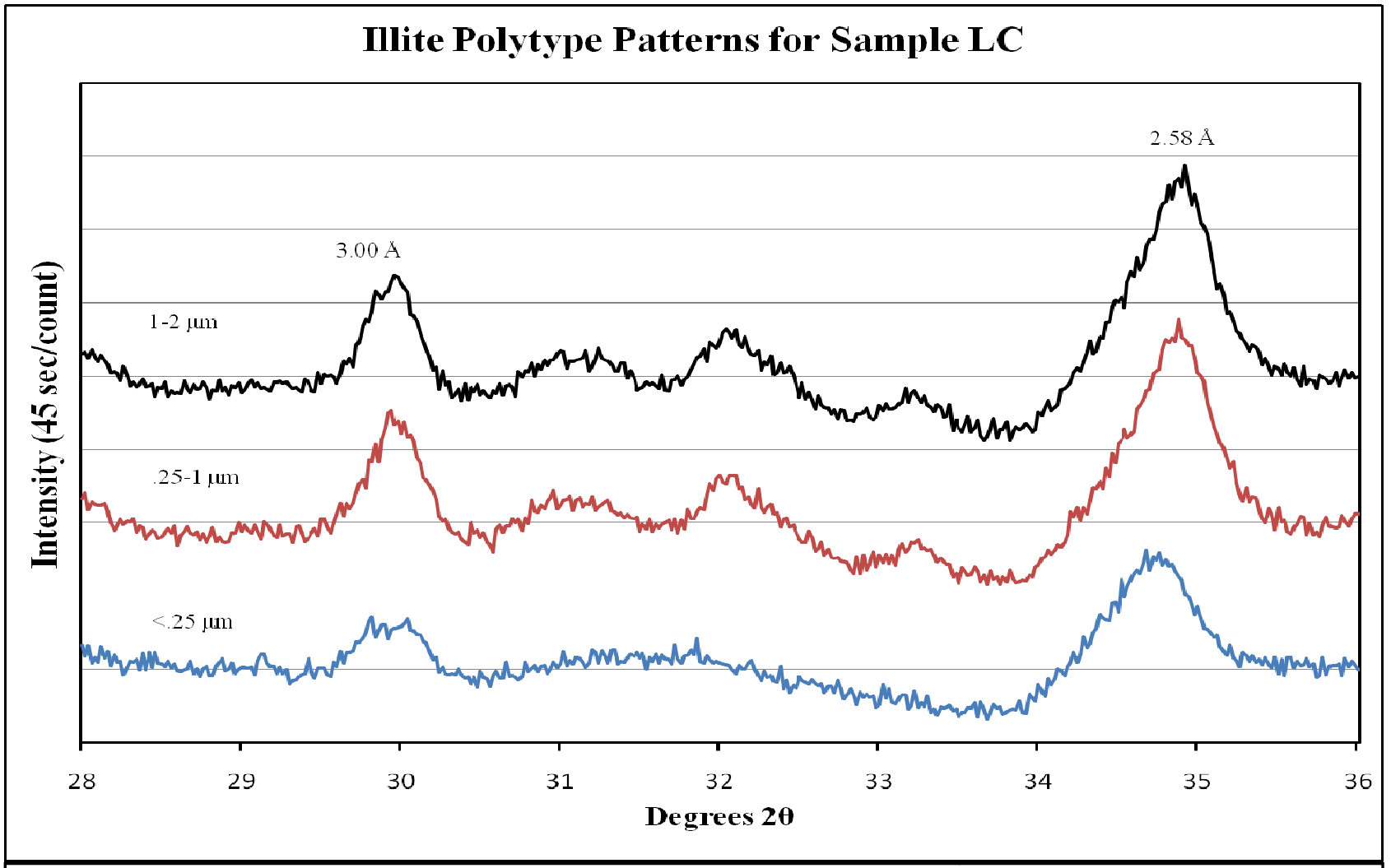

Figure C.3- Illite polytype patterns for sample LC.

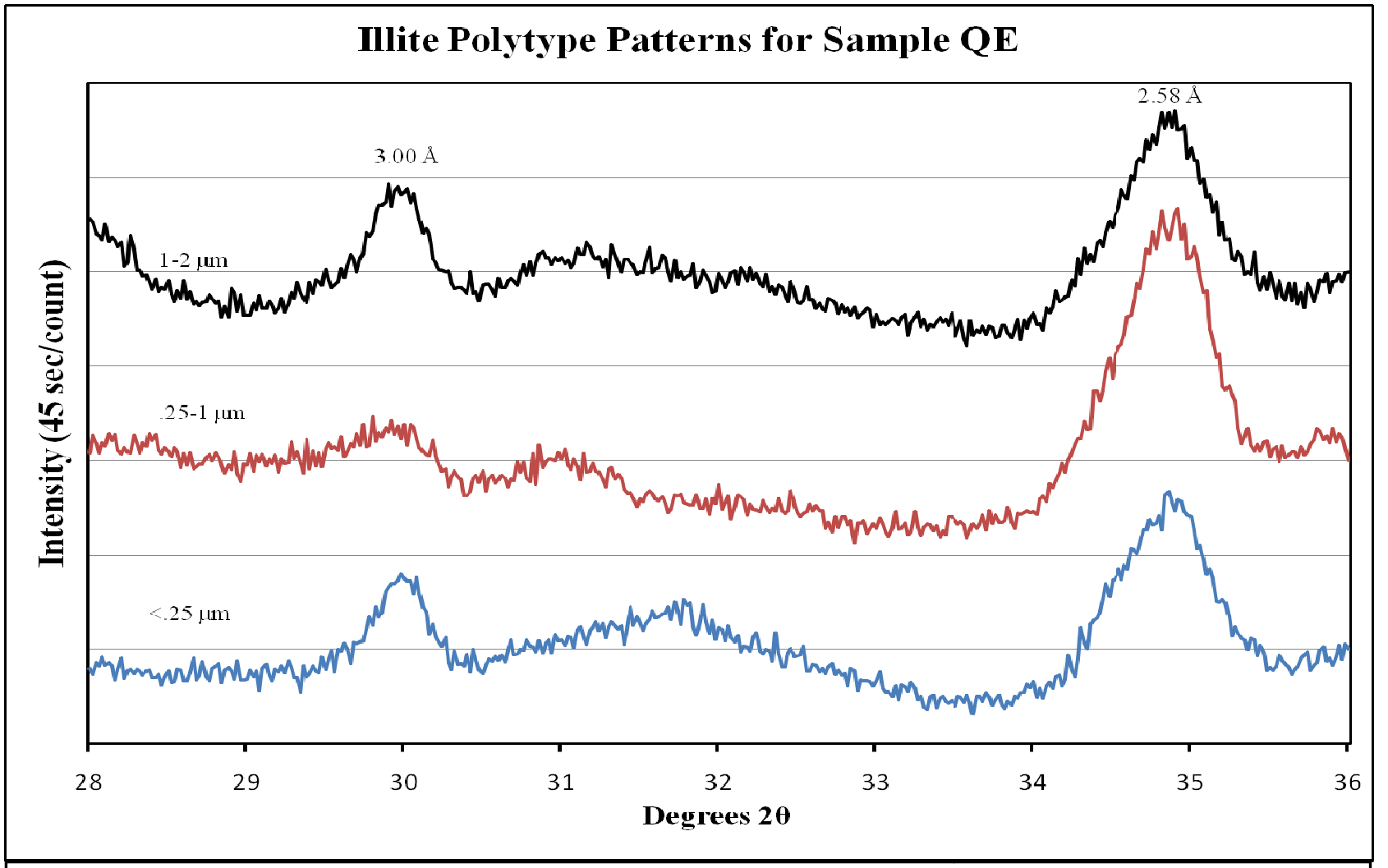

Figure C.4- Illite polytype patterns for sample QE.

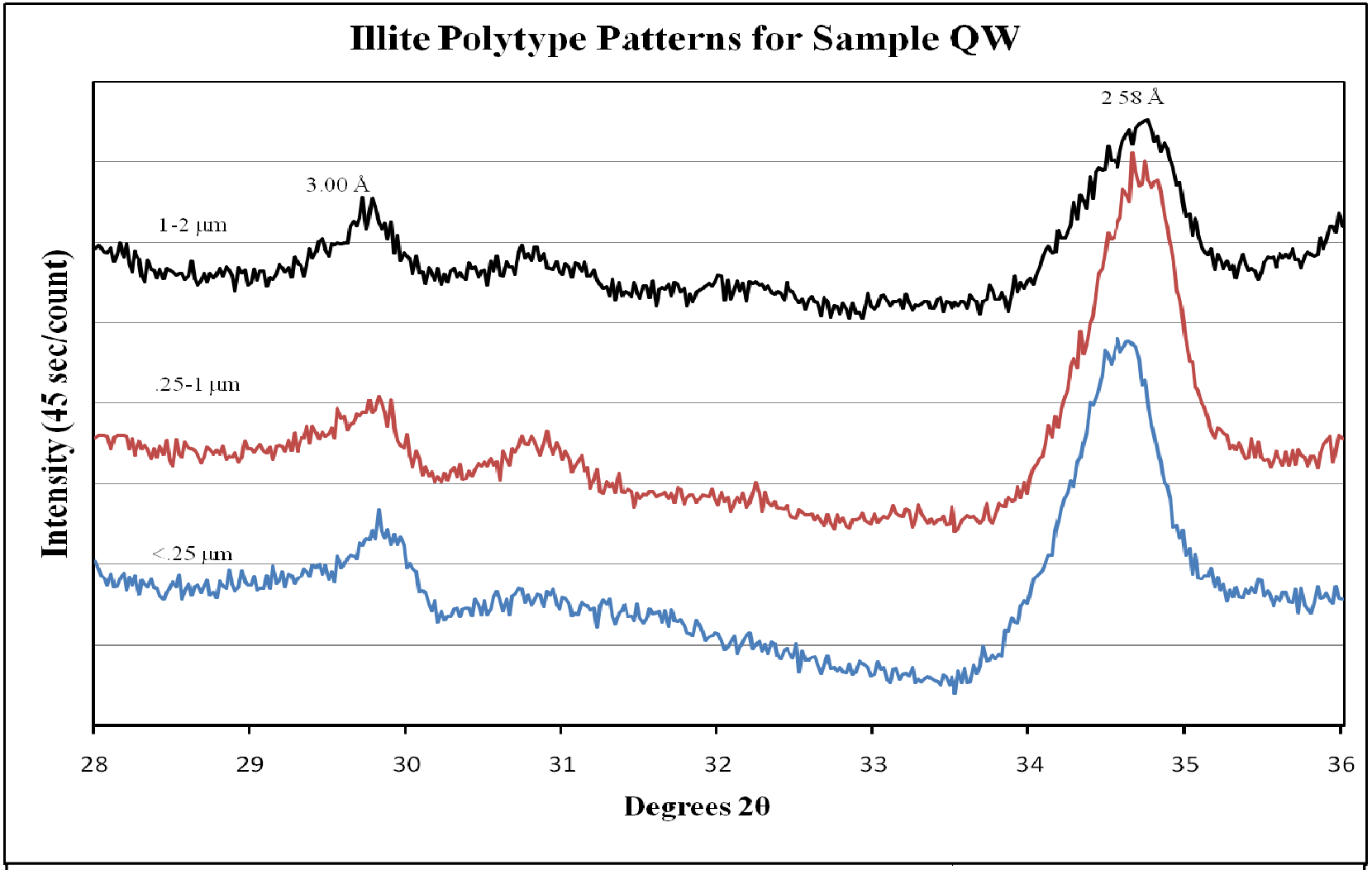

Figure C.5- Illite polytype patterns for sample QW.

Appendix D: Illite (001) Peak Deconvolution

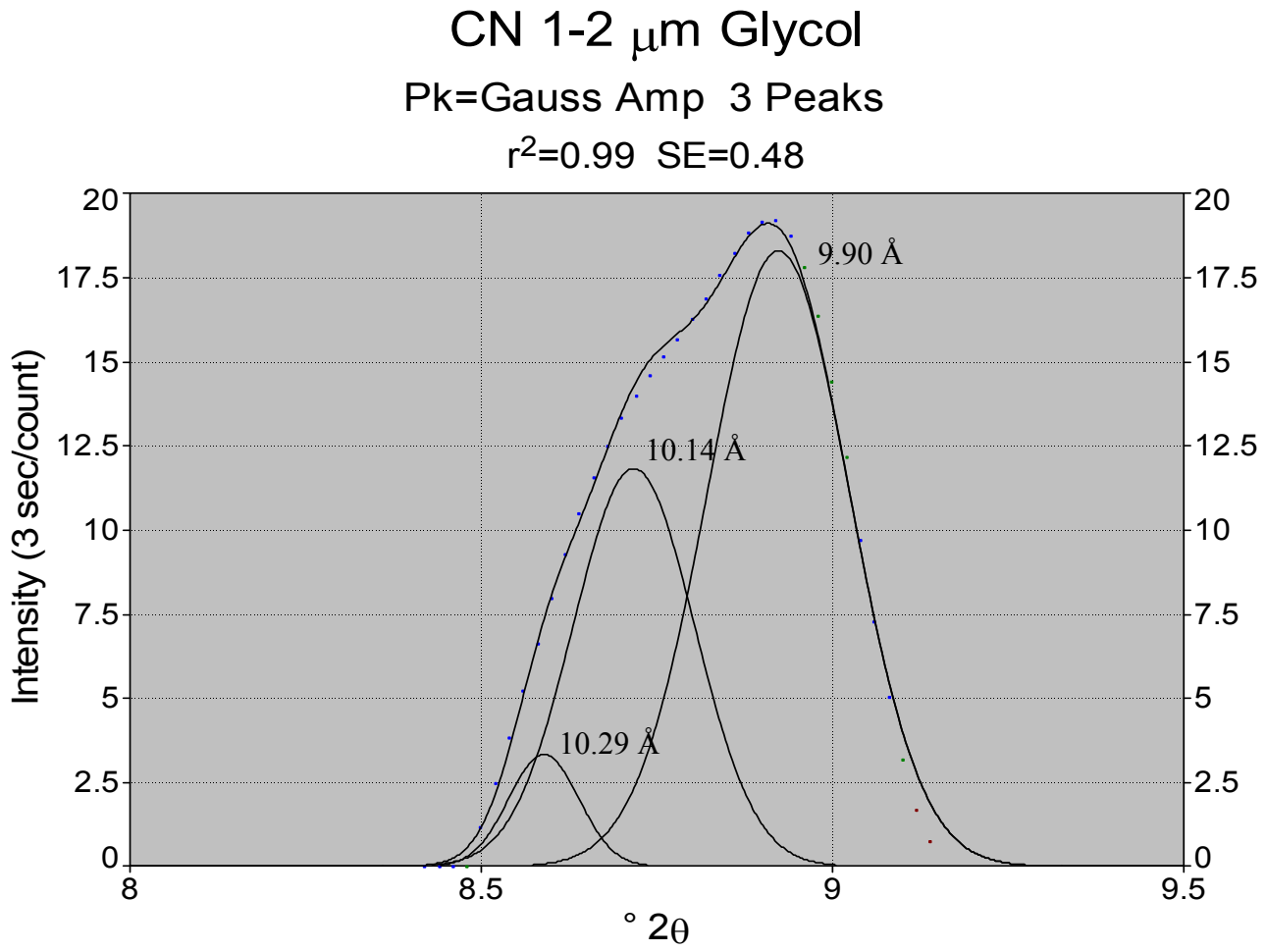

Figure D.1- Deconvolution of the ethylene glycol solvated illite (001) peak of sample CN 1-2 μm.

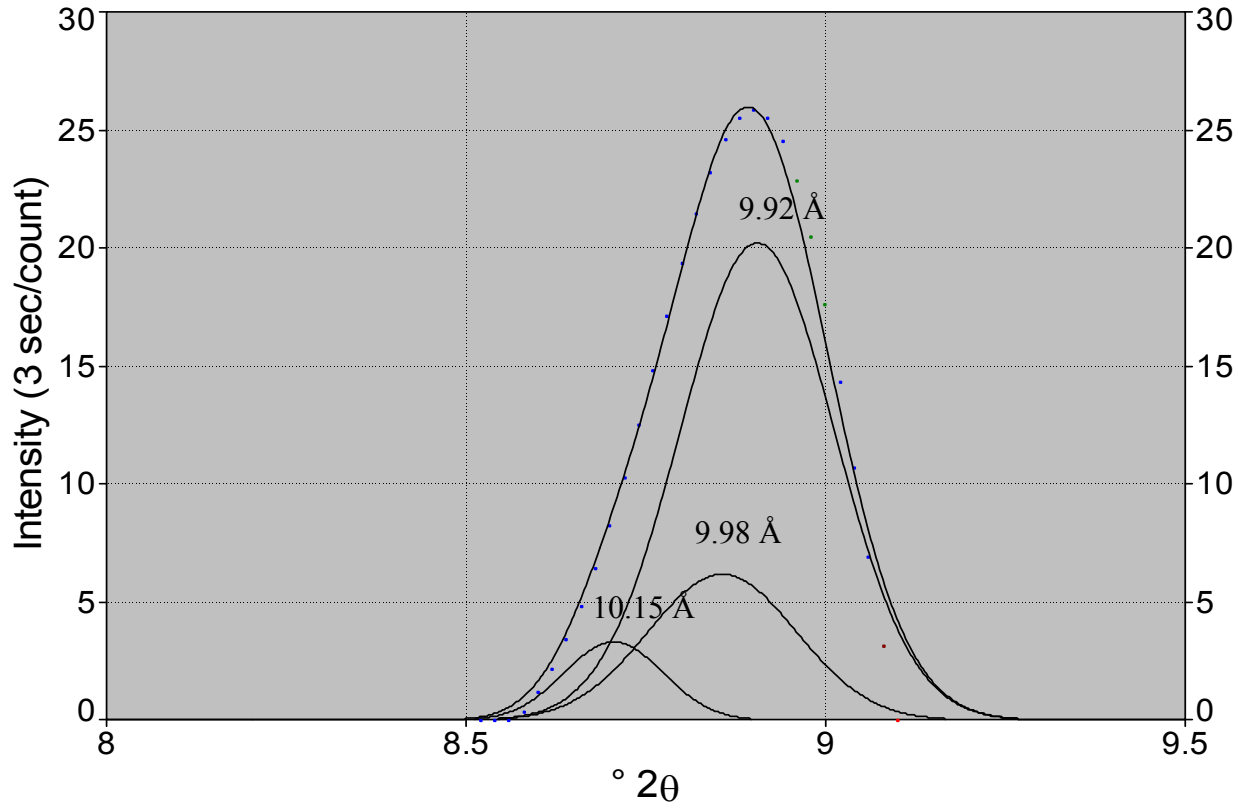

Figure D.2- Deconvolution of the ethylene glycol solvated illite (001) peak of sample CS 1-2 μm.

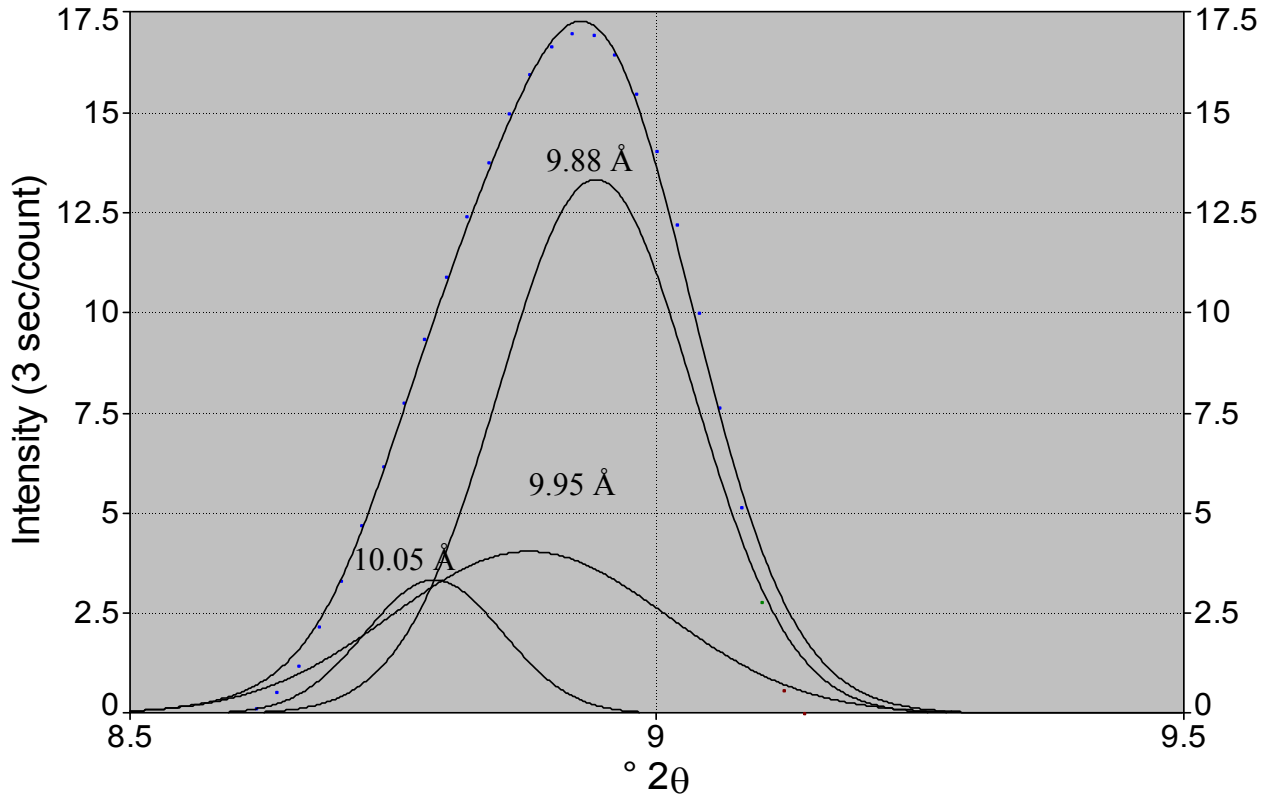

Figure D.3- Deconvolution of the ethylene glycol solvated illite (001) peak of sample LC 1-2 μm.

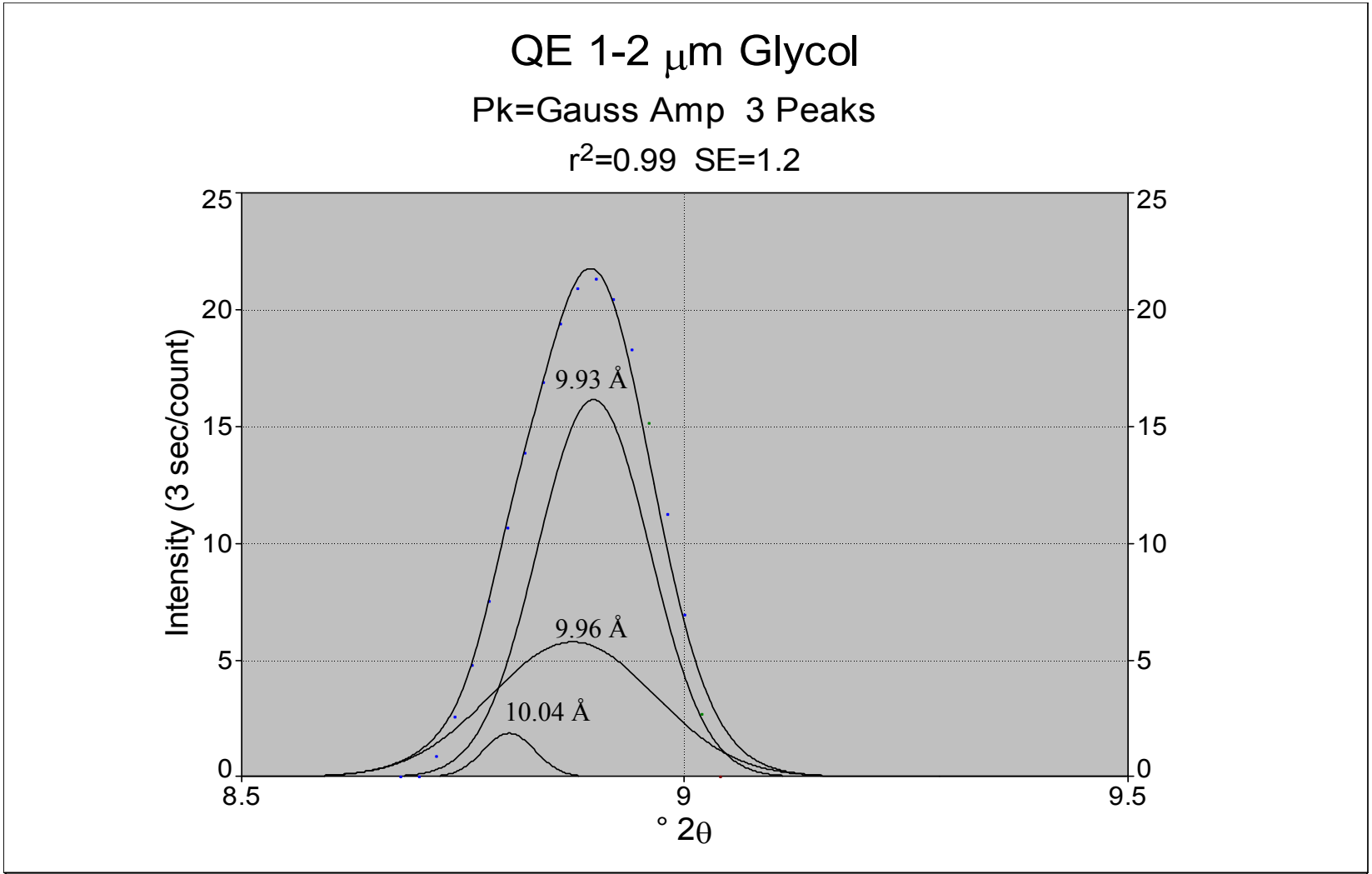

Figure D.4- Deconvolution of the ethylene glycol solvated illite (001) peak of sample QE 1-2 μm.

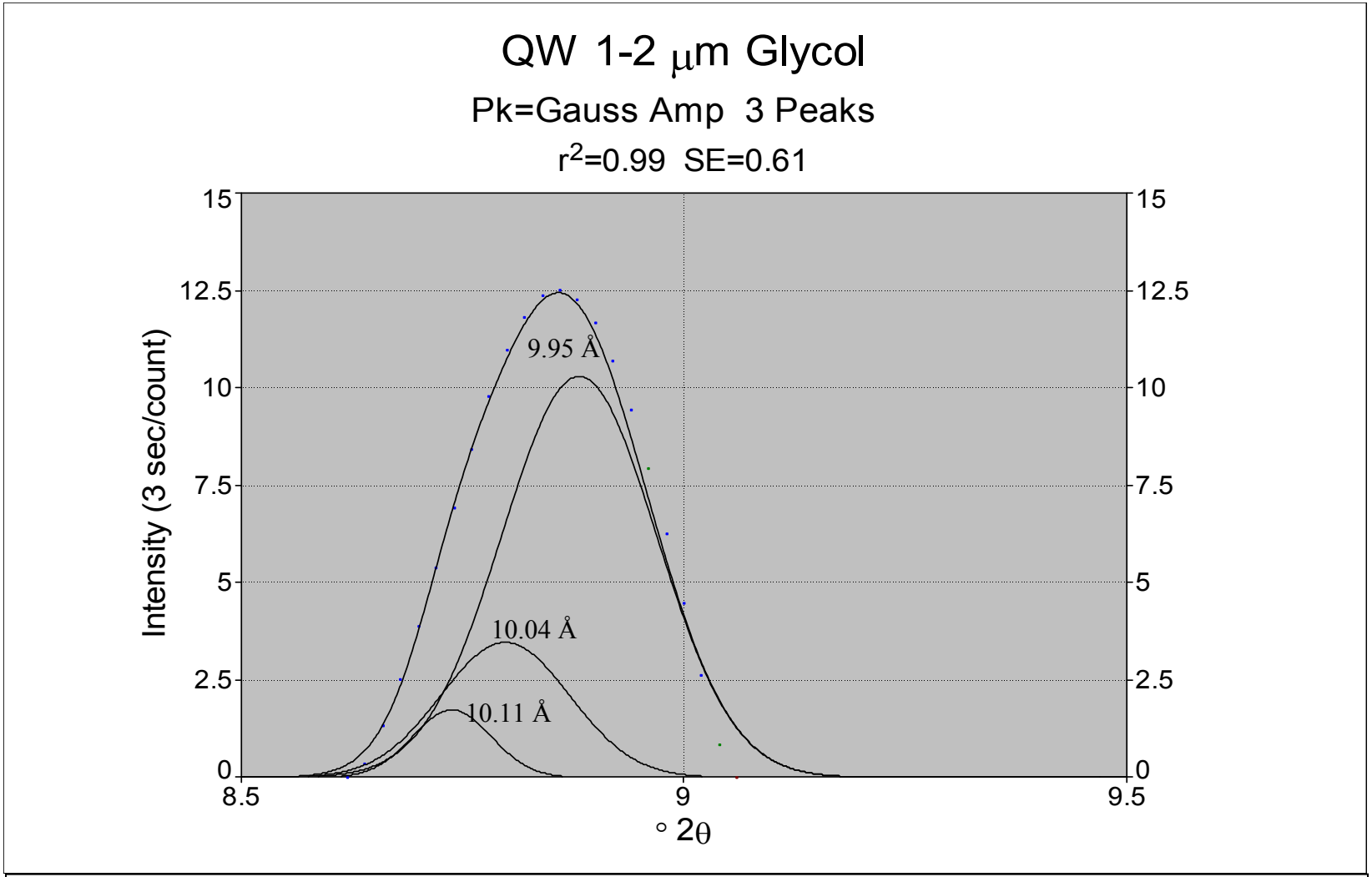

Figure D.5- Deconvolution of the ethylene glycol solvated illite (001) peak of sample QW 1-2 μm.

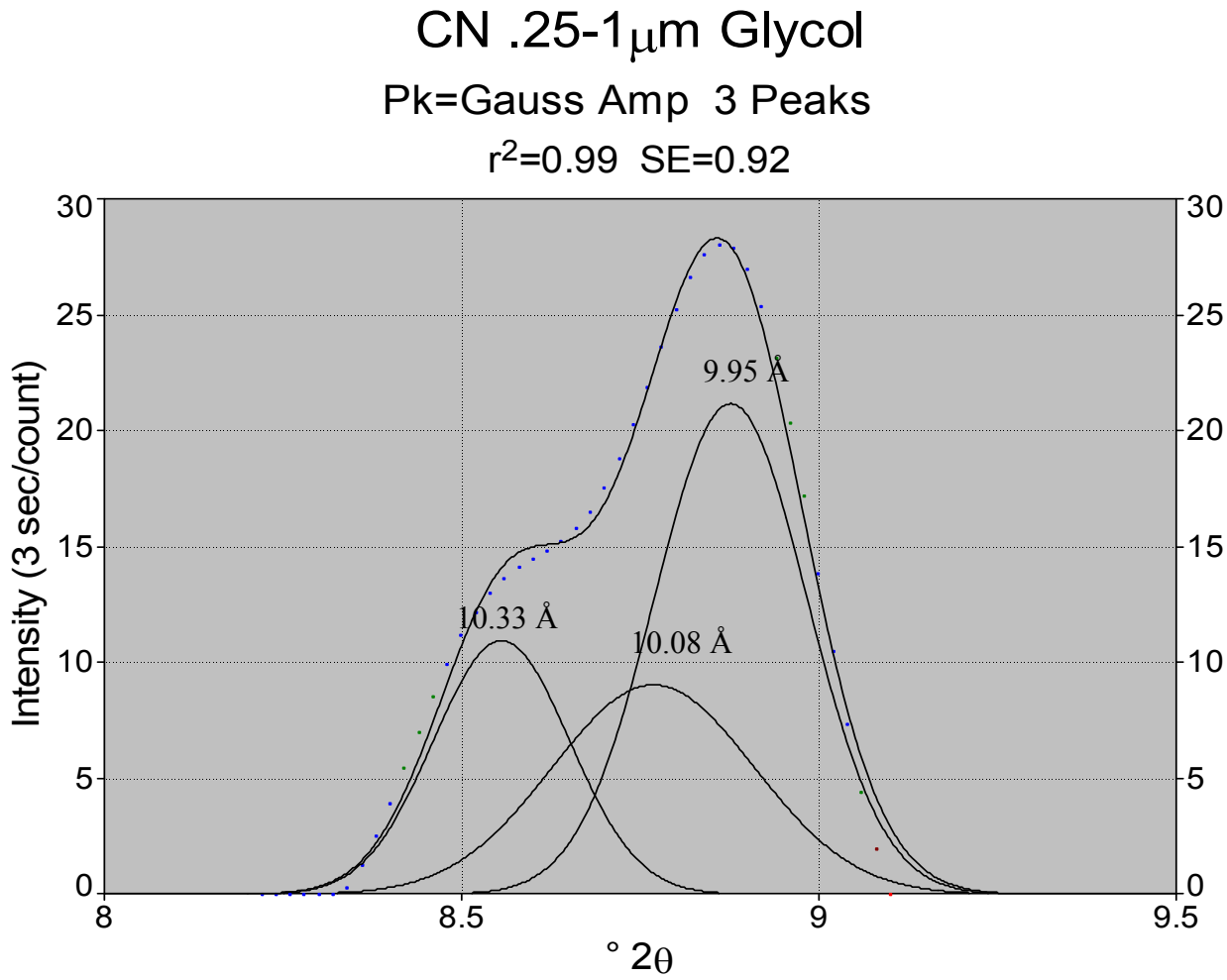

Figure D.6- Deconvolution of the ethylene glycol solvated illite (001) peak of sample CN 0.25-1 μm.

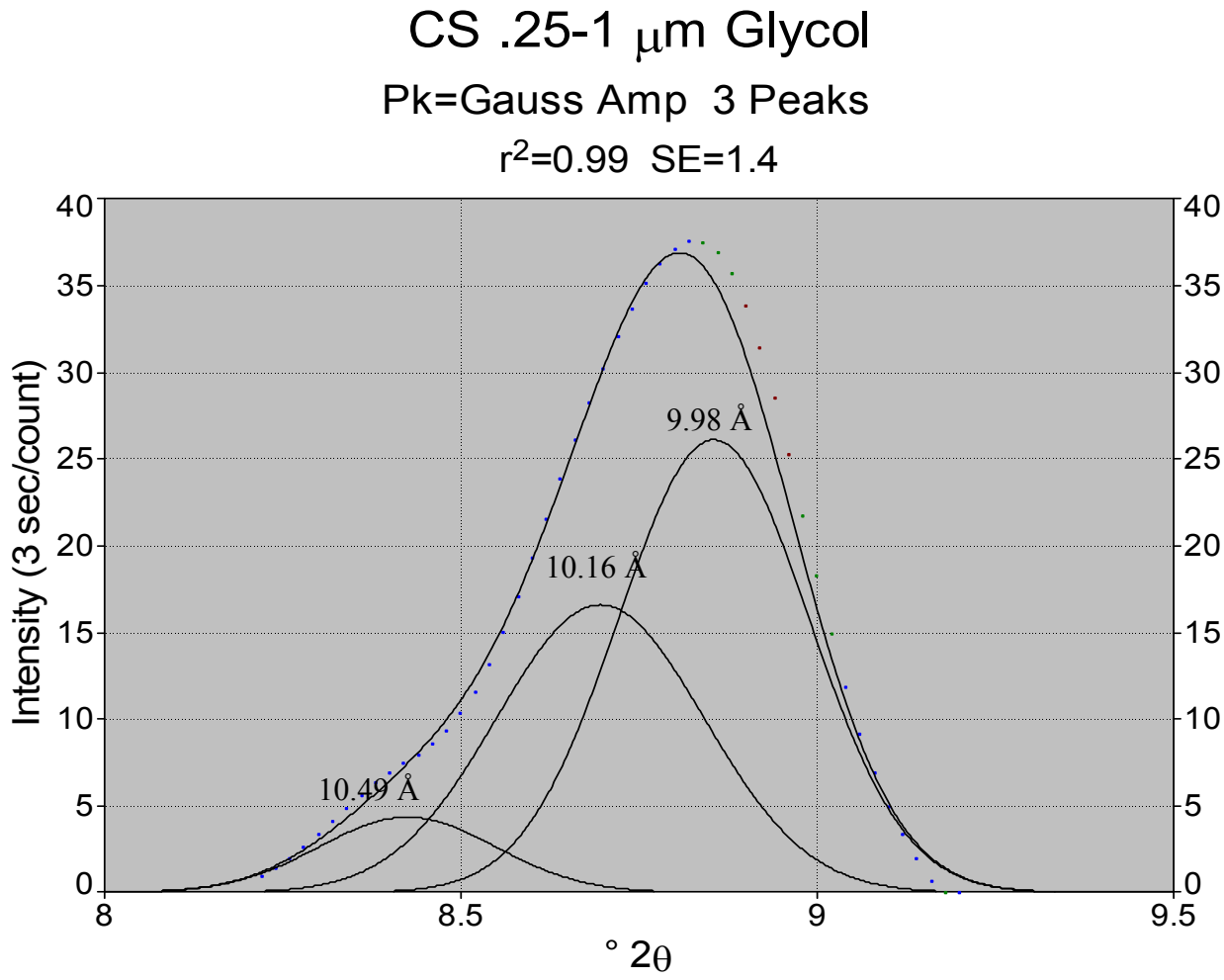

Figure D.7- Deconvolution of the ethylene glycol solvated illite (001) peak of sample CS 0.25-1 μm.

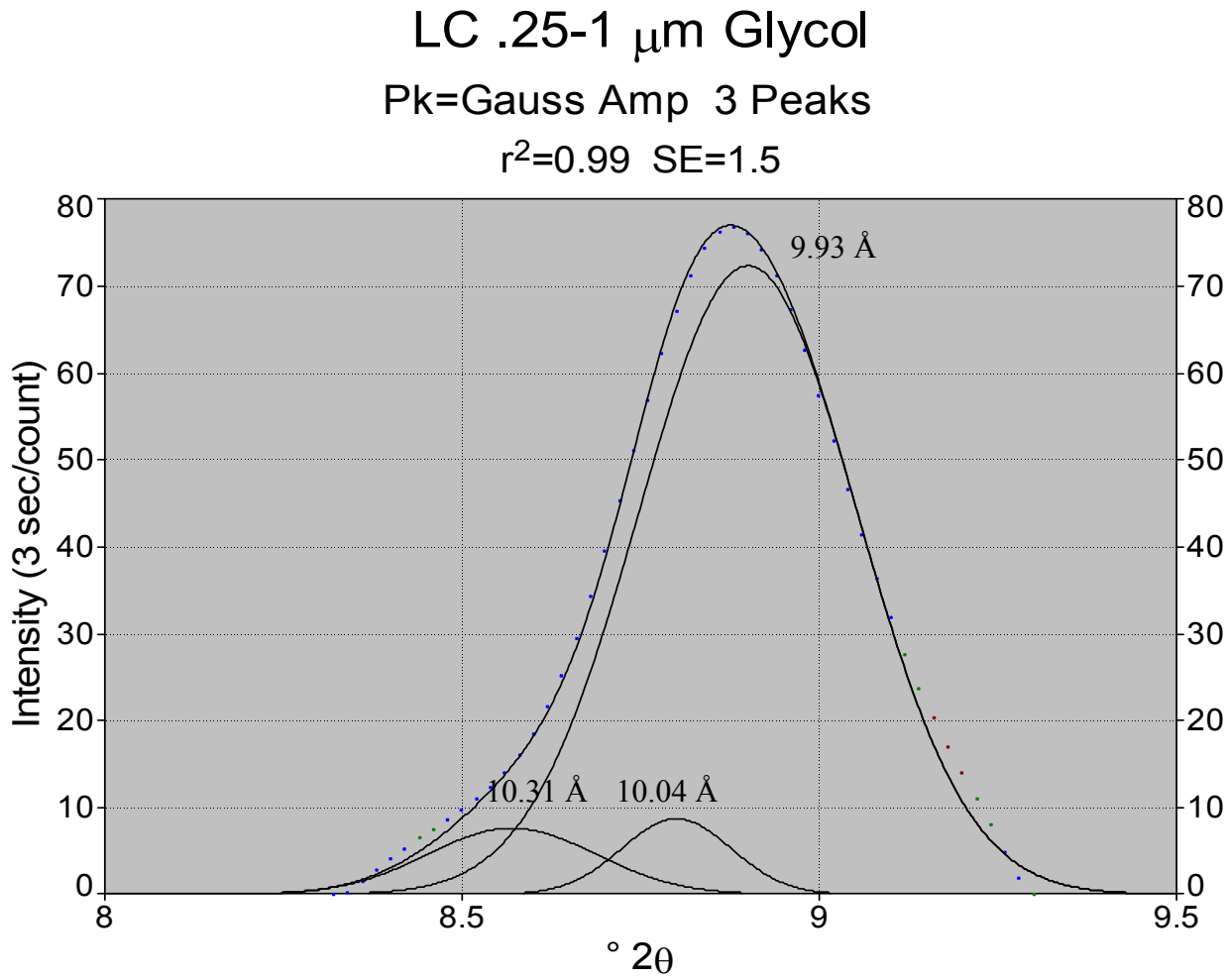

Figure D.8- Deconvolution of the ethylene glycol solvated illite (001) peak of sample LC 0.25-1 μm.

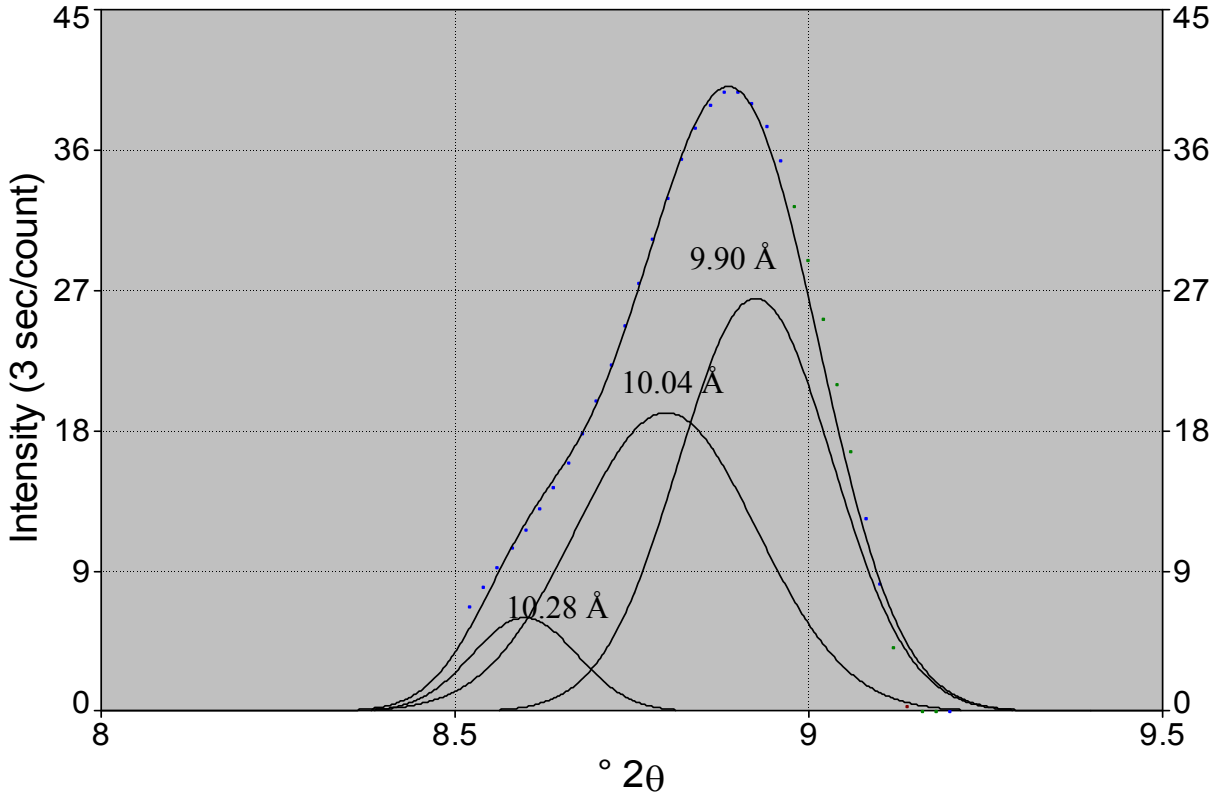

Figure D.9- Deconvolution of the ethylene glycol solvated illite (001) peak of sample QE 0.25-1 μm.

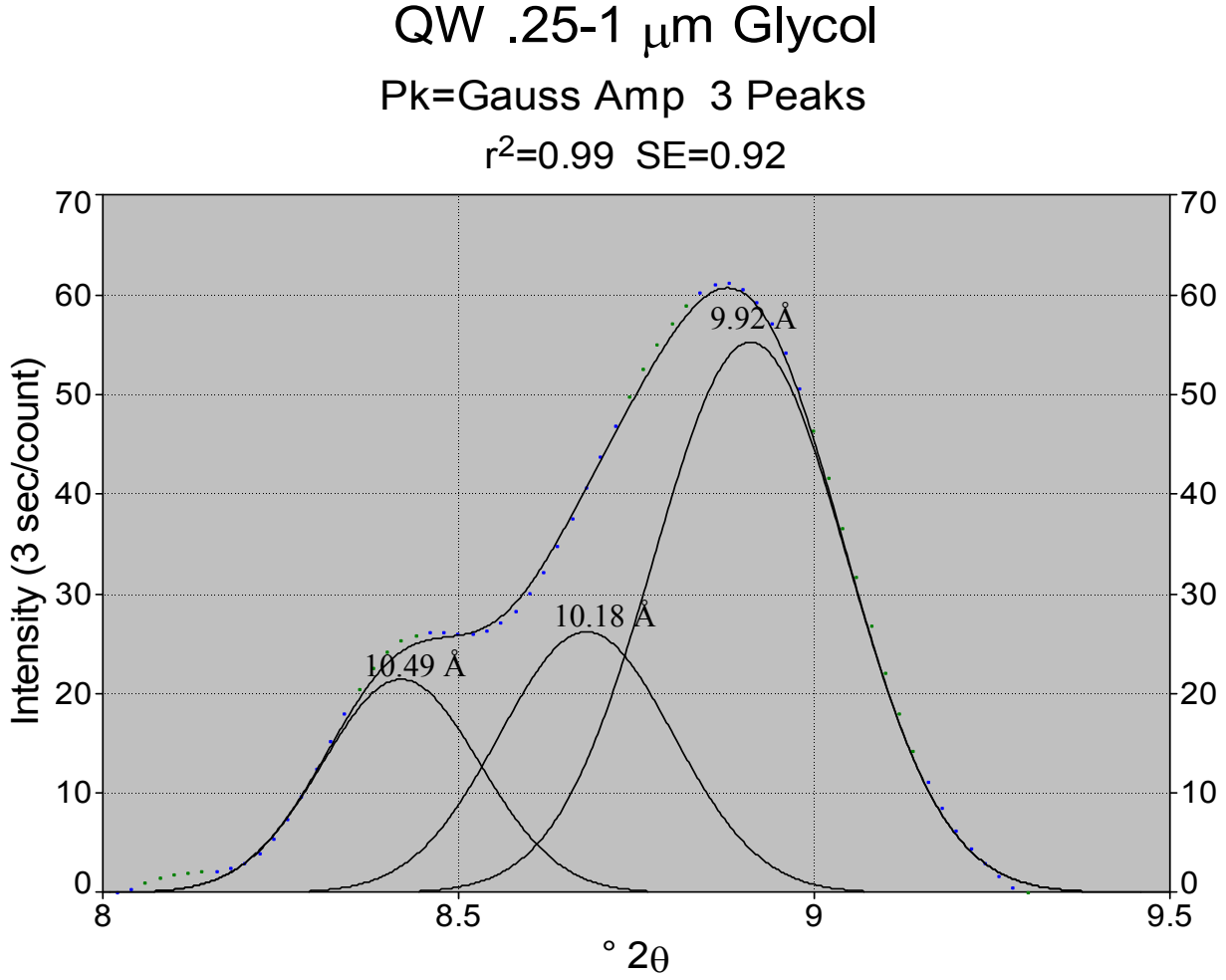

Figure D.10- Deconvolution of the ethylene glycol solvated illite (001) peak of sample QW 0.25-1 μm.

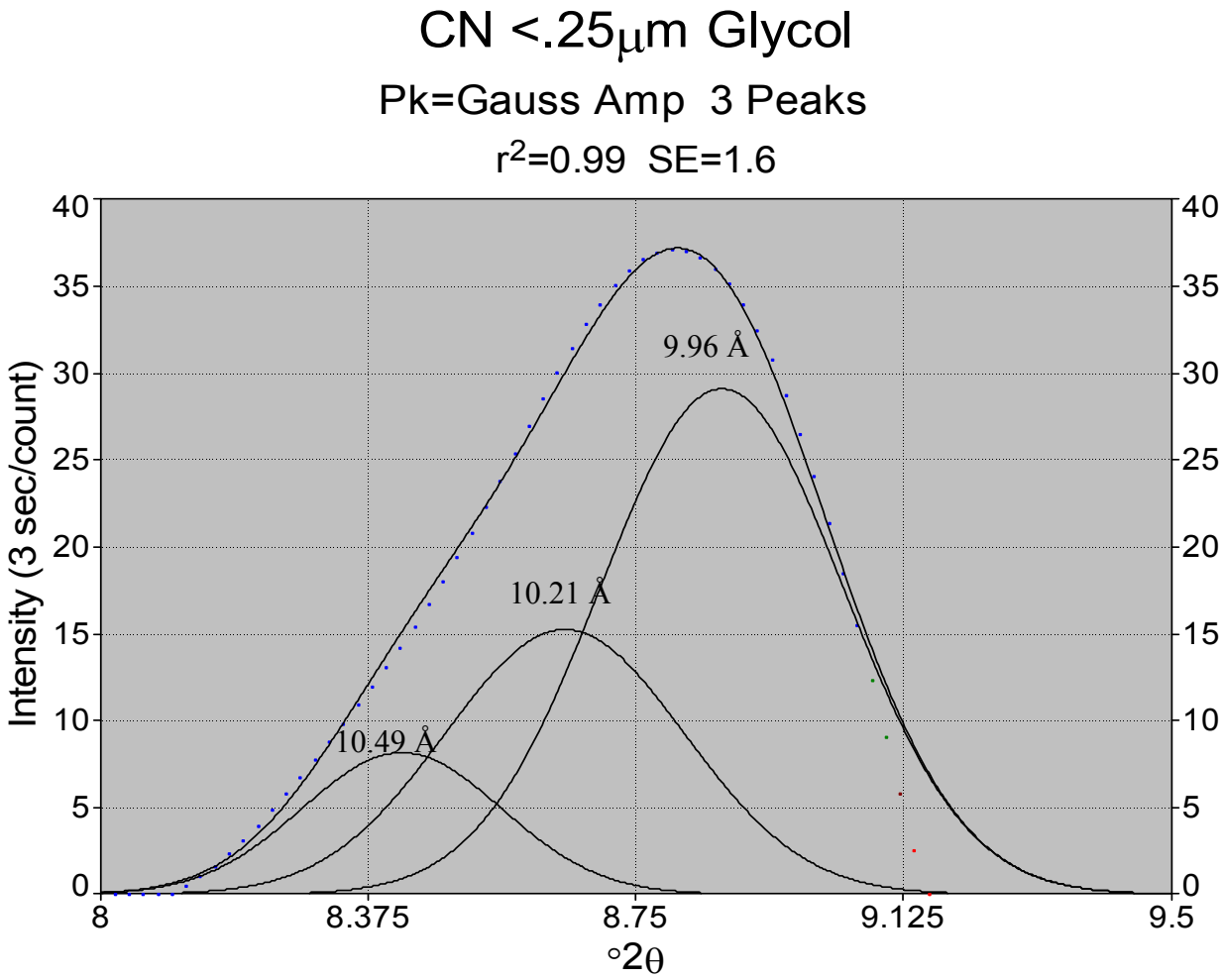

Figure D.11- Deconvolution of the ethylene glycol solvated illite (001) peak of sample CN <0.25 μm.

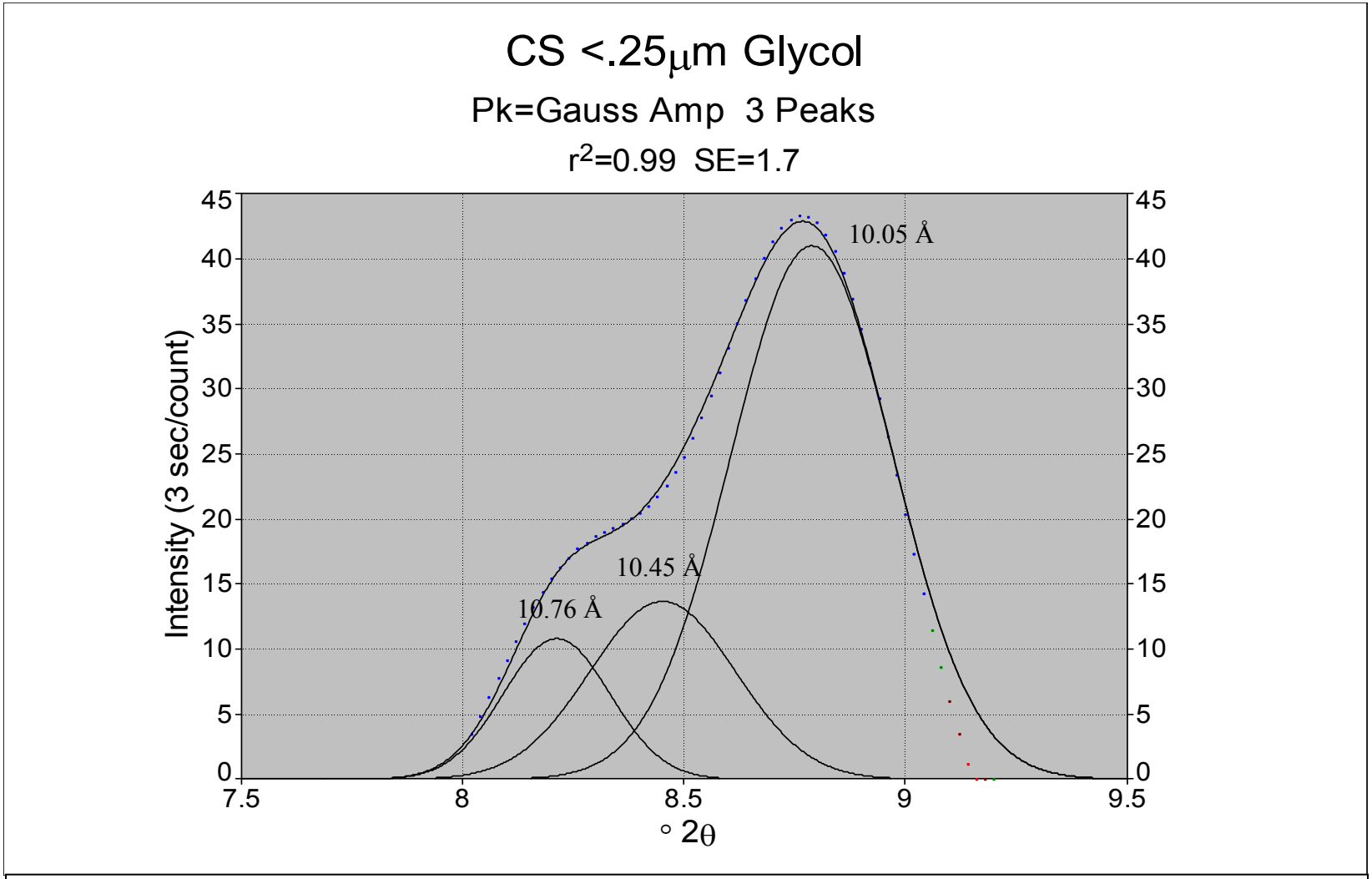

Figure D.12- Deconvolution of the ethylene glycol solvated illite (001) peak of sample CS <0.25 μm.

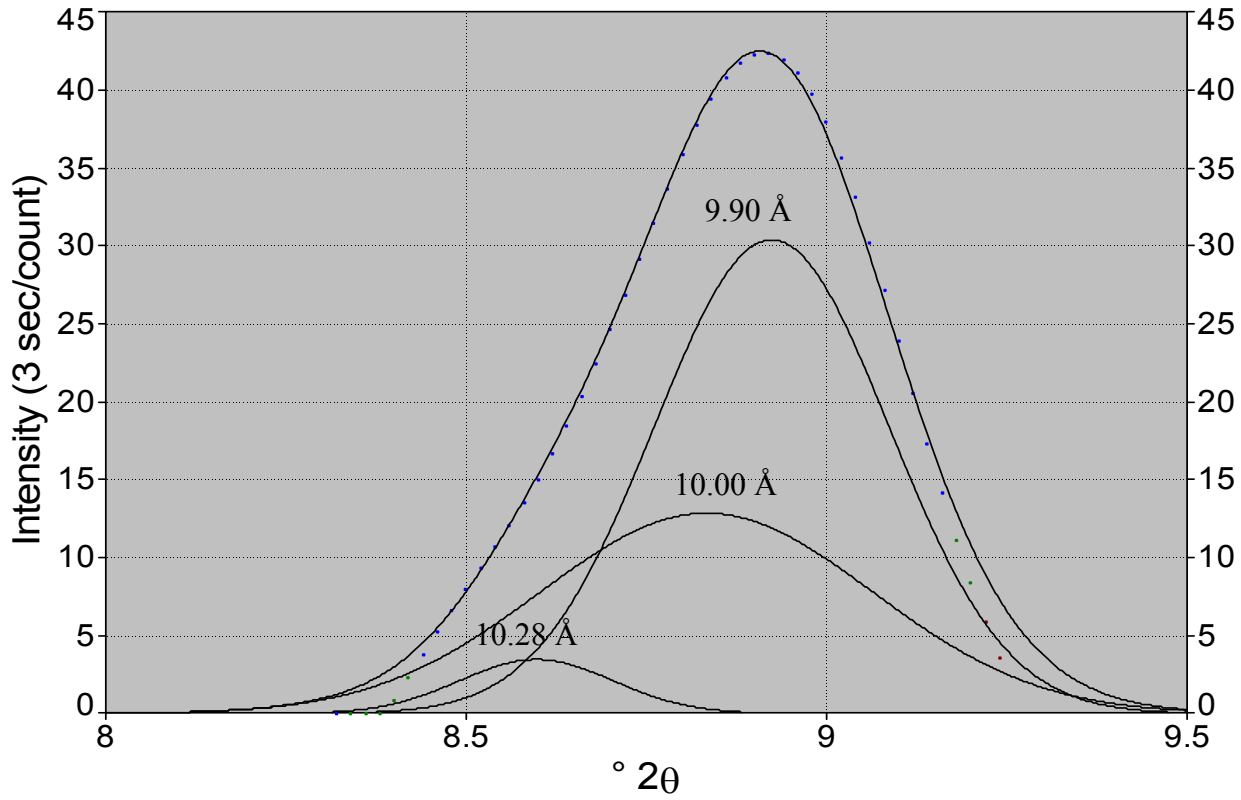

Figure D.13- Deconvolution of the ethylene glycol solvated illite (001) peak of sample LC <0.25 μm.

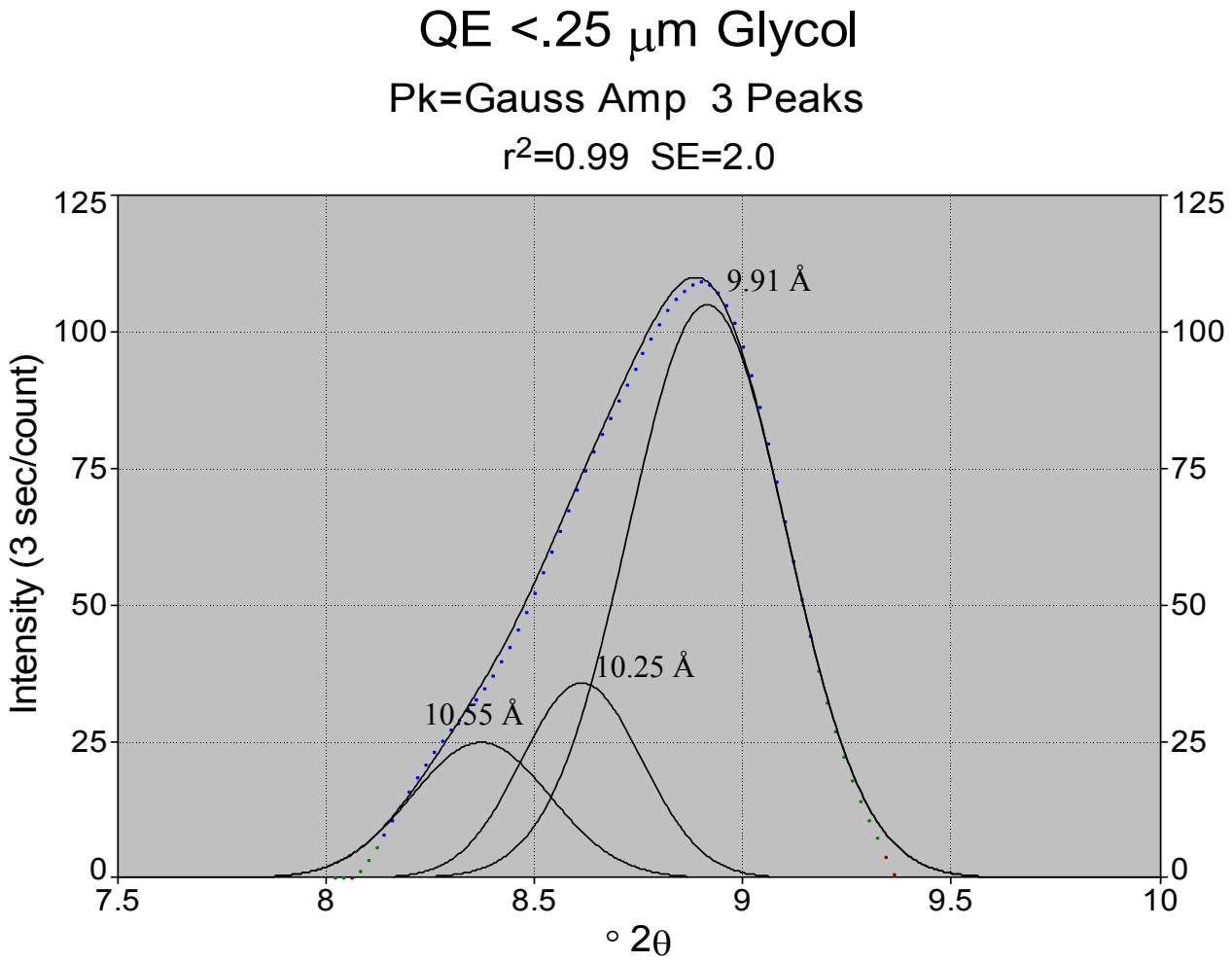

Figure D.14- Deconvolution of the ethylene glycol solvated illite (001) peak of sample QE <0.25 μm.

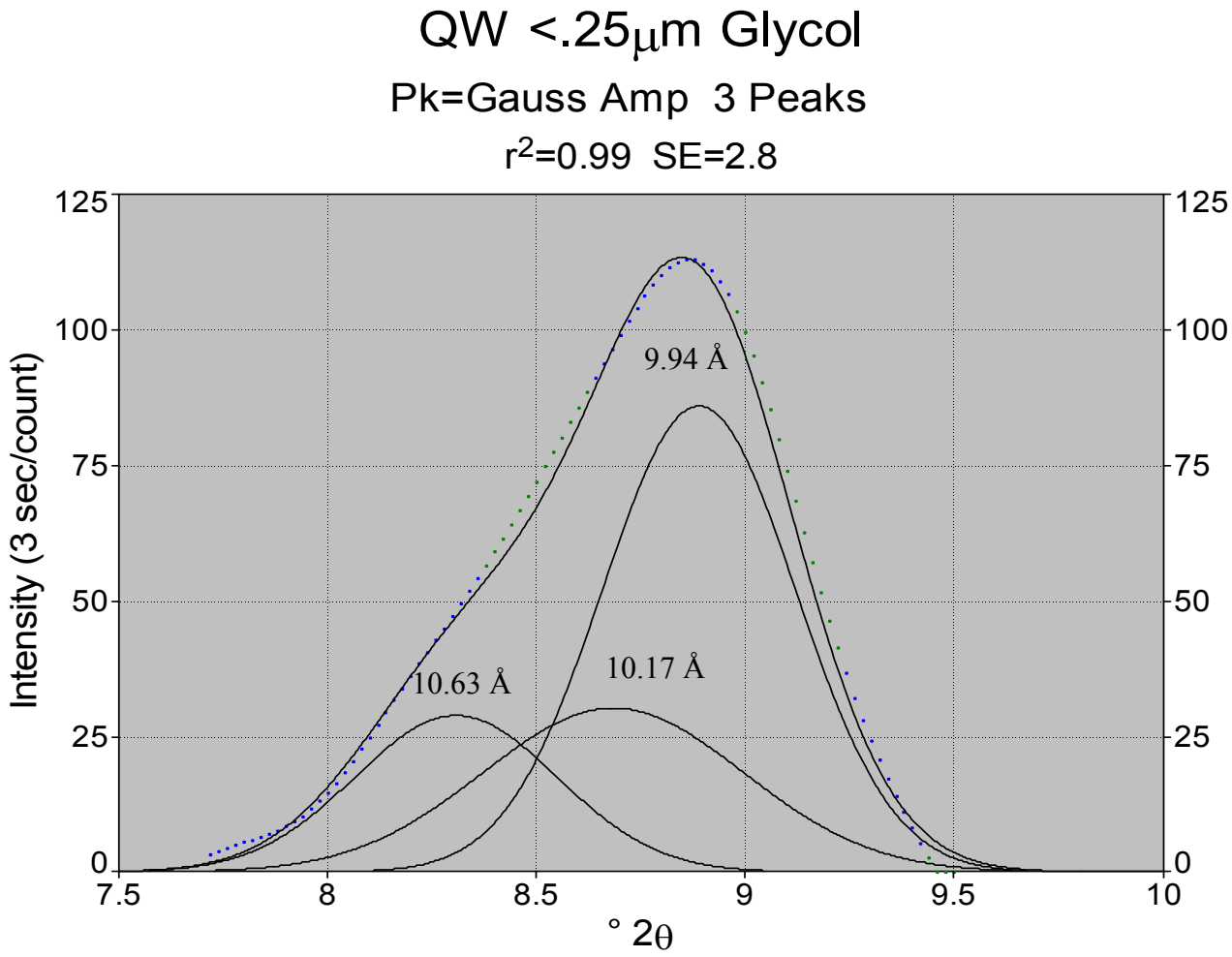

Figure D.15- Deconvolution of the ethylene glycol solvated illite (001) peak of sample QW <0.25 μm.